THREE DIMENSIONAL FRACTURE ANALYSIS OF ORTHOTROPIC MATERIALS

A THESIS SUBMITTED TO
THE GRADUATE SCHOOL OF NATURAL AND APPLIED SCIENCES
OF
MIDDLE EAST TECHNICAL UNIVERSITY

BY

GÖRKEM AKGÜL

IN PARTIAL FULLFILLMENT OF THE REQUIREMENTS
FOR
THE DEGREE OF MASTER OF SCIENCE
IN
MECHANICAL ENGINEERING

JUNE 2012

Approval of the thesis:

THREE DIMENSIONAL FRACTURE ANALYSIS OF ORTHOTROPIC MATERIALS

submitted by **GÖRKEM AKGÜL** in partial fulfillment of the requirements for the degree of **Master of Science in Mechanical Engineering Department, Middle East Technical University** by,

Prof. Dr. Canan Özgen
Dean, Graduate School of **Natural and Applied Sciences** _____

Prof. Dr. Suha Oral
Head of Department, **Mechanical Engineering** _____

Assoc. Prof. Dr. Serkan Dağ
Supervisor, **Mechanical Engineering Dept.,METU** _____

Examining Committee Members:

Prof. Dr. Suat Kadıoğlu
Mechanical Engineering Dept., METU _____

Assoc. Prof. Dr. Serkan Dağ
Mechanical Engineering Dept., METU _____

Assist. Prof. Dr. Ender Ciğeroğlu
Mechanical Engineering Dept., METU _____

Assist. Prof. Dr. Gökhan Özgen
Mechanical Engineering Dept., METU _____

Dr. Tunç Apatay
Mechanical Engineering Dept., GAZI UNIVERSITY _____

Date: **05.06.2012**

I hereby declare that all information in this document has been obtained and presented in accordance with academic rules and ethical conduct. I also declare that, as required by these rules and conduct, I have fully cited and referenced all material and results that are not original to this work.

Name, Last name: Görkem AKGÜL

Signature:

ABSTRACT

THREE DIMENSIONAL FRACTURE ANALYSIS OF ORTHOTROPIC MATERIALS

Akgül, Görkem

M. Sc., Department of Mechanical Engineering

Supervisor: Assoc. Prof. Dr. Serkan Dağ

June 2012, 104 pages

The main objective of this study is to examine the three-dimensional surface crack problems in orthotropic materials subjected to mechanical or thermal loading. The cracks are modeled and embedded in the orthotropic material by considering semi-elliptical crack front geometry. In the model special elements are embedded in the crack front region, in this way it is possible to include crack tip singular fields along the crack front. Three-dimensional finite element analyses are conducted to obtain mode I stress intensity factors. The stress intensity factor is calculated by using the displacement correlation technique. In the analysis, collapsed 20-node iso-parametric elements are utilized to simulate strain singularity around the semi-elliptical crack front. The surface crack problem is analyzed under both mechanical and thermal stresses. In the case of mechanical loading, uniform tension and fixed grip tension loading cases are applied on the model. In thermal analysis, thermal boundary conditions are defined. Comparisons of the results generated to those available in the literature verify the developed techniques.

Keywords: Fracture mechanics, semi-elliptical crack, orthotropic materials, stress intensity factors, thermal stresses

ÖZ

ORTOTROPİK MALZEMELERİN ÜÇ BOYUTLU KIRILMA ANALİZİ

Akgül, Görkem

Yüksek Lisans, Makina Mühendisliği Bölümü

Tez Yöneticisi: Doç. Dr. Serkan Dağ

Haziran 2012, 104 sayfa

Bu çalışmanın temel amacı, mekanik veya ısıl yüklemeye maruz kalan ortotropik malzemelerin üç boyutlu yüzey çatlak sorunlarını incelemektir. Çatlaklar, yarı-eliptik geometriye sahip olacak şekilde modellenerek ortotropik malzeme içine yerleştirilmiştir. Modelde özel elemanlar kullanmak, çatlak ucu bölgesi boyunca tekil alan çözümlerini de elde edebilmeyi mümkün kılmaktadır. Gerilme şiddet faktörünü hesaplamak için üç boyutlu sonlu eleman çözüm teknikleri uygulanmıştır. Gerilim şiddeti faktörü, deplasman korelasyon tekniği kullanılarak hesaplanmıştır. 20-düğümlü izo-parametrik elemanlar yarı eliptik çatlak ucu çözümlerinde kullanılmıştır. Yüzey çatlakları, hem mekanik, hem ısıl gerilme etkisi altında analiz edilmiştir. Mekanik yükleme analizlerinde, sabit noktadan gerilme yükleme ve sabit gerginlik durumları uygulanmıştır. Isıl yüklemede ise sınır koşulları tanımlanmıştır. Literatürde bulunan, doğruluğu ispatlanmış sonuçlar, geliştirilen yöntemin doğrulanmasında kullanılacaktır.

Anahtar Kelimeler: Kırılma mekaniği, yarı eliptik çatlak, ortotropik malzemeler, gerilme şiddeti faktörü

To my family

ACKNOWLEDGEMENTS

I would like to express my sincere gratitude to my advisor, Assoc. Prof. Dr. Serkan Dağ for his guidance, support and suggestions throughout the study. I would also like to thank Barış Sabuncuoğlu for his valuable advises and help on the ANSYS APDL coding.

I would also like to express my sincere appreciation for A. Sinem Konu, Furkan Lüleci, Ahmet Muaz Ateş, Duygu Tekbaş, Kadir İşeri, Egemen Yıldırım for their valuable friendship, support and help.

For their understanding my spending lots of time on this work, my sincere thanks go to my sister and to my mother.

Lastly, for his great support, understanding and help, I am also grateful to my father.

TABLE OF CONTENTS

LIST OF TABLES

TABLES

LIST OF FIGURES

FIGURES

LIST OF SYMBOLS

a	Radius of the Circular Surface Crack
$\emptyset$	Parametric Angle
h_1	Thickness of the Substrate
h_2	Thickness of the FGM Coating
b	Half - Width of the Cracked Plate
l	Half - Length of the Cracked Plate
p	Material Nonhomogeneity Parameter for the FGM Layers
T	Temperature
E_c	Elastic Modulus of the Ceramic Component (ZrO2)
v_c	Poisson's Ratio of the Ceramic Component
k_c	Thermal Conductivity of the Ceramic Component
c_c	Specific Heat of the Ceramic Component
ρ_c	Density of the Ceramic Component
h_c	Thermal Expansion Coefficient of the Ceramic Component
E_s	Elastic Modulus of the Metal Component (Ti-6Al-4V)
v_s	Poisson's Ratio of the Metal Component
k_s	Thermal Conductivity of the Metal Component
c_s	Specific Heat of the Metal Component
ρ_s	Density of the Metal Component
h_s	Thermal Expansion Coefficient of the Metal Component
K_I	Mode I Stress Intensity Factor

K_{In}	Normalized Mode I Stress Intensity Factor
Q	Shape Factor for a Semi - Elliptical Crack
σ_t	Uniform Tension Stress
σ_b	Normal Stress on the Outer Fiber for Bending Load
v_0	Uniform Normal Displacement for Fixed – Grip Tension
σ	Uniform Compressive Traction for Three Point Bending
δ	Half – Length of the Rectangular Region
P	The Resultant Force due to Loading in Three Point Bending
T_0	Environment Temperature
h	Convection Coefficient
T_m	Average of the Environment and Processing Temperatures
S	Normalization Stress
D	Thermal Diffusivity Coefficient
t	Time
τ	Normalized Time
u_b	Normal Displacement Component on the Crack Front
σ_{bb}	Normal Stress Component on the Crack Front
r	Distance from the Crack Tip
θ	Angle from the Crack Plane
σ_{ij}	The Components of Stresses
u_i	The Components of Displacements
K_{II}	Mode II Stress Intensity Factor
K_{III}	Mode III Stress Intensity Factor
μ	Shear Modulus

CHAPTER 1

INTRODUCTION

1.1 Introduction

In the present study, three-dimensional semi elliptic crack problems are studied for orthotropic materials. There are nine independent characterizing variables of orthotropic materials, which means that there are three planes of elastic symmetry in the structure.

In order to obtain asymptotic stress and displacement fields of a crack in a three-dimensional orthotropic material, stress and displacement fields close to the tip of a straight crack in a generally rectilinear anisotropic elastic body are resolved. As in the isotropic analysis, the stress singularity $r^{1/2}$, where r is the distance from the tip, is handled in a complicated way because of the angular changes due to the anisotropy around the crack front. In some special cases, where some elements of the compliance matrix are zero, the asymptotic stress and displacement fields should be redefined for these special cases. These cases are called degeneracy cases such as anti plane shear and plane strain decoupling case and x-y plane isotropy case. As a result of the material used for the analysis is not fully anisotropic in this study, the degeneracy cases are used to obtain asymptotic field expressions. The crack front in a three dimensional orthotropic medium is modeled using these anisotropic asymptotic field expressions [1].

Composites have wide application areas in the world. Due to their advantageous mechanical and thermal properties in engineering applications, composites are preferred. Their high stiffness to weight ratios, low thermal conductivity constants and design flexibilities make the composite structures comparable with traditional materials. These materials generally possess anisotropic or orthotropic materials.

Different numerical methods can be used to conduct fracture analysis. Boundary Element Method (BEM) and Finite Difference Method (FDM) are two of these solution techniques. Moreover, there is also meshless method to solve the structure model numerically, different from BEM and FDM. But the most popular method is the Finite Element Method (FEM). By using this method, most of the problems can be modeled and solved by defining boundary conditions and the physics of the environment. However, the elements at the crack faces should be handled in a different way compared to the other elements. In order to simulate and solve the crack propagation using the fracture mechanics approach, re-meshing techniques and prediction methods for singular stress field around a crack tip should be applied. Due to the difficulties in modeling these singular stress fields around a crack tip by using finite element method, in certain cases the Extended Finite Element Method (XFEM) could be preferred to solve the problems, which contain singular fields and discontinuities in material and geometry. The XFEM method is originally applied by Belytschko and Black [2]. They use the advantages of the conventional FEM and improve the method by modeling the discontinuities.

In analysis based on fracture mechanics, the most important parameter is the stress intensity factor. Therefore, in fracture mechanics based finite element analyses it is important to calculate the stress intensity factors accurately.

In fracture mechanics, the three-dimensional crack problems have been considered as important problems to be solved analytically and numerically. For three dimensional anisotropic and orthotropic materials, there exists very limited research. Therefore, in this study, these materials will be studied in detail, and finally three-dimensional orthotropic materials will be modeled and meshed in order to compute stress intensity factors for certain configurations.

There are several finite element analysis programs available. These programs are used for commercial and academic purposes. Because of the large variety of approaches and finite element analysis software programs for three-dimensional structures, crack geometries in three-dimensional bodies have been studied with great interest in recent years. However, finite element techniques are not capable of solving crack geometries accurately without considering the crack faces, asymptotic fields and stress fields around crack tips [3]. Therefore, some modifications should be applied to the software program by embedding the asymptotic field expressions using parametric design language of the program. The use of the asymptotic field expressions allows the evaluation of the stress intensity factors from stress and displacement values around the crack front. Asymptotic fields for plane strain configurations of anisotropic materials can be used also for three-dimensional problems involving such materials [4]. In the present study, we employ plane strain fields to generate the stress intensity factors for cracks located in three-dimensional structures.

The $r^{1/2}$ stress singularity method is used in 3D fracture analyses. In this method mid side nodes are placed at the quarter of the element size from the crack front location, thus this method is also known as quarter point technique. Although this method is highly dependent on the mesh quality, it can be successfully used to solve three-dimensional problems. Ozkan [5], illustrated that quarter point technique can be applied to both three-dimensional isotropic materials and three-dimensional

anisotropic materials. Disadvantages of this method are the necessity of using wedge elements along the crack front and dependence of the solutions on mesh refinement.

1.2 Literature Survey

The goal of this study is to develop a method to carry out fracture analyses of orthotropic materials. Mode I stress intensity factor for three-dimensional composite structures is calculated by applying the displacement correlation technique. In the past, various researchers studied surface crack problems. However, these crack problems are handled for two dimensional planar structures or three-dimensional isotropic structures, or three-dimensional FGM coating materials, in which the material properties change continuously as a function of thickness dimension of the structure. This study can be considered as one of the first studies in the literature, dealing with three-dimensional fracture problems in orthotropic materials.

Although the literature related to three-dimensional analysis on orthotropic materials is very limited, in previous studies numerous results have been reported for three-dimensional cracks in an isotropic media. Hence, certain methods to solve these have been developed in literature. Especially, three-dimensional homogenous isotropic materials have been considered in the FEM analysis. There are large number of techniques available to obtain stress intensity factors for three-dimensional isotropic crack fronts [3],[6],[7]. Semicircular cracks in semi-infinite structures are considered under different types of mechanical loading cases, such as tension and bending by Smith et al. [8]. The stress intensity factors are also calculated under thermal loading situation [9]. There are also empirical solutions for semi elliptic cracks in the literature. Raju and Newman [10] derived expressions to obtain stress intensity factors. In this research, they derived the empirical stress intensity factor equations of a semi-elliptical surface crack by using FEA.

Due to the complex nature of material behavior of anisotropic materials, most of the researchers focused on the two-dimensional formulations. Sih et al. [11] extended the isotropic local crack tip stress fields for general plane problems to the rectilinear anisotropic case. Hoenig [1], Embley [12], and Sih [13], extended the analysis of crack tip stress fields to the case of generalized plane deformation for an anisotropic body. Stress and strain fields for plane strain configurations of anisotropic materials can be used also for three-dimensional problems involving such materials [4]. Ozkan [14] observed the asymptotic stress and displacement fields around crack tip for three-dimensional cracks on both isotropic and homogeneous anisotropic materials. A valuable research on cracks in anisotropic materials using ANSYS and 3DFAS has prepared by Ozkan et al. [5]. In this research, it is proved that quarter point technique can be applied for both three-dimensional isotropic materials and three-dimensional anisotropic materials.

There are also other studies related to the analysis of three-dimensional crack problems. These problems are examined by various researchers in the past [4],[14],[15]. In these studies, it is demonstrated that the enriched finite element method is a useful technique for obtaining stress intensity factors for general three-dimensional crack problems. This method gives accurate results for cracks in isotropic or anisotropic materials. The engineering fracture mechanics parameters are calculated by the help of the known parameters obtained from the finite element solution results, such as displacements of the nodes at the crack front. For this reason, this method can be used for various types of crack singularity fields [4].

Kirilyuk [16] has studied static equilibrium problems for a three-dimensional elastic orthotropic material with an internal circular (penny-shaped) crack. In this research, to solve the problem, Willis' approach is used and the influence of anisotropy on the stress intensity factors is studied. In this paper, this approach is based on the triple Fourier transform, the Fourier-transformed Green's function for an orthotropic medium, and Cauchy's residue theorem.

1.3 Goal of the Study

The goal of this study is to develop a method to conduct three-dimensional fracture analysis of orthotropic materials. Firstly, the three-dimensional orthotropic material structure is modeled by finite element analysis. In this study, ANSYS Parametric Design Language is used to create the geometry of the model. Moreover, this software is used to mesh the geometry, to load the model structurally and thermally; and to calculate the fracture mechanics parameters. By using ANSYS, parametric design language complex geometries with different type of crack geometries and orientation are possible to be worked on. In this study surface crack geometry is modeled in a three-dimensional orthotropic material. Considering the crack front location, quarter point technique is used to simulate the $r^{1/2}$ stress singularities. The material properties can be considered as isotropic, orthotropic or anisotropic material. Hence, the asymptotic crack tip stress and displacement fields become crucial. The fracture mechanics based expressions are different for different type of materials. After creating, meshing, defining the material, and setting the boundary conditions finite element model is solved in the software. Displacements are obtained for the cracked three-dimensional orthotropic materials. After that, displacement correlation technique is used to obtain fracture mechanics parameters, such as stress intensity factors.

In this study, three-dimensional orthotropic materials are analyzed using asymptotic fields for plane strain configurations of anisotropic materials. Three-dimensional finite element analyses are conducted to obtain mode I stress intensity factors. The stress intensity factor is calculated by using the displacement correlation technique. In addition to these, comparisons of the results generated to those available in the literature verify the developed techniques.

This study consists of five chapters. Chapter I contains the following sections: introduction, literature survey and the goal of the study. In Chapter 2, constitutive relations of anisotropic materials are given. In Chapter 3, finite element method,

asymptotic stress and strain fields at the crack tip and displacement correlation technique are studied. In Chapter 4, problem is defined. Moreover, three-dimensional fracture analysis techniques, geometry of the problem and loading types, results and discussion are given in this section. Finally, an outcome of the results and concluding remarks are given in Chapter 5.

CHAPTER 2

CONSTITUTIVE RELATIONS FOR ANISOTROPIC MATERIALS

2.1 Mechanical Behavior of Anisotropic Materials

The stress strain relations for anisotropic materials are more complex than the relation for isotropic materials. There are also more independent material constants compared to the linear elastic and isotropic material. The general stress and strain relationship is given in Cartesian coordinate system as follows:

$$\begin{Bmatrix} \epsilon_1 \\ \epsilon_2 \\ \epsilon_3 \\ \gamma_{23} \\ \gamma_{13} \\ \gamma_{12} \end{Bmatrix} = \begin{bmatrix} S_{11} & S_{12} & S_{13} & S_{14} & S_{15} & S_{16} \\ S_{21} & S_{22} & S_{23} & S_{24} & S_{25} & S_{26} \\ S_{31} & S_{32} & S_{33} & S_{34} & S_{35} & S_{36} \\ S_{41} & S_{42} & S_{43} & S_{44} & S_{45} & S_{46} \\ S_{51} & S_{52} & S_{53} & S_{54} & S_{55} & S_{56} \\ S_{61} & S_{62} & S_{63} & S_{64} & S_{65} & S_{66} \end{bmatrix} \begin{Bmatrix} \sigma_1 \\ \sigma_2 \\ \sigma_3 \\ \tau_{23} \\ \tau_{13} \\ \tau_{12} \end{Bmatrix} \tag{2.1}$$

6x6 [S] matrices are called compliance matrix. The compliance matrix has 36 constants. However, due to the symmetry of the compliance matrix, the numbers of material constants are reduced to 21 [17]. Nonzero engineering constants for monoclinic, orthotropic, transversely isotropic and isotropic materials are tabulated in Table 2.1.

Table 2 . 1 The nonzero engineering constants [17]

	Nonzero engineering constants	
Material	*Independent*	*Dependent*
Monoclinic	E_1, E_2, E_3 G_{23}, G_{13}, G_{12} v_{12}, v_{13}, v_{23} $v_{16}, v_{26}, v_{45}, v_{36}$	
Orthotropic	E_1, E_2, E_3 G_{23}, G_{13}, G_{12} v_{12}, v_{13}, v_{23}	
Transversely isotropic	E_1, E_2 G_{12} v_{12}, v_{23}	$E_3 = E_2, G_{13} = G_{12}$ $G_{23} = \frac{E_1}{2(1+v_{23})}$ $v_{13} = v_{12}$
Isotropic	$E_1 \quad (= E)$ $v_{12} \quad (= v)$	$E_2 = E_3 = E, v_{13} = v_{23} = v$ $G_{23} = G_{13} = G_{12} = \frac{E_1}{2(1+v)}$

Considering the nonzero engineering constants for monoclinic, orthotropic, transversely isotropic, and isotropic materials the compliance matrices can be tabulated in Table 2.2.

Table 2 . 2 Compliance matrices [18]

The compliance matrices in terms of the engineering constants for monoclinic, orthotropic, transversely isotropic, and isotropic materials
$S = \begin{bmatrix} 1/E_1 & -\upsilon_{23}/E_2 & -\upsilon_{31}/E_3 & 0 & 0 & \upsilon_{61}/G_{12} \\ -\upsilon_{32}/E_1 & 1/E_2 & -\upsilon_{32}/E_3 & 0 & 0 & \upsilon_{62}/G_{12} \\ -\upsilon_{13}/E_1 & -\upsilon_{23}/E_2 & 1/E_3 & 0 & 0 & \upsilon_{63}/G_{12} \\ 0 & 0 & 0 & 1/G_{23} & -\upsilon_{54}/G_{23} & 0 \\ 0 & 0 & 0 & -\upsilon_{45}/G_{23} & 1/G_{13} & 0 \\ 0 & 0 & 0 & 0 & 0 & 1/G_{12} \end{bmatrix}$ Monoclinic
$S = \begin{bmatrix} 1/E_1 & -\upsilon_{21}/E_2 & -\upsilon_{31}/E_3 & 0 & 0 & 0 \\ -\upsilon_{12}/E_1 & 1/E_2 & -\upsilon_{32}/E_3 & 0 & 0 & 0 \\ -\upsilon_{13}/E_1 & -\upsilon_{23}/E_2 & 1/E_3 & 0 & 0 & 0 \\ 0 & 0 & 0 & 1/G_{23} & 0 & 0 \\ 0 & 0 & 0 & 0 & 1/G_{13} & 0 \\ 0 & 0 & 0 & 0 & 0 & 1/G_{12} \end{bmatrix}$ Orthotropic
$S = \begin{bmatrix} 1/E_1 & -\frac{\upsilon_{21}}{E_2} & -\frac{\upsilon_{31}}{E_2} & 0 & 0 & 0 \\ -\frac{\upsilon_{12}}{E_1} & \frac{1}{E_2} & -\frac{\upsilon_{32}}{E_2} & 0 & 0 & 0 \\ -\frac{\upsilon_{13}}{E_1} & -\frac{\upsilon_{23}}{E_2} & \frac{1}{E_2} & 0 & 0 & 0 \\ 0 & 0 & 0 & \frac{2(1+\upsilon_{23})}{E_2} & 0 & 0 \\ 0 & 0 & 0 & 0 & \frac{1}{G_{13}} & 0 \\ 0 & 0 & 0 & 0 & 0 & \frac{1}{G_{13}} \end{bmatrix}$ Transversely isotropic
$S = \begin{bmatrix} 1/E & -\upsilon/E & -\upsilon/E & 0 & 0 & 0 \\ -\upsilon/E & 1/E & -\upsilon/E & 0 & 0 & 0 \\ -\upsilon/E & -\upsilon/E & 1/E & 0 & 0 & 0 \\ 0 & 0 & 0 & 2(1+\upsilon)/E & 0 & 0 \\ 0 & 0 & 0 & 0 & 2(1+\upsilon)/E & 0 \\ 0 & 0 & 0 & 0 & 0 & 2(1+\upsilon)/E \end{bmatrix}$ Isotropic

2.1.1 Generally Anisotropic Materials

When the fibers are oriented in a non-symmetrical manner in the matrix medium, the material has 21 independent elastic constants. This material is called generally anisotropic material. An example of a generally anisotropic material is shown in Figure 2.1. The properties of that anisotropic material are found at a particular point and the relationships for stress and strains are derived considering that point. Furthermore, for non-homogeneous anisotropic material the properties can be different from one point to another in the structure. If it is assumed that the material is homogenous, the 21 independent elastic constants should be found analytically or experimentally [17].

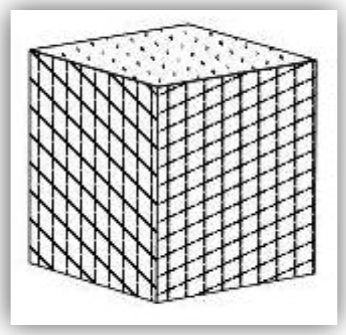

Figure 2 . 1 Example of a generally anisotropic material [19]

Considering fiber reinforced materials, the structure is assumed anisotropic when the fibers are oriented in three non-orthogonal directions [18].

2.1.2 Monoclinic Materials

In monoclinic materials, there is a symmetry plane with respect to the alignment of the fibers. If there is a one plane of symmetry, the independent elastic constants of the compliance matrix are reduced to 13. Material symmetry indicates that the material and its mirror images about the plane of symmetry are identical [17].

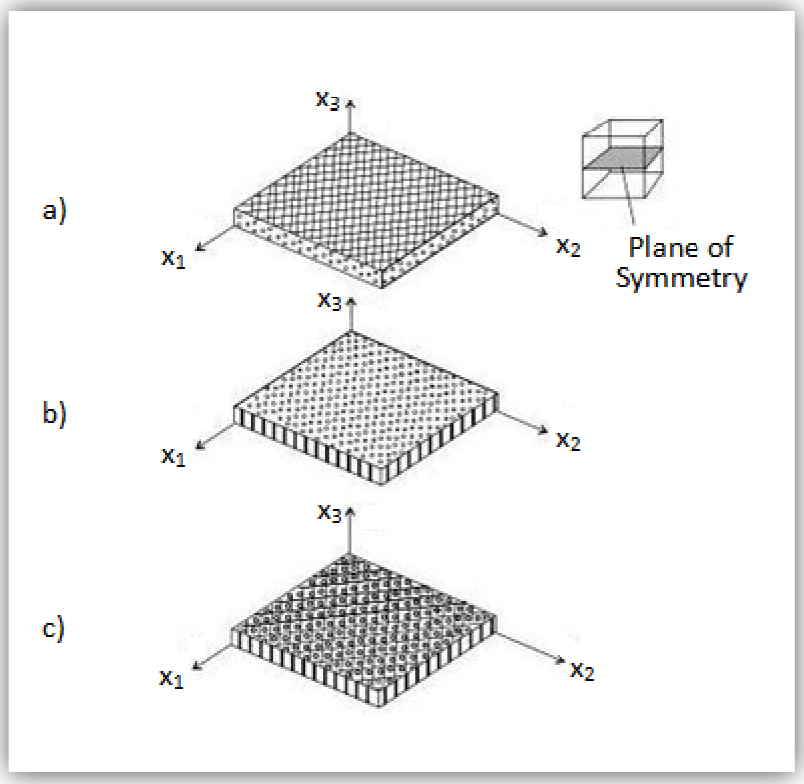

Figure 2 . 2 Illustrations of Fiber-Reinforced Monoclinic Materials [19]

In Figure 2.2(a), fibers are oriented parallel to the x_1-x_2 plane, which is the plane of symmetry. In Figure 2.2(b), fibers are oriented parallel to the plane of symmetry and in Figure 2.2(c) the fibers are in the plane of symmetry and perpendicular to the plane of symmetry [18].

The compliance matrix for monoclinic materials is obtained by reducing the compliance matrix of generally anisotropic materials. Because of the symmetry plane the out of plane shear strains does not exist, therefore the S_{41} , S_{42} , S_{52} , S_{43} , S_{53} , S_{64} , S_{65} elements of the compliance matrix is zero. Similarly, due to the symmetry of the compliance matrix, the S_{41} , S_{42} , S_{52} , S_{43} , S_{53} , S_{64} , S_{65} elements are also equal to zero. Then, the compliance matrix can be rewritten as follows:

$$S = \begin{bmatrix} S_{11} & S_{12} & S_{13} & 0 & 0 & S_{16} \\ S_{12} & S_{22} & S_{23} & 0 & 0 & S_{26} \\ S_{13} & S_{23} & S_{33} & 0 & 0 & S_{36} \\ 0 & 0 & 0 & S_{44} & S_{45} & 0 \\ 0 & 0 & 0 & S_{45} & S_{55} & 0 \\ S_{16} & S_{26} & S_{36} & 0 & 0 & S_{66} \end{bmatrix} \quad (2.2)$$

2.1.3 Orthotropic Materials

Orthotropic materials have three mutually perpendicular planes of symmetry with respect to the orientation of the material. For orthotropic materials, the compliance matrix has nine independent elastic constant as seen following compliance matrix:

$$S = \begin{bmatrix} S_{11} & S_{12} & S_{13} & 0 & 0 & 0 \\ S_{12} & S_{22} & S_{23} & 0 & 0 & 0 \\ S_{13} & S_{23} & S_{33} & 0 & 0 & 0 \\ 0 & 0 & 0 & S_{44} & 0 & 0 \\ 0 & 0 & 0 & 0 & S_{55} & 0 \\ 0 & 0 & 0 & 0 & 0 & S_{66} \end{bmatrix} \quad (2.3)$$

Fibers oriented in a rectangular array in a single lamina constitute an example of an orthotropic material.

2.1.4 Transversely Isotropic Materials

A transversely isotropic material has a plane of material isotropy in one of the planes of an orthotropic material. This situation can occur when the unidirectional fibers are oriented in the x_1 direction. Because of the material isotropy, the compliance matrix for transversely isotropic materials has five independent elastic constants. Furthermore, the following simplifications can be valid because of the isotropy.

$$E_2 = E_3 \quad (2.4)$$
$$G_{13} = G_{12} \quad (2.5)$$
$$v_{13} = v_{12} \quad (2.6)$$

Since, for the isotropic material, the shear modulus is expressed as:

$$G = \frac{E}{2(1+v)} \tag{2.7}$$

Therefore, the shear modulus for a material that shows isotropic in the plane x_2 and x_3, is written as follows:

$$G_{23} = \frac{E_2}{2(1+v_{23})} \tag{2.8}$$

By applying the simplification to the compliance matrix for transversely isotropic material, the compliance matrix takes the following form:

$$S = \begin{bmatrix} S_{11} & S_{12} & S_{12} & 0 & 0 & 0 \\ S_{12} & S_{22} & S_{23} & 0 & 0 & 0 \\ S_{12} & S_{23} & S_{22} & 0 & 0 & 0 \\ 0 & 0 & 0 & 2(S_{22}-S_{23}) & 0 & 0 \\ 0 & 0 & 0 & 0 & S_{66} & 0 \\ 0 & 0 & 0 & 0 & 0 & S_{66} \end{bmatrix} \tag{2.9}$$

2.1.5 Isotropic Materials

For isotropic materials, every plane is a plane of symmetry. Material symmetry planes are shown in Figure 2.3.

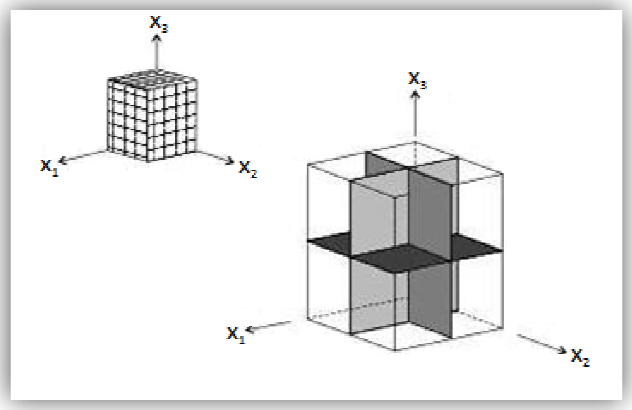

Figure 2 . 3 Material with three planes of symmetry [19]

Due to the symmetry planes, engineering constants can be simplified as follows:

$$E_1 = E_2 = E_3 = E \tag{2.10}$$
$$G_{23} = G_{13} = G_{12} = G \tag{2.11}$$
$$v_{23} = v_{13} = v_{12} = v \tag{2.12}$$
$$G = \frac{E}{2(1+v)} \tag{2.13}$$

The compliance matrix for isotropic materials has 3 independent elastic constants and can be written as follows:

$$S = \begin{bmatrix} S_{11} & S_{12} & S_{12} & 0 & 0 & 0 \\ S_{12} & S_{11} & S_{12} & 0 & 0 & 0 \\ S_{12} & S_{12} & S_{11} & 0 & 0 & 0 \\ 0 & 0 & 0 & 2(S_{11}-S_{12}) & 0 & 0 \\ 0 & 0 & 0 & 0 & 2(S_{11}-S_{12}) & 0 \\ 0 & 0 & 0 & 0 & 0 & 2(S_{11}-S_{12}) \end{bmatrix} \tag{2.14}$$

2.2 Plane Strain Condition

In engineering problems, there are situations considering the change in the stress and strains. For plane strain condition, along direction x_3-axis or z-axis the stresses and strains do not change. However, the stresses and strains can still vary in planes perpendicular to the x_3-axis or z-axis. This circumstance is called the plane strain condition. For instance, the plane strain condition for isotropic structures creates planes perpendicular to the x_3-axis or z-axis. This situation may occur also considerably far from the boundary of a large homogenous body exposed to uniform load along the longitudinal axis.

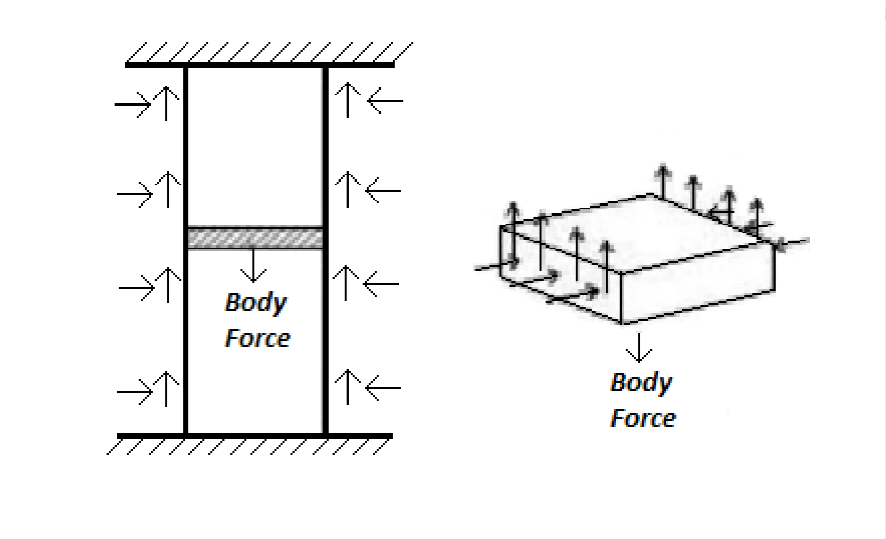

Figure 2 . 4 Surface and body forces that may be applied under plane-strain condition. The applied forces must be uniform along the longitudinal axis and must be in equilibrium for each segment [19]

From the definition of the plane strain condition, the strains do not change along the longitudinal axis. Therefore, following expressions are valid for the plane stain condition.

$$\epsilon_{xx}=\epsilon_{xx}\ (x,y) \quad (2.15)$$
$$\epsilon_{xy}=\epsilon_{xy}\ (x,y) \quad (2.16)$$
$$\epsilon_{yy}=\epsilon_{yy}\ (x,y) \quad (2.17)$$
$$\epsilon_{z}=\gamma_{YZ}=\gamma_{XZ}=0 \quad (2.18)$$

2.3 Plane Stress Condition

Under plane stress condition, normal stresses in z-direction and out of plane shear stresses in the x-y plane are zero. Plane stress condition can be used for thin plates. An example of this situation occurs in fiber-reinforced materials. If the fibers are parallel to the x-y plane and the plate is loaded along the edges, plane stress condition can be applied. This results from the fact that the forces are parallel to the

plane of plate and distributed uniformly over the thickness [19]. Figure 2.5 shows the stresses under plane stress conditions and the zero stress values are as follows:

$$\sigma_z = 0 \quad (2.19)$$

$$\tau_{yz} = 0 \quad (2.20)$$

$$\tau_{xz} = 0 \quad (2.21)$$

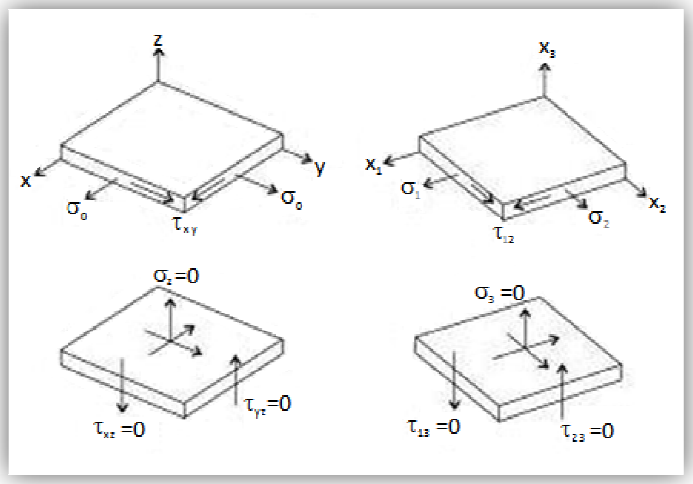

Figure 2 . 5 The stresses under plane-stress condition [19]

2.4 Bases Change Formulas

Material properties are usually used in a basis with coordinate axes aligned with the material symmetry planes. While dealing with the anisotropic materials it is frequently required to transform compliance matrices to a coordinate system that is oriented to the boundaries of the structure. In this study, the compliance matrices are recalculated considering the crack front location in the three dimensional orthotropic body by using these bases change formulas. Following formulation can be used to change the basis of the material properties [20].

Supposing that compliance tensors are given in a basis, $\{e_1, e_2, e_3\}$, and the transformation is applied to the second basis, $\{m_1, m_2, m_3\}$. The transformation tensor Ω in matrix form can be written as follows:

$$[\Omega] = \begin{bmatrix} m_1 e_1 & m_1 e_2 & m_1 e_3 \\ m_2 e_1 & m_2 e_2 & m_2 e_3 \\ m_3 e_1 & m_3 e_2 & m_3 e_3 \end{bmatrix} \tag{2.22}$$

The basis change expressions for the elasticity tensor in matrix form can be written in the following form:

$$C^{(m)} = K C^{(e)} K^T \tag{2.23}$$

Where the basis change matrix can be defined as

$$K = \begin{bmatrix} K^{(1)} & 2K^{(2)} \\ K^{(3)} & K^{(4)} \end{bmatrix} \tag{2.24}$$

$$K_{ij}^{(1)} = \Omega_{ij}^2 \tag{2.25}$$

$$K_{ij}^{(2)} = \Omega_{imod(j+1,3)}\, \Omega_{imod(j+2,3)} \tag{2.26}$$

$$K_{ij}^{(3)} = \Omega_{mod(i+1,3)j}\, \Omega_{mod(i+2,3)j} \tag{2.27}$$

$$K_{ij}^{(4)} = \Omega_{mod(i+1,3)mod(j+1,3)}\, \Omega_{mod(i+2,3)mod(j+2,3)} + \Omega_{mod(i+1,3)mod(j+2,3)}\, \Omega_{mod(i+2,3)mod(j+1,3)} \tag{2.28}$$

The expressions are for $i, j = 1..3$ and the modulo function yields

$$mod(i,3) = \begin{cases} i & , i \leq 3 \\ i-3 & , i > 3 \end{cases} \tag{2.29}$$

For compliance tensor, the basis change expression is as follows:

$$S^{(m)} = K^{-1} S^{(e)} K^{-1} \tag{2.30}$$

where,

$$K^{-T} = \begin{bmatrix} K^{(1)} & K^{(2)} \\ 2K^{(3)} & K^{(4)} \end{bmatrix} \tag{2.31}$$

For a special case of rotation through an angle θ, in a counterclockwise sense about the e_1, e_2, e_3 axes, respectively, the rotation matrix can be defined as the following form:

$$\begin{bmatrix} 1 & 0 & 0 & 0 & 0 & 0 \\ 0 & c^2 & s^2 & 2cs & 0 & 0 \\ 0 & s^2 & c^2 & -2cs & 0 & 0 \\ 0 & -cs & cs & c^2 - s^2 & 0 & 0 \\ 0 & 0 & 0 & 0 & c & -s \\ 0 & 0 & 0 & 0 & s & c \end{bmatrix}.$$

$$\begin{bmatrix} 1 & 0 & 0 & 0 & 0 & 0 \\ 0 & c^2 & s^2 & 2cs & 0 & 0 \\ 0 & s^2 & c^2 & -2cs & 0 & 0 \\ 0 & -cs & cs & c^2 - s^2 & 0 & 0 \\ 0 & 0 & 0 & 0 & c & -s \\ 0 & 0 & 0 & 0 & s & c \end{bmatrix}.$$

$$\begin{bmatrix} 1 & 0 & 0 & 0 & 0 & 0 \\ 0 & c^2 & s^2 & 2cs & 0 & 0 \\ 0 & s^2 & c^2 & -2cs & 0 & 0 \\ 0 & -cs & cs & c^2 - s^2 & 0 & 0 \\ 0 & 0 & 0 & 0 & c & -s \\ 0 & 0 & 0 & 0 & s & c \end{bmatrix} \quad (2.32)$$

where $c = \cos\theta$ and $s = \sin\theta$.

In this study, the compliance matrices are recalculated taking into account the crack front location in the orthotropic body by using these bases change formulas.

CHAPTER 3

FINITE ELEMENT METHOD, THE ASYMPTOTIC FIELD EXPRESSIONS AND THE DISPLACEMENT CORRELATION TECHNIQUE

3.1 The Finite Element Method

The finite element model is generated step by step ANSYS analysis procedure. The three-dimensional model is created with the help of the ANSYS Parametric Design Language (APDL). The Mechanical APDL application is very useful, especially when working with linked analysis (e.g., thermal-mechanical analysis, substructuring of submodeling, etc.)

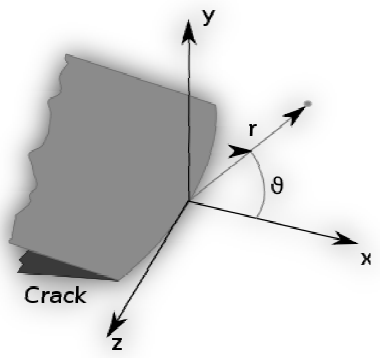

Figure 3 . 1 Polar coordinates at the crack front region [21]

Fracture mechanics provides a tool to evaluate the criticality of the cracks in structures. The main attainment in the theoretical foundation of linear elastic

fracture mechanics was the introduction of the stress intensity factor (K) as a parameter for the intensity of stresses close to the crack tip and this parameter is related to the energy release rate [22].

The wide range of structural configurations, loading conditions and crack geometries with the material property changes make the analytical prediction of the stress intensity factors (SIFs) complicated.

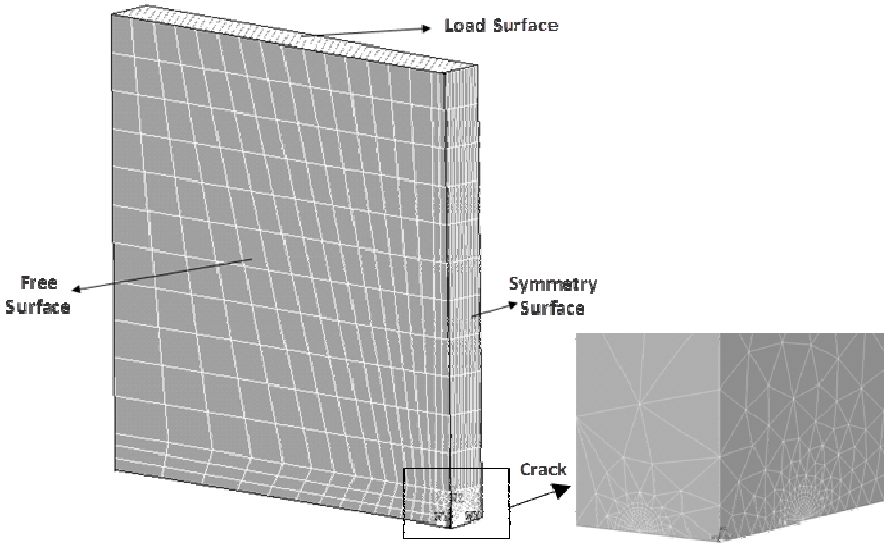

Figure 3 . 2 Finite element model of the three-dimensional structure

In this study, analysis of the three-dimensional fracture problems is carried out to obtain linear elastic fracture mechanics parameter, namely mode-I stress intensity factors. Stress intensity factors (SIFs) can be calculated in the ANSYS APDL software and other computer programs. To evaluate the stress intensity factors, there are a number of methods available for cracked bodies.

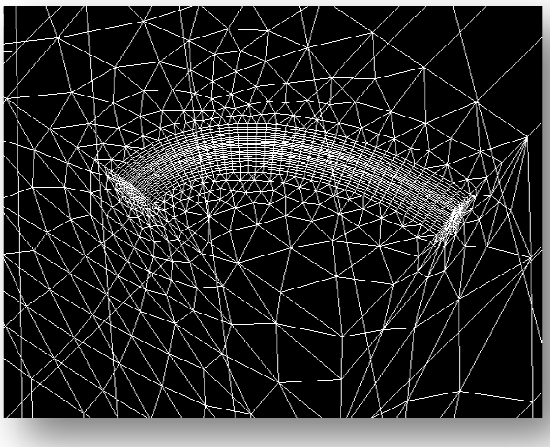

Figure 3 . 3 Elements at the crack front region (Surface crack geometry, quarter model)

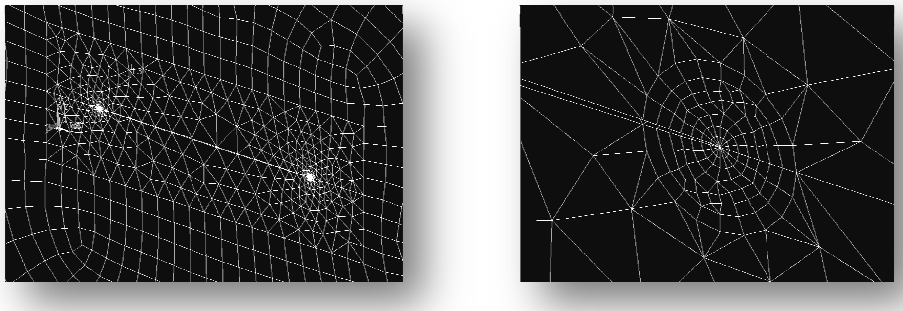

Figure 3 . 4 Elements at the crack front region (Internal penny-shaped geometry, half model)

There are two ways of creating the model in the finite element programs. First of them is to have the two-dimensional and three-dimensional solid model of the geometry. It is possible to mesh this solid model and to generate nodes and elements for this geometry. The other method is to create the model directly from the nodes. In this method after generating the nodes, the elements are created from these nodes and the body is created by merging these elements together. In this study, second method is preferred to generate the model of the geometry. The generated

finite element model of the three dimensional structure is shown in Figure 3.2. The generated meshes are given in Figure 3.3 and in Figure 3.4.

Second step is to mesh the model to obtain the elements in order to compute the displacements. Meshing is the important step in the analysis; the crack front region, which is the most critical region in the analysis, is defined in the meshing procedure. Since small deformations are taken into account in the calculations, fine mesh should be used in the crack front region to obtain reliable results. There are three steps to mesh the model. Firstly, element attributes are defined. Secondly, mesh controls are specified and lastly mesh is generated.

Element attributes are characteristics of the finite element model that have to be established prior to meshing. These element attributes include:

-Element types

-Real constants

-Material properties

-Section properties

The element type is important selection that determines the degree of freedom set and element shape. ANSYS has a library of over 170 element types. In this study, as an element type MESH200, SOLID87 and SOLID92 are used.

MESH200 is a “mesh-only” element, and it does not include in the solution. It is used for temporary storage elements when the analysis physics has not been defined. It is also used for multistep meshing operations. In extrusion process, the lower

dimensionality mesh is needed for the creation of a higher dimensionality mesh; MESH200 is required for these type operations.

SOLID87 is a three-dimensional 10-node tetrahedral thermal solid element type and this element type is preferred to model irregular meshes. This type of element has one degree of freedom. At each node of the element, temperatures can be defined. The element is suitable for three-dimensional steady state or transient thermal analysis. In this study, the model is analyzed both thermally and structurally; therefore, the element type is changed from SOLID87 to SOLID92, which is the equivalent structural element. They are shown in Figure 3.5.

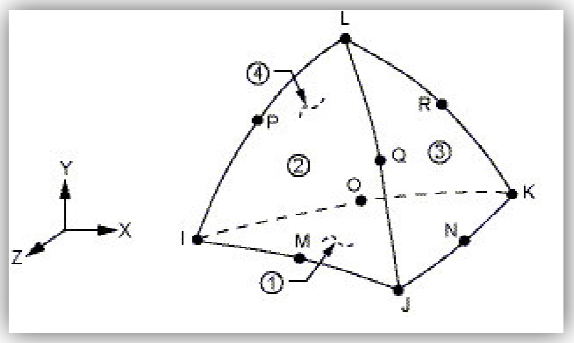

Figure 3 . 5 SOLID87 and SOLID92 Geometry [23]

SOLID92 is three-dimensional 10 node tetrahedral structural solid element type and is well suited with irregular meshes. Different from the SOLID87 type, it has three degrees of freedom at each nod. Translations of nodes in x, y and z directions can be defined at each node. The element type shows quadratic displacement behavior and has plasticity, creep, swelling and stiffening capabilities.

3.2 The Asymptotic Fields at the Crack Tip

In this section, asymptotic fields for the orthotropic materials are studied. The solid body is considered as a plane, therefore, the formulation depends only on the x and y coordinates. These asymptotic field expressions can be used for orthotropic materials [1].

Considering the Hook's Law, the equilibrium equations can be written by taking the body forces equal to zero. Linear operators L_2, L_3 and L_4 can be expressed in terms of material constants. Two coupled partial differential equations give the solution such that:

$$\left(L_2 L_4 - {L_2}^2\right)F = 0 \tag{3.1}$$

Closely associated with these operators are four polynomials:

$$l_2(x) = S_{22}x^2 - 2S_{45}x + S_{44} \tag{3.2}$$
$$l_3(x) = S_{15}x^3 - (S_{14} + S_{56})x^2 + (S_{25} + S_{46})x - S_{24} \tag{3.3}$$
$$l_4(x) = S_{11}x^4 - 2S_{16}x^3 + (2S_{12} + S_{66})x^2 - 2S_{26}x + S_{22} \tag{3.4}$$
$$l_6(x) = l_4(x)l_2(x) - [l_3(x)]^2 \tag{3.5}$$

The characteristic roots of the $l_6(x)$ function govern the structure of the stress functions. The roots are expressed with μ and they are always complex numbers, which will occur in pairs of complex conjugates [24]. There are six roots (μ), three distinct roots are chosen; such that imaginary parts of the roots are greater than zero. ($\mathrm{Im}(\mu) > 0$)

By defining $\lambda_i = -l_3(\mu_i)/l_2(\mu_i)$, the displacement and stress equations along the crack tip can be obtained as explained in [1]. The coordinate system at the crack front region is given in Figure 3.6.

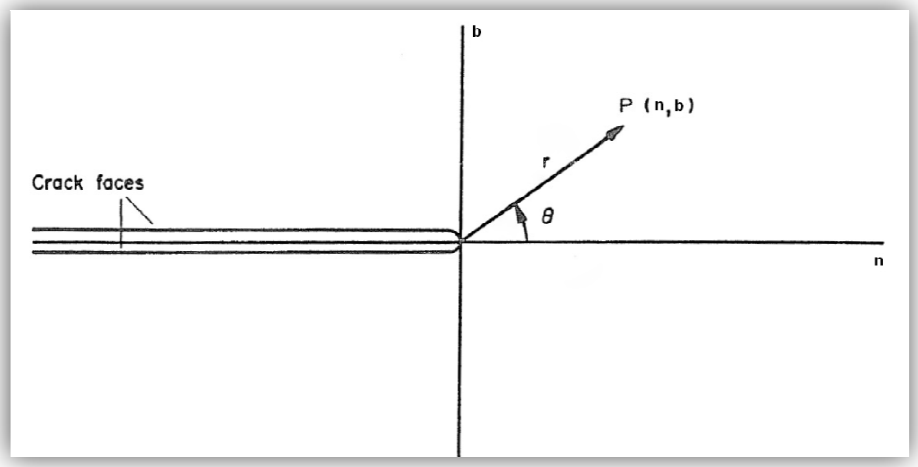

Figure 3 . 6 The semi-infinite crack and associated coordinate system [1]

The stress and strain displacements can now be written in terms of the stress intensity factor, p_{ij} and N_{ij}, since the mode-I stress intensity factor is studied and the direction is taken in the direction of b axis, which is the direction of the tensile mode where the crack surfaces move directly apart.

In this study, only the mode I stress intensity factor (K_I) will be examined, therefore, mode II and mode III stress intensity factors will be assumed as zero. $(K_{II} = 0 \text{ and } K_{III} = 0)$. There are also some special cases where these results are inapplicable. For these cases, the formulations and the solution method will be explained.

3.2.1 Anisotropic Degeneracy Cases

There are several ways, which make the above formulations inapplicable. One of them occurs when any two roots of the characteristic equation (μ_j) are equal to each other. Therefore, the inverse of the N_{ij} matrix does not exist. The other situation occurs when the $l_{2,3,4,6}(x)$ functions are identically zero. These types of

situations, where the results for anisotropic case vanish, are called anisotropic degeneracy situations [1].

3.2.1.1 Anti-Plane Shear and Plane Strain Decoupling Case

Degeneracy occurs if the anti-plane shear and plane strain displacements decouple. This situation exists where the following compliance matrix expressions are equal to zero [1]:

$$S_{14} = S_{24} = S_{15} = S_{25} = S_{46} = S_{56} = 0 \tag{3.6}$$

In anti-plane shear and plane strain displacements decouple situation, matrix form of the compliance matrix is as follows:

$$S = \begin{bmatrix} S_{11} & S_{12} & S_{13} & 0 & 0 & S_{16} \\ S_{21} & S_{22} & S_{23} & 0 & 0 & S_{26} \\ S_{31} & S_{32} & S_{33} & S_{34} & S_{35} & S_{36} \\ 0 & 0 & S_{43} & S_{44} & S_{45} & 0 \\ 0 & 0 & S_{53} & S_{54} & S_{55} & 0 \\ S_{61} & S_{62} & S_{63} & 0 & 0 & S_{66} \end{bmatrix} \tag{3.7}$$

In this situation $l_3(x)$, and consequently, L_3 are equal to zero. Therefore the characteristic roots μ_1 and μ_2 are taken from the equation $l_4(x) = 0$ such that $\mathrm{Im}(\mu_{1,2}) > 0$.

The p_{ij} matrix, which depends on the material properties and the characteristic root, is defined as follows:

$$p_{1\alpha} = S_{11}\mu_\alpha^2 + S_{12} - S_{16}\mu_\alpha \tag{3.8}$$
$$p_{2\alpha} = S_{12}\mu_\alpha + S_{22}/\mu_\alpha - S_{26} \tag{3.9}$$
$$p_{33} = S_{45} - S_{44}/\mu_\alpha \tag{3.10}$$
$$p_{31} = p_{32} = p_{13} = p_{23} = 0 \tag{3.11}$$

Matrix form of p_{ij} and N_{ij} ,which consists of the characteristics roots, are in the following manner:

$$p = \begin{bmatrix} p_{11} & p_{12} & 0 \\ p_{21} & p_{22} & 0 \\ 0 & 0 & p_{33} \end{bmatrix} \tag{3.12}$$

$$N = \begin{bmatrix} 1 & 1 & 0 \\ -\mu_1 & -\mu_2 & 0 \\ 0 & 0 & -1 \end{bmatrix} \tag{3.13}$$

Open forms of the displacement equation for mode I type of loading is given as:

$$u_2 = \sqrt{\left(\frac{2r}{\pi}\right)}\,\mathrm{Re}\left\{p_{21}\left(N_{11}{}^{-1}K_I + N_{12}{}^{-1}K_I\right)\sqrt{\left(\cos\theta + \mu_1 \sin\theta\right)}\right\} \tag{3.14}$$

Because of anti-plane shear and plane strain displacement decoupling the above formulation should be used in calculation of the stress intensity factors. The anisotropic expressions are no longer valid [1].

3.2.1.2 The x-y Plane Isotropy Case

The other case for anisotropic degeneracy situation occurs when the body is isotropic in the x and y planes. There are actually additional situations occurred, such as the anti-plane shear and the plane strain displacement case. The two of roots of the characteristic equation are equal to each other $(\mu_1 = \mu_2 = 0)$, therefore, the inverse of the N_{ij} does not exist. Considering the x-y plane isotropy, the elastic constants should be defined. There are five independent elastic constants, namely elastic modulus, Poisson ratios, and shear modulus. (E, E_2, v, v_2 and G_2) The relationship between the elastic constants and the compliance matrix is as follows [1]:

$$S_{14} = S_{24} = S_{15} = S_{25} = S_{16} = S_{26} = S_{46} = S_{56} = S_{45} = 0 \tag{3.15}$$

$$S_{11} = S_{22} = \frac{1}{E} \tag{3.16}$$

$$S_{12} = \frac{-v}{E} \tag{3.17}$$

$$S_{66} = \frac{2(1+v)}{E} \tag{3.18}$$

$$S_{44} = S_{55} = \frac{1}{G_2} \tag{3.19}$$

$$S_{33} = \frac{1}{G_2} \tag{3.20}$$

$$S_{13} = S_{23} = \frac{-\nu_2}{E_2} \tag{3.21}$$

Considering above relation, compliance matrix for a transversely isotropic body can be written as follows:

$$S = \begin{bmatrix} \frac{1}{E} & \frac{-\nu}{E} & \frac{-\nu_2}{E_2} & 0 & 0 & 0 \\ \frac{-\nu}{E} & \frac{1}{E} & \frac{-\nu_2}{E_2} & 0 & 0 & 0 \\ \frac{-\nu_2}{E_2} & \frac{-\nu_2}{E_2} & \frac{1}{E_2} & 0 & 0 & 0 \\ 0 & 0 & 0 & \frac{1}{G_2} & 0 & 0 \\ 0 & 0 & 0 & 0 & \frac{1}{G_2} & 0 \\ 0 & 0 & 0 & 0 & 0 & \frac{2(1+\nu)}{E} \end{bmatrix} \tag{3.22}$$

The asymptotic expressions for displacements and stress components are same for the isotropic case, and they are given in the [25] for mode I stress intensity factor as follows:

$$\begin{bmatrix} u_1 \\ u_2 \end{bmatrix} = \frac{K_I}{2G}\sqrt{\frac{r}{2\pi}}\begin{bmatrix} \cos(\theta/2)(\kappa - 1 + 2\sin^2(\theta/2)) \\ \sin(\theta/2)(\kappa + 1 - 2\cos^2(\theta/2)) \end{bmatrix} \tag{3.23}$$

In the above displacement expression, κ value is $\kappa = (3 - 4\nu)$ for plane strain and $\kappa = (3 - \nu)/(1 + \nu)$ for plane stress. In addition, shear modulus can be expressed in terms of modulus of elasticity. Then, the displacement formulation can be rewritten for plane strain condition [1].

$$\begin{bmatrix} u_1 \\ u_2 \end{bmatrix} = \frac{(1+\nu)}{E}\sqrt{\frac{2r}{\pi}}K_I\begin{bmatrix} \cos(\theta/2)(1 - 2\nu) + \sin^2(\theta/2)) \\ \sin(\theta/2)(2(1 - \nu) - \cos^2(\theta/2)) \end{bmatrix} \tag{3.24}$$

3.3 The Displacement Correlation Technique (DCT)

In the finite element analysis, displacements of the nodes are computed in both mechanical and thermal loading cases. The coordinates of the nodes of the deformed geometry and undeformed geometry are used as inputs for the displacement correlation technique (DCT). The displacement correlation technique can be used to compute mode I, mode II and mode III, stress intensity factors.

A three-dimensional crack front, which is embedded in the composite medium, is given in Figure 3.7. Arc length of the crack front is given as *s,* and the local coordinate axes are located at point *P,* the components of the local coordinate axes are given in the figure with parameters tangential *(t)*, normal *(n)* and binormal *(b)* directions. In addition to these, parameters *(r) and (Θ)* are the polar coordinates in the normal plane.

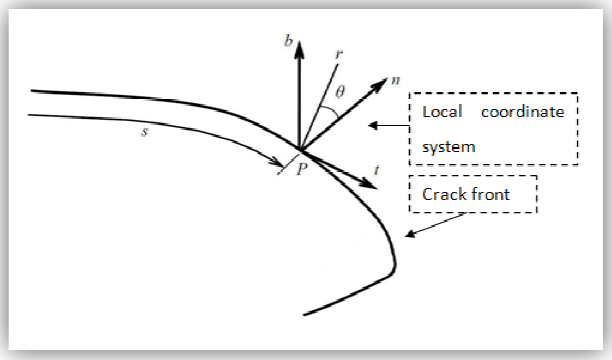

Figure 3 . 7 Local coordinate system at the crack front region [26]

The displacement component $u_b(r,\theta)$ is evaluated at point P on the deformed shape of the crack surface. For mode I type SIF calculations, the displacement component is required. $C(\theta)$ is function of (θ) and also contains material properties. The displacement parameters can be expressed as follows:

$$u_b(r,\theta) = C(\theta)\, K_I(s) \sqrt{\frac{2r}{\pi}} \tag{3.25}$$

For isotropic material, the $C(\theta)$ value can be replaced with the following expression:

$$C(\theta) = \frac{1 + v_{tip}}{E^{tip}} sin\left(\frac{\theta}{2}\right)\left[2(1 - v_{tip}) - cos^2\left(\frac{\theta}{2}\right)\right] \tag{3.26}$$

For orthotropic materials, $C(\theta)$ value should be calculated as follows:

$$C(\theta) = Re\left\{p_{21}(N_{11}{}^{-1})\sqrt{(\cos\theta + \mu_1 \sin\theta)} + p_{22}(N_{21}{}^{-1})\sqrt{(\cos\theta + \mu_2 \sin\theta)}\right\} \tag{3.27}$$

The material properties are taken from where the point P is located. Considering the crack front, a section is taken parallel to the normal plane, which consists of normal and binormal axes. In Figure 3.8, three nodes constitute the edge of a collapsed 20-node quarter point brick element. These points that are taken along the deformed crack surface placed with a space ratio, $R_2 = R_3/4$. At the point, where, $\theta = \pi$, Equation 3.25 can be expressed as

$$u_b(r, \pi) = C(\pi)\sqrt{\frac{2r}{\pi}} K_I \tag{3.28}$$

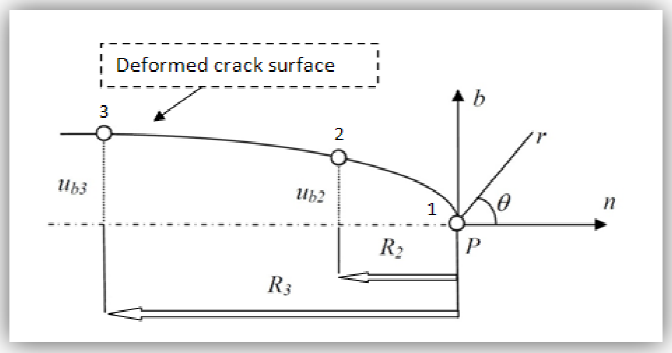

Figure 3 . 8 Deformed shape of the crack surface (symmetric)[26]

The mode I stress intensity factor can be calculated by using the above equation and can be expressed as

$$K_I = \frac{\sqrt{\pi/2}}{C(\pi)}\left[\lim_{r\to 0}\left\{\frac{u_b(r,\pi)}{\sqrt{r}}\right\}\right] \tag{3.29}$$

In the Equation 3.29, suppose that limit term is linear, therefore, it can be written as follows:

$$\frac{u_b(r,\pi)}{\sqrt{r}} = A + Br \tag{3.30}$$

There are two conditions: $u_b = u_{b2}$ at $r = R_2$ and $u_b = u_{b3}$ at $r = R_3$. After applying these conditions to the Equation 3.30, one can obtain below equations.

$$A + BR_2 = \frac{u_{b2}}{\sqrt{R_2}} \tag{3.31}$$

$$A + BR_3 = \frac{u_{b3}}{\sqrt{R_3}} \tag{3.32}$$

By using above equations the constant A can be expressed as

$$A = \frac{R_3^{3/2}u_{b2} - R_2^{3/2}u_{b3}}{\sqrt{R_2}\sqrt{R_3}(R_3 - R_2)} \tag{3.33}$$

Finally, the mode I stress intensity factor can be computed at the crack tip, where r goes to zero. $(r \to 0)$

$$K_I = \frac{\sqrt{\pi/2}}{C(\pi)}\left[\frac{R_3^{3/2}u_{b2} - R_2^{3/2}u_{b3}}{\sqrt{R_2}\sqrt{R_3}(R_3 - R_2)}\right] \tag{3.34}$$

The above equation can be used if the crack region is symmetric. The mode I stress intensity factor can now be computed by using Equation 3.34, after obtaining the displacements of the crack front nodes.

For unsymmetrical cases, such as the fully anisotropic materials and unsymmetrical loading cases, full model is used for mode I stress intensity factor calculations. Figure 3.9 shows a complete crack model to apply the displacement correlation technique.

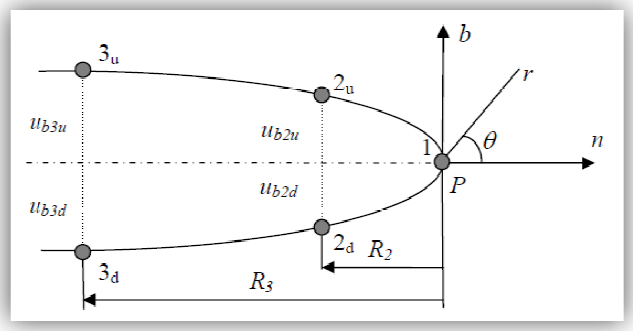

Figure 3 . 9 Deformed shape of the crack surface (non symmetric)[27]

For unsymmetrical case, substituting $\theta = -\pi$ into Equation 3.25 yields

$$u_b(r,-\pi) = C(-\pi)\sqrt{\frac{2r}{\pi}}K_I \tag{3.35}$$

Subtracting Equation 3.28 from Equation 3.35 the below expression is obtained.

$$u_b(r,\pi) - u_b(r,-\pi) = [C(\pi) - C(-\pi)]\sqrt{\frac{2r}{\pi}}K_I \tag{3.36}$$

Since $C(\pi)$expression is equal to $-C(-\pi)$, following expression is obtained

$$K_I = \frac{\sqrt{\pi/2}}{2C(\pi)}\left[\lim_{r\to 0}\left\{\frac{u_b(r,\pi) - u_b(r,-\pi)}{\sqrt{r}}\right\}\right] \tag{3.37}$$

Similarly, the mode I stress intensity factor can be computed at the crack tip, where r goes to zero $(r \to 0)$ as follows.

$$K_I = \frac{\sqrt{\pi/2}}{2C(\pi)}\left[\frac{R_3^{3/2}(u_{b2u} - u_{b2d}) - R_2^{3/2}(u_{b3u} - u_{b3d})}{\sqrt{R_2}\sqrt{R_3}(R_3 - R_2)}\right] \quad (3.38)$$

The mode I stress intensity factor can be evaluated for non-symmetrical cases by using Equation 3.38, after obtaining the displacements of the crack front nodes.

CHAPTER 4

RESULTS AND DISCUSSION

4.1 Introduction

In this chapter, sample results generated are presented and compared to the corresponding results in the literature.

First, the code for three-dimensional model is verified comparing with the results of Walters et al. [24]. After this verification, present study percent differences are determined comparing with Newman and Raju equations [28]. Thus, the accuracy of the numerical solution technique is checked out. After obtaining results and checking the accuracy of finite element solution method, the code is used to obtain normalized mode-I stress intensity factors for three-dimensional structures. Anisotropic asymptotic stress and strain fields are embedded to the code for three dimensional model. The three-dimensional edge crack problem is solved for various orthotropic material properties. These results are obtained for orthotropic materials under mechanical loading conditions such as uniform tension and fixed grip tension. Another analysis is done for polystal material under thermal loading condition. Three dimensional transient thermal analysis results are also presented in this section.

4.2 Comparisons to Results of Walters et al.

In this section, the results of uniform tension on three-dimensional isotropic structure analysis are compared to the results given by Walters et al. [24]. These

comparisons are made to verify the three-dimensional surface semi-elliptical edge crack model. Therefore, the crack geometry parameters such as, crack depth, thickness of the plate, exponentially varying Young's modulus and Poisson's ratios are taken same with the reference values. The selected ranges of specimen and crack geometries are exposed to mechanical loading. In this type of loading, the body is exposed to uniform stress σ_t at the edge of the end of longitudinal axis of the structure, i.e. stress is applied at the ends $y = \pm l$. In Figure 4.1 - 4.2 the geometry of the model is given. Presented results show normalized mode-I stress intensity factors for $a/c = 2$ semi elliptical crack geometry with variable crack depth to thickness ($a/h = 0.2, 0.4, 0.6\ and\ 0.8$). As a material property, the Poisson's ratio is taken as 0.25. Furthermore, exponentially varying Young's moduli are used such as, $E(h)/E_1 = 0.2, 1.0\ and\ 5.0$. Elastic modulus variation in the structure is given as

$$E(x) = E_1 \exp(\beta x) \tag{3.39}$$

As a result of these analyses, percent differences are found and the accuracy of finite element solution procedures is verified.

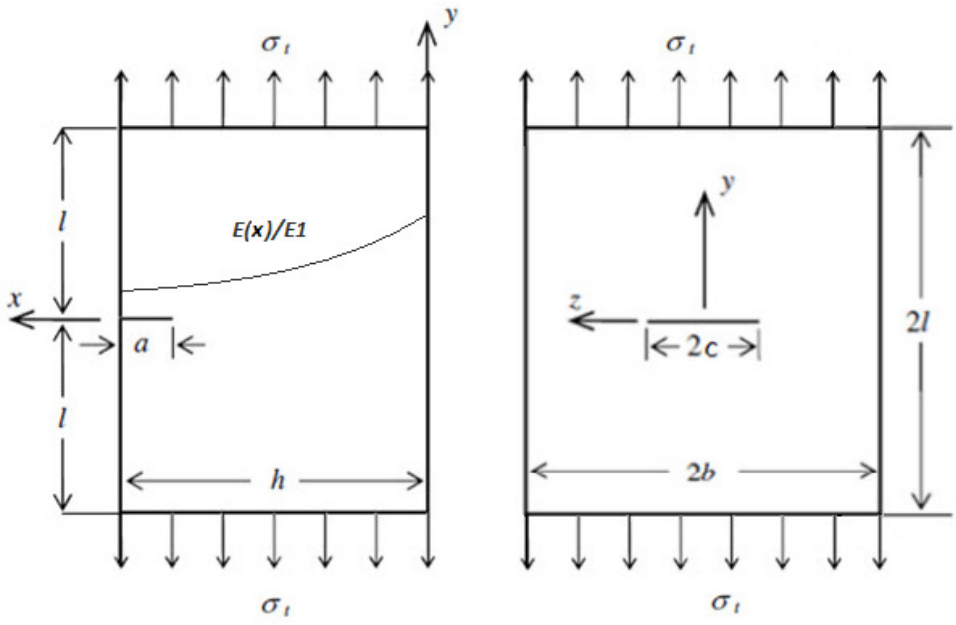

Figure 4 . 1 Material subjected to uniform tension at the ends

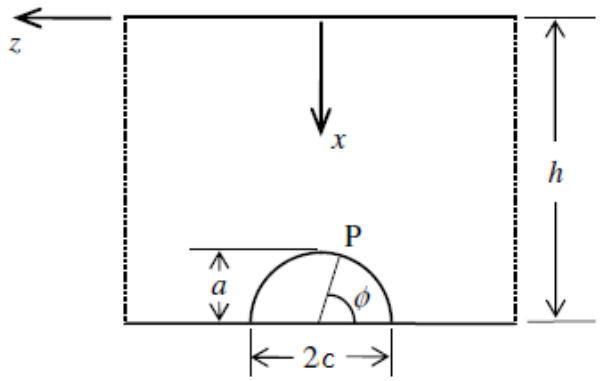

Figure 4 . 2 Top view of the material

Results of the present study, the results of reference [24] and the percent differences are given in Table 4.1 - 4.10.

Table 4 . 1 Comparison of the normalized mode I stress intensity factors for uniform tension

$2\phi/\pi$	*a/h=0.2, a/c=2, E(h)/E₁=0.2*		
	Walters et al. (2004)	*Present study*	*% Diff.*
0.000	0.612	0.642	4.947
0.125	0.623	0.629	0.982
0.250	0.608	0.615	1.211
0.375	0.595	0.602	1.214
0.500	0.574	0.582	1.456
0.625	0.547	0.554	1.241
0.750	0.516	0.521	0.914
0.875	0.486	0.492	1.244
1.000	0.473	0.480	1.408

Table 4 . 2 Comparison of the normalized mode I stress intensity factors for uniform tension

$2\phi/\pi$	*a/h=0.2, a/c=2, E(h)/E₁=1*		
	Walters et al. (2004)	*Present study*	*% Diff.*
0.000	0.763	0.782	2.552
0.125	0.755	0.754	0.177
0.250	0.716	0.713	0.379
0.375	0.677	0.676	0.105
0.500	0.637	0.637	0.014
0.625	0.595	0.594	0.145
0.750	0.554	0.551	0.494
0.875	0.516	0.517	0.200
1.000	0.499	0.503	0.745

Table 4 . 3 Comparison of the normalized mode I stress intensity factors for uniform tension

$2\phi/\pi$	*a/h=0.2, a/c=2, E(h)/E₁=5.0*		
	Walters et al. (2004)	*Present study*	*% Diff.*
0.000	0.615	0.646	5.008
0.125	0.636	0.638	0.305
0.250	0.625	0.627	0.241
0.375	0.610	0.612	0.380
0.500	0.588	0.591	0.555
0.625	0.561	0.562	0.220
0.750	0.529	0.529	0.000
0.875	0.499	0.500	0.243
1.000	0.484	0.488	0.776

Table 4 . 4 Comparison of the normalized mode I stress intensity factors for uniform tension

$2\phi/\pi$	*a/h=0.5, a/c=2, E(h)/E₁=0.2*		
	Walters et al. (2004)	*Present study*	*% Diff.*
0.000	0.736	0.772	4.925
0.125	0.746	0.753	0.891
0.250	0.719	0.727	1.106
0.375	0.690	0.698	1.115
0.500	0.651	0.659	1.172
0.625	0.606	0.612	0.913
0.750	0.561	0.564	0.457
0.875	0.522	0.526	0.709
1.000	0.506	0.510	0.801

Table 4 . 5 Comparison of the normalized mode I stress intensity factors for uniform tension

$2\phi/\pi$	*a/h=0.5, a/c=2, E(h)/E₁=1.0*		
	Walters et al. (2004)	*Present study*	*% Diff.*
0.000	0.782	0.807	3.162
0.125	0.774	0.775	0.092
0.250	0.731	0.730	0.157
0.375	0.689	0.689	0.029
0.500	0.646	0.647	0.144
0.625	0.603	0.602	0.185
0.750	0.560	0.557	0.468
0.875	0.521	0.522	0.221
1.000	0.504	0.507	0.691

Table 4 . 6 Comparison of the normalized mode I stress intensity factors for uniform tension

$2\phi/\pi$	a/h=0.5, a/c=2, E(h)/E_1=5.0		
	Walters et al. (2004)	Present study	% Diff.
0.000	0.596	0.647	8.492
0.125	0.656	0.661	0.687
0.250	0.677	0.680	0.413
0.375	0.685	0.688	0.429
0.500	0.679	0.682	0.402
0.625	0.659	0.659	0.074
0.750	0.629	0.627	0.289
0.875	0.595	0.596	0.194
1.000	0.580	0.582	0.393

Table 4 . 7 Comparison of the normalized mode I stress intensity factors for uniform tension

$2\phi/\pi$	*a/h=0.8, a/c=2, E(h)/E_1=0.2*		
	Walters et al. (2004)	*Present study*	*% Diff.*
0.000	0.849	0.875	3.01
0.125	0.836	0.837	0.13
0.250	0.775	0.779	0.46
0.375	0.712	0.716	0.50
0.500	0.643	0.647	0.63
0.625	0.577	0.579	0.43
0.750	0.519	0.519	0.05
0.875	0.475	0.477	0.33
1.000	0.457	0.460	0.59

Table 4 . 8 Comparison of the normalized mode I stress intensity factors for uniform tension

$2\phi/\pi$	*a/h=0.8, a/c=2, E(h)/E₁=1.0*		
	Walters et al. (2004)	*Present study*	*% Diff.*
0.000	0.823	0.841	2.164
0.125	0.806	0.803	0.365
0.250	0.755	0.751	0.587
0.375	0.707	0.705	0.343
0.500	0.659	0.658	0.137
0.625	0.612	0.610	0.392
0.750	0.566	0.562	0.713
0.875	0.525	0.525	0.047
1.000	0.507	0.509	0.460

Table 4 . 9 Comparison of the normalized mode I stress intensity factors for uniform tension

$2\phi/\pi$	*a/h=0.8, a/c=1/3, E(h)/E₁=1*		
	Walters et al. (2004)	*Present study*	*% Diff.*
0.000	1.378	1.305	5.272
0.125	1.244	1.271	2.198
0.250	1.300	1.319	1.436
0.375	1.380	1.395	1.121
0.500	1.441	1.456	1.053
0.625	1.476	1.489	0.863
0.750	1.485	1.505	1.354
0.875	1.483	1.500	1.153
1.000	1.481	1.497	1.091

Table 4 . 10 Comparison of the normalized mode I stress intensity factors for uniform tension

$2\phi/\pi$	*a/h=0.8, a/c=2, E(h)/E$_1$=5.0*		
	Walters et al. (2004)	*Present study*	*% Diff*
0.000	0.602	0.665	10.448
0.125	0.698	0.700	0.266
0.250	0.748	0.749	0.098
0.375	0.774	0.776	0.215
0.500	0.772	0.775	0.392
0.625	0.746	0.744	0.295
0.750	0.700	0.694	0.804
0.875	0.648	0.648	0.061
1.000	0.625	0.627	0.355

Taking into account the results of the Table 4.1-4.10, the largest percent difference is 2.198% excluding the differences at the free surface $\phi = 0$. Since the square root singularity is not valid at the free surface, where the crack front intersects with outer surface. In the previous researches, it is substantiated that free surface effect is crucial only in a small zone around the crack front [29]. Hence, the free surface effect is not taken into account. Instead, the mesh of crack region is refined. Because of this phenomenon percent differences at the crack tips are high, considering other crack parametric polar angles. Considering the tabulated results, normalized mode I stress intensity factors of the three-dimensional surface crack problems are given in Figure 4.3- Figure 4.11. In these figures, the variation of the normalized mode I stress intensity factors are presented with respect to normalized polar angle $(2\phi/\pi)$ for different crack to thickness ratios and varying elastic modulus.

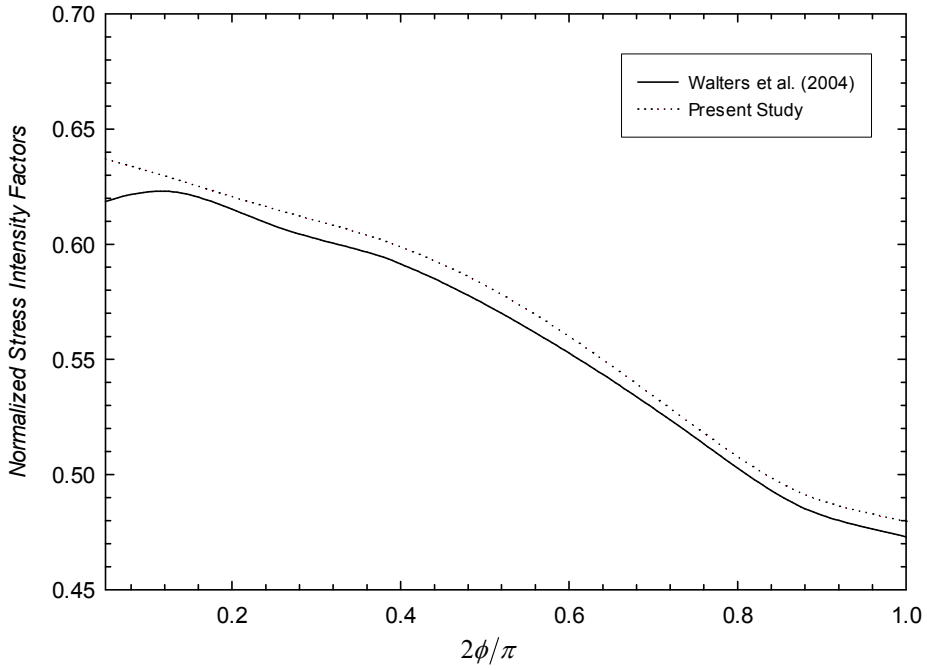

Figure 4 . 3 Uniform tension for a/h=0.2, a/c=2, E(h)/E1=0.2

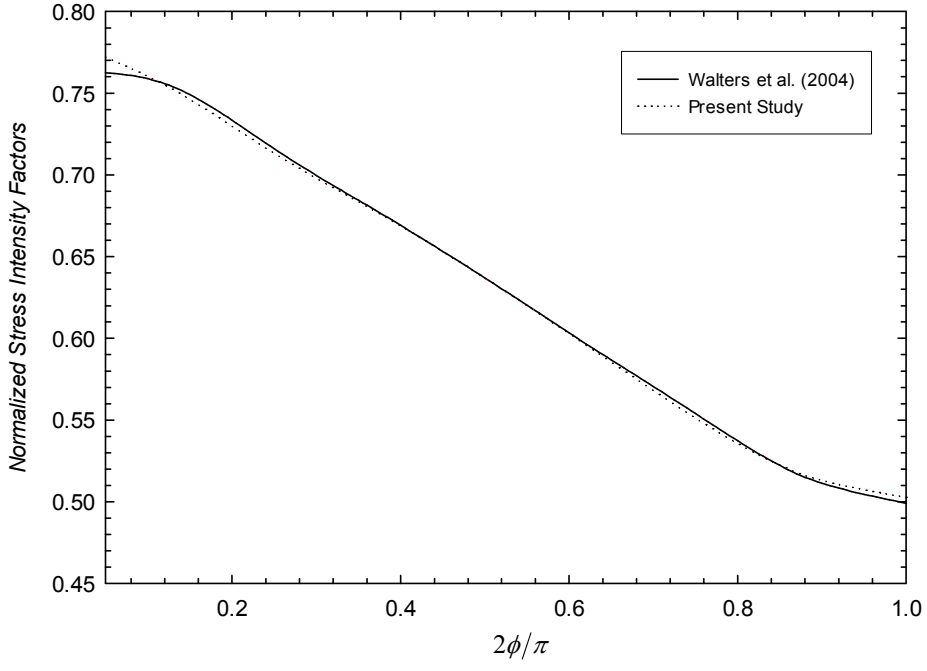

Figure 4 . 4 Uniform tension for a/h=0.2, a/c=2, E(h)/E1=1.0

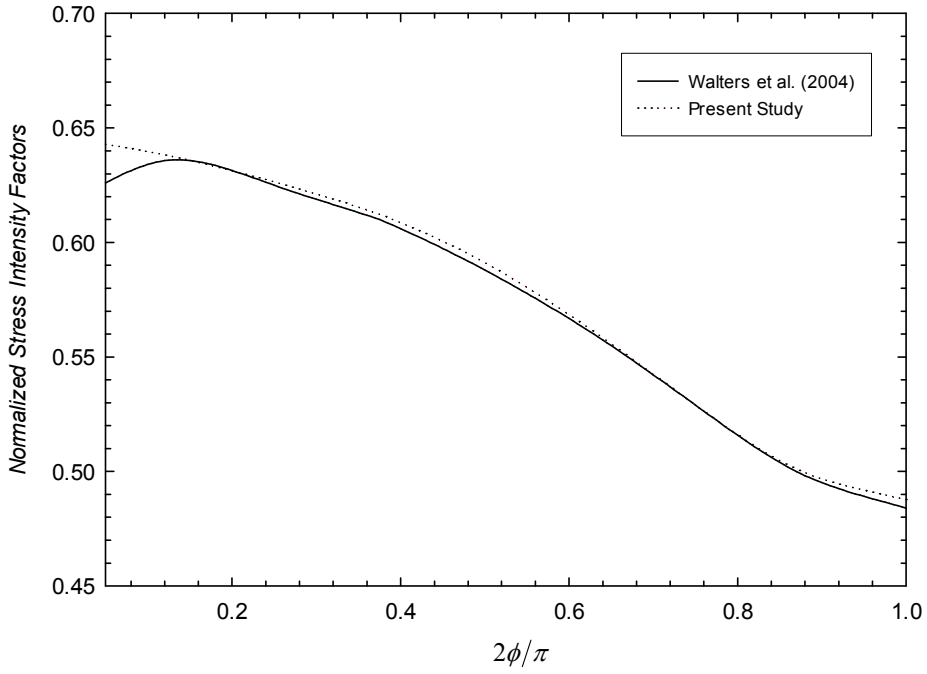

Figure 4 . 5 Uniform tension a/h=0.2, a/c=2, E(h)/E1=5.0

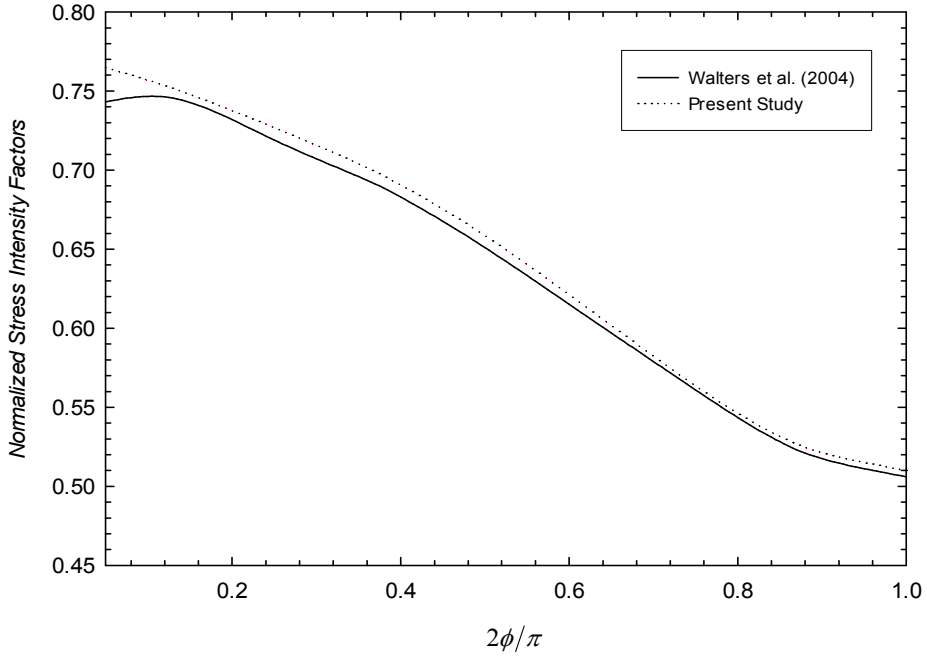

Figure 4 . 6 Uniform tension for a/h=0.5, a/c=2, E(h)/E1=0.2

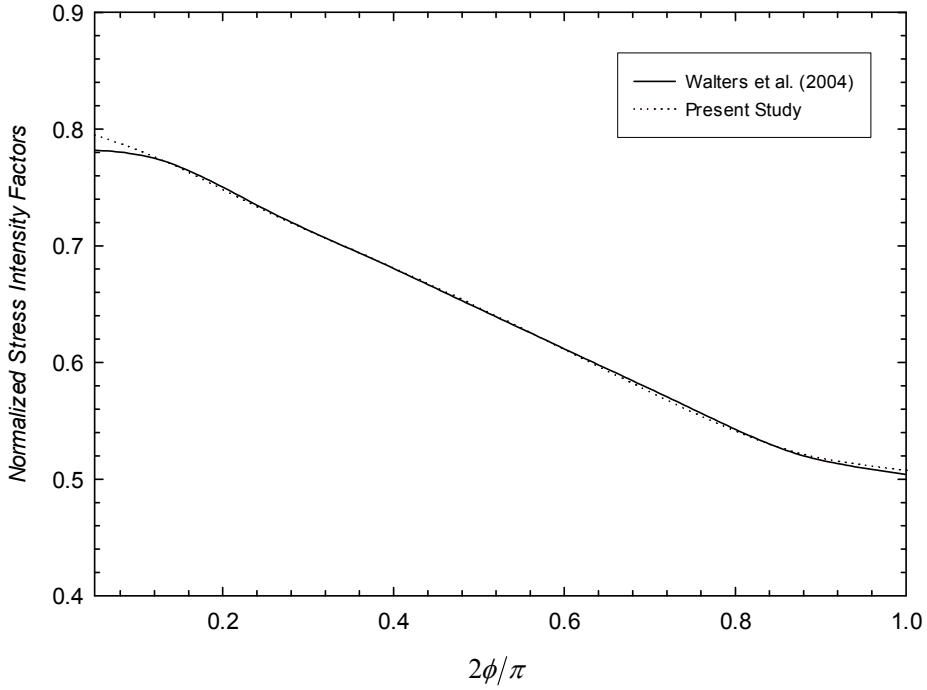

Figure 4 . 7 Uniform tension for a/h=0.5, a/c=2, E(h)/E1=1.0

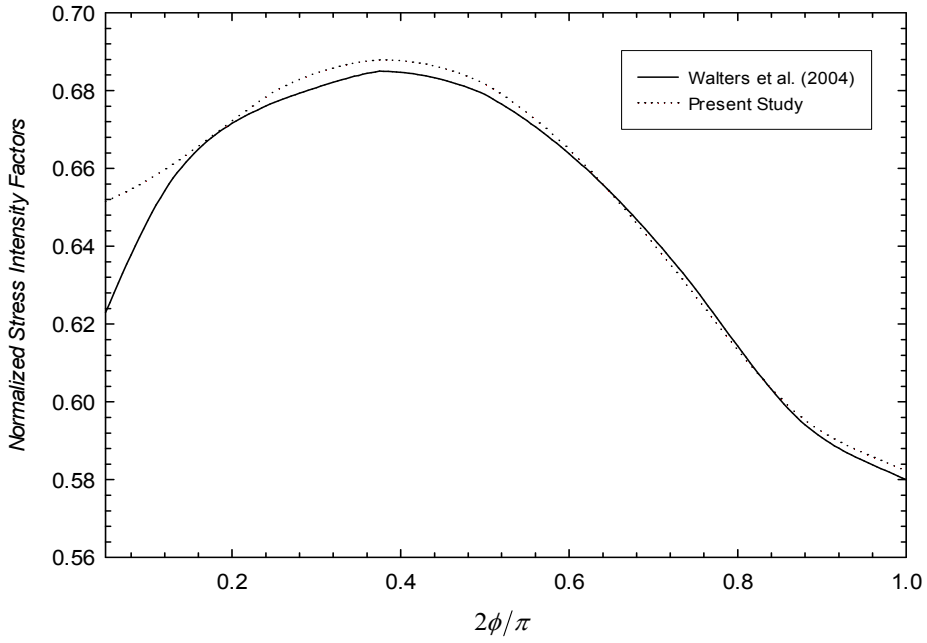

Figure 4 . 8 Uniform tension for a/h=0.5, a/c=2, E(h)/E1=5.0

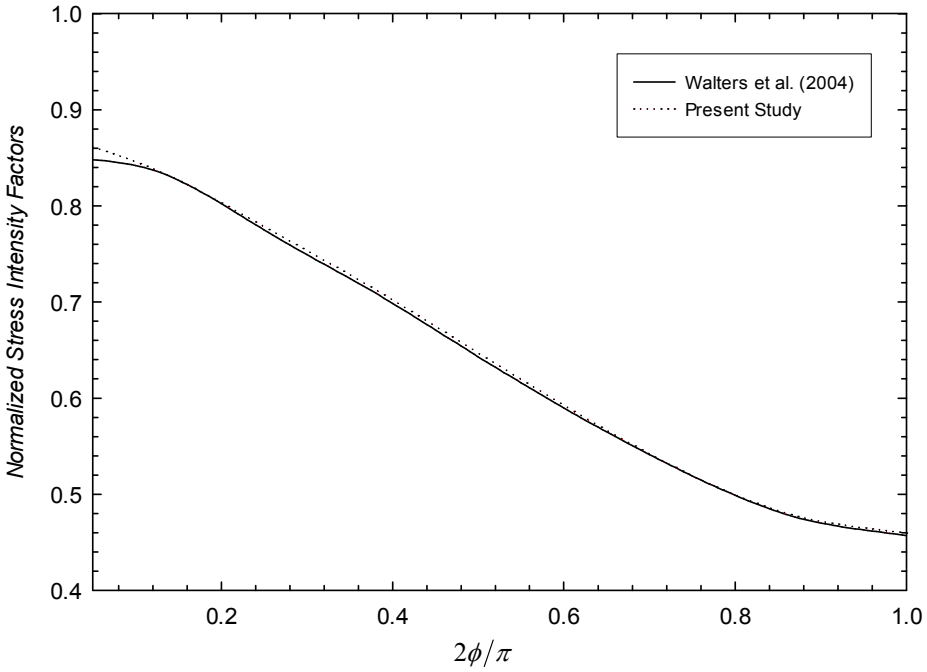

Figure 4 . 9 Uniform tension for a/h=0.8, a/c=2, E(h)/E1=0.2

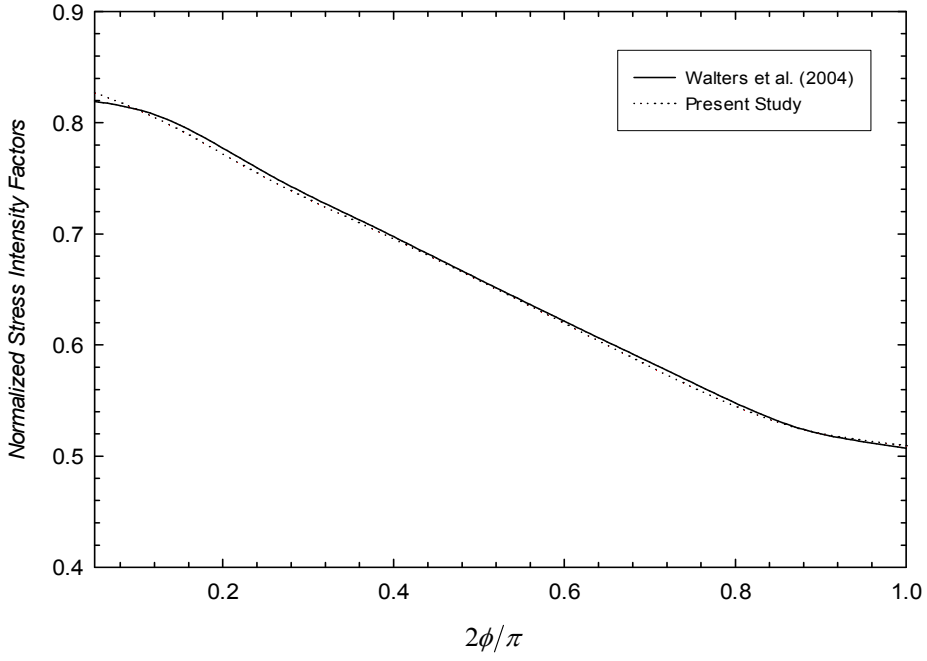

Figure 4 . 10 Uniform tension for a/h=0.8, a/c=2, E(h)/E1=1.0

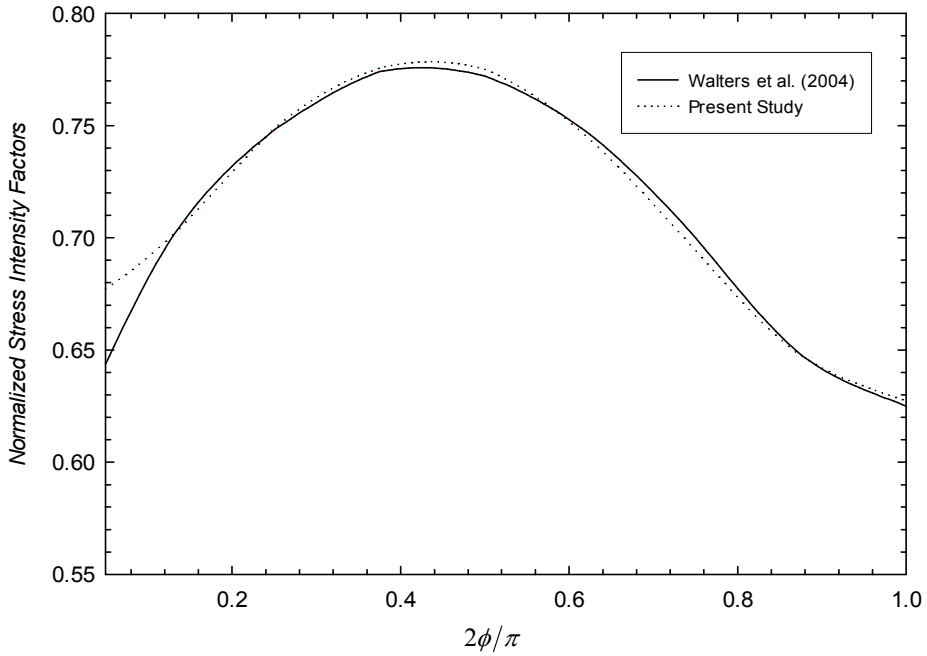

Figure 4 . 11 Uniform tension for a/h=0.8, a/c=2, E(h)/E1=5.0

In all geometries, all of the percent differences between the results of [24] and the present study, the accuracy of the three-dimensional finite element model and the numerical implementation of the asymptotic field expressions are acceptable.

4.3 Comparisons to Newman and Raju Equations

In this type of loading, there dimensional isotropic body exposed to uniform stress σ_t at the edge of the end of longitudinal axis of the structure, i.e. stress is applied at the ends $y = \pm l$. Elastic modulus of the isotropic material is taken as 105.8 GPa and the Poisson's ratio is taken as 0.298. These properties are taken at a temperature of 300 K for metallic alloy (Ti-6Al-4V). Because of this uniform stress at the edges, deformation and the strain displacements are calculated to obtain normalized stress intensity factors. The structure subjected to uniform tension is shown in Figure 4.12 and Figure 4.13.

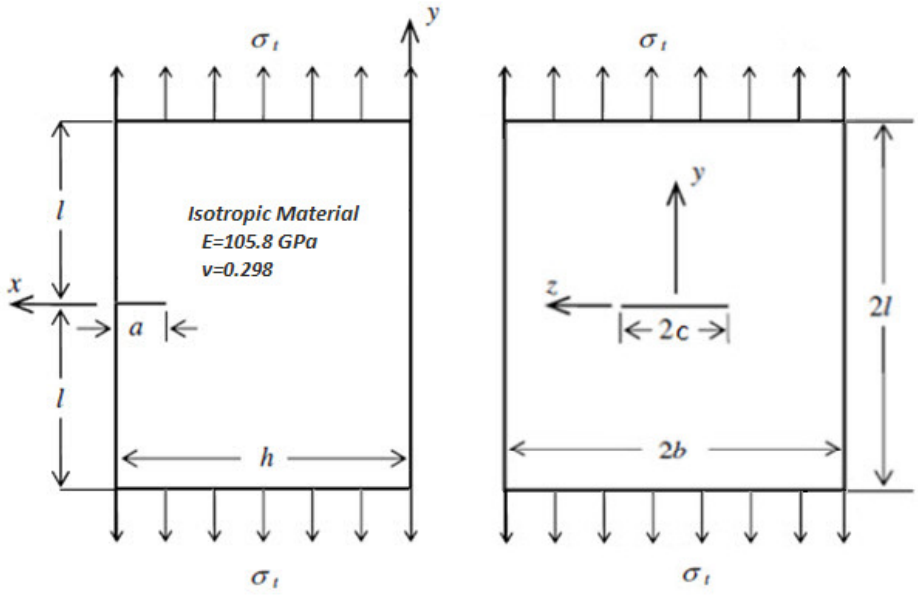

Figure 4 . 12 Isotropic material subjected to uniform tension at the ends $y = \pm l$

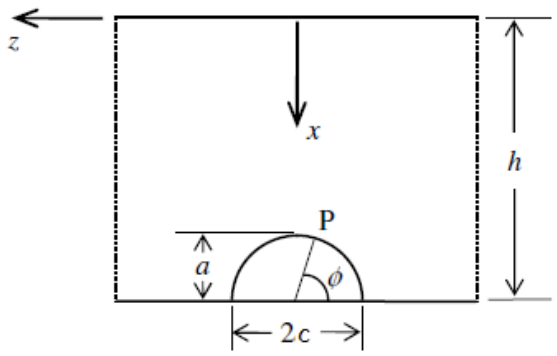

Figure 4 . 13 Parametric angle (ϕ) and the corresponding point P on the semi elliptical crack front.

The Mode I type normalized stress intensity factors are tabulated and percent differences between the reference results [30] are presented. In order to verify the three-dimensional model and the accuracy of the results, normalized mode-I stress intensity factors of the homogeneous isotropic structure are compared to the reference results. Present study results are obtained from the isotropic degeneracy case of the anisotropic asymptotic field expressions given in Chapter 3.2. Sample

calculation steps are given in Appendix A. Asymptotic field displacement constant $C(\theta)$ is calculated and this value is used in the finite element code.

Results of the present study, the results of reference [30] and the percent differences are given in Table 4.11 – Table 4.12.

Table 4 . 11 Comparison of the normalized mode I stress intensity factors for three-dimensional homogeneous plate subjected to uniform tension

$2\phi/\pi$	*a/h=0.4, a/c=1*		
	Present study results	*Newman and Raju (1981)*	*% Diff*
0.0000	1.120	1.146	2.226
0.1250	1.146	1.109	3.339
0.1875	1.124	1.094	2.739
0.2500	1.107	1.081	2.400
0.3125	1.094	1.070	2.230
0.3750	1.084	1.061	2.126
0.4375	1.076	1.055	2.015
0.5000	1.070	1.050	1.894
0.5625	1.065	1.046	1.785
0.6250	1.061	1.044	1.644
0.6875	1.058	1.042	1.497
0.7500	1.055	1.041	1.330
0.8125	1.053	1.041	1.179
0.8750	1.052	1.041	1.051
0.9375	1.051	1.041	0.956
1.0000	1.050	1.041	0.916

Table 4 . 12 Comparison of the normalized mode I stress intensity factors for three-dimensional homogeneous plate subjected to uniform tension

$2\phi/\pi$	*a/h=0.8, a/c=1*		
	Present study results	*Newman and Raju (1981)*	*% Diff*
0.0000	1.109	1.152	3.678
0.1250	1.148	1.113	3.152
0.1875	1.126	1.098	2.553
0.2500	1.110	1.084	2.354
0.3125	1.098	1.073	2.303
0.3750	1.084	1.064	1.885
0.4375	1.074	1.057	1.583
0.5000	1.069	1.052	1.631
0.5625	1.065	1.049	1.608
0.6250	1.062	1.046	1.539
0.6875	1.059	1.044	1.402
0.7500	1.057	1.044	1.331
0.8125	1.057	1.043	1.319
0.8750	1.054	1.043	1.049
0.9375	1.053	1.043	1.010
1.0000	1.056	1.043	1.299

In Tables 4.11 and 4.12 three-dimensional crack models and numerical solution technique are verified. The stress intensity factors of the models are compared with the Raju et al. [3]. The percent differences can indicate that the three-dimensional finite element model appropriate to calculate stress intensity factor of three-dimensional structures with semi-elliptical surface cracks.

Considering Table 4.11, for this crack dimensions maximum percent difference is 3.339% at the polar angle $\phi = 1.250$. Taking into account Table 4.12 results, maximum percent difference is 3.678% and it is calculated at the free surface. These results are acceptable results. Thus, verification of the three-dimensional finite element model is accomplished. Furthermore, the asymptotic expressions are also verified with the result presented in Table 4.11 and in Table 4.12.

With these comparisons not only the finite element models are verified, but also the asymptotic expressions are also verified with the result presented in Table 4.11 and Table 4.12. Therefore, analysis for orthotropic materials can be accomplished with this model and asymptotic field constant embedded in the finite element software.

Tabulated results are shown in Figure 4.14 and Figure 4.15.

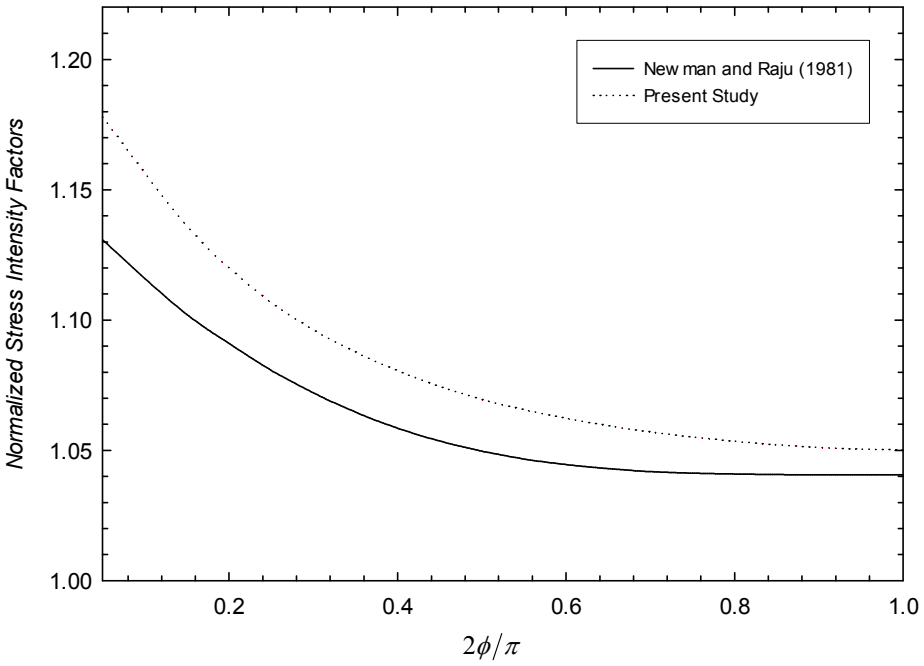

Figure 4 . 14 Uniform tension for a/h=0.4, a/c=1

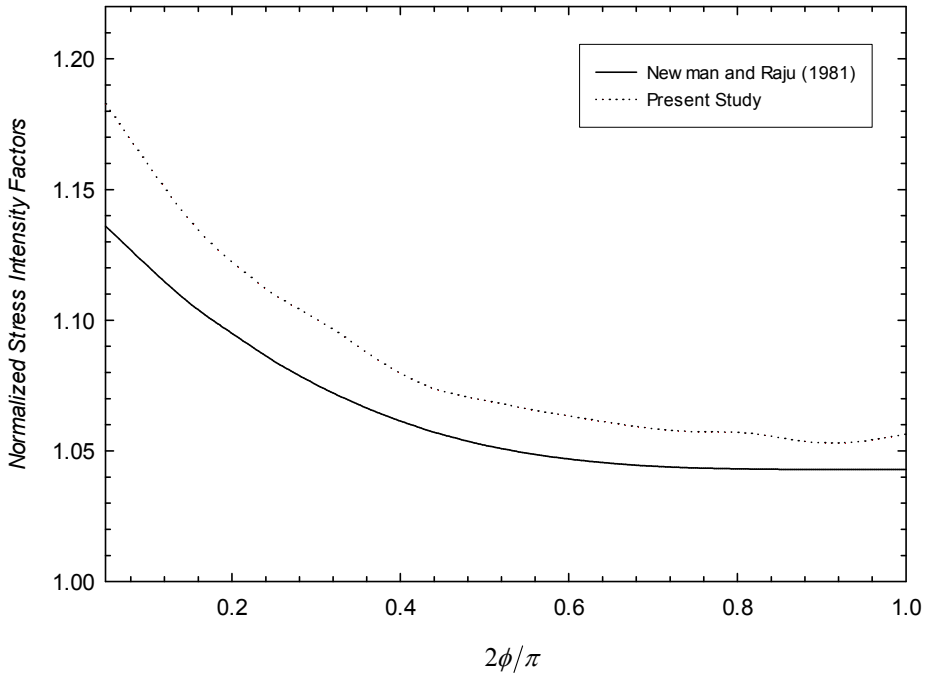

Figure 4 . 15 Uniform tension for a/h=0.8, a/c=1

4.4 Comparisons to Kirilyuk

In this section, three-dimensional orthotropic model and asymptotic field expressions are verified comparing with the internal three-dimensional penny-shaped crack in an infinite orthotropic medium as stated in the reference [16]. The geometry of the model is given in Figure 4.16.

The stress intensity factors are analyzed for an orthotropic material with a circular crack in the x-y plane in an infinite medium. In the analysis, four types of materials are considered with the elastic properties given in Table 4.13. In this case, only the half of the geometry is modeled.

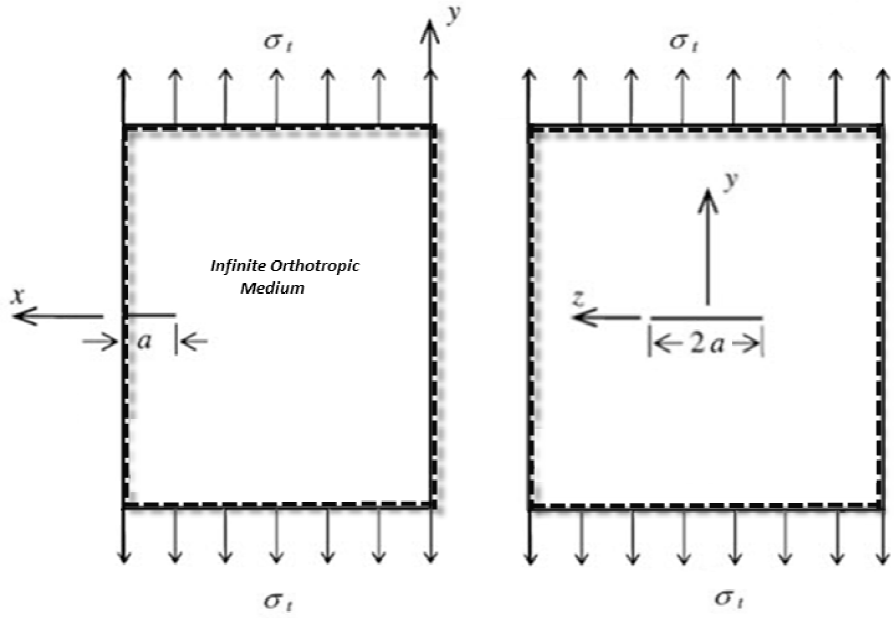

Figure 4 . 16 Orthotropic infinite medium subjected to uniform tension at the ends $y = \pm l$

Table 4 . 13 Orthotropic material properties used in numerical examples (elastic moduli units given in Pa) [16]

	Mat. I	*Mat. II*	*Mat. III*	*Mat. IV*
E_x	55.90 x10^9	36.10 x10^9	35.21 x10^9	17.55 x10^9
E_y	13.73 x10^9	26.28 x10^9	28.73 x10^9	12.85 x10^9
E_z	13.73 x10^9	10.79 x10^9	17.95 x10^9	4.22 x10^9
v_{xy}	0.28	0.11	0.18	0.15
v_{yz}	0.40	0.43	0.37	0.31
v_{xz}	0.07	0.41	0.16	0.08
G_{xy}	5.59 x10^9	4.90 x10^9	7.45 x10^9	2.75 x10^9
G_{yz}	4.90 x10^9	4.02 x10^9	6.18 x10^9	2.35 x10^9
G_{xz}	5.59 x10^9	4.41 x10^9	6.47 x10^9	2.35 x10^9

Tabulated results are given in Table 4.14 – Table 4.17.

Table 4 . 14 Comparison of penny-shaped crack in orthotropic medium results with Kirilyuk [16]

Angle (deg.)	*Mat. I*		
	Present Study	*K_{In} [16]*	*% Diff*
0.0	1.298	1.250	3.862
3.2	1.294	1.249	3.571
15.6	1.235	1.220	1.248
28.0	1.175	1.180	0.465
40.4	1.134	1.130	0.344
52.8	1.107	1.090	1.520
65.2	1.086	1.060	2.785
77.6	1.117	1.045	3.646
90.0	1.134	1.040	4.403

Table 4 . 15 Comparison of penny-shaped crack in orthotropic medium results with Kirilyuk [16]

Angle (deg.)	*Mat. II*		
	Present Study	*K_{In} [16]*	*% Diff*
0.0	1.095	1.090	0.449
3.2	1.093	1.089	0.3787
15.6	1.059	1.070	1.0303
28.0	1.036	1.055	1.793
40.4	1.027	1.050	2.156
52.8	1.039	1.055	2.188
65.2	1.065	1.090	2.278
77.6	1.195	1.210	1.266
90.0	1.453	1.440	0.917

Table 4 . 16 Comparison of penny-shaped crack in orthotropic medium results with Kirilyuk [16]

Angle (deg.)	*Mat. III*		
	Present Study	*K_{In} [16]*	*% Diff*
0	1.155	1.165	0.781
3.2	1.154	1.164	0.858
15.6	1.129	1.145	1.356
28	1.106	1.128	1.960
40.4	1.094	1.118	2.181
52.8	1.088	1.110	1.986
65.2	1.089	1.111	1.988
77.6	1.100	1.116	0.143
90	1.112	1.119	0.666

Table 4 . 17 Comparison of penny-shaped crack in orthotropic medium results with Kirilyuk [16]

Angle (deg.)	*Mat. IV*		
	Present Study	*K_{In} [16]*	*% Diff*
0.0	1.124	1.156	2.757
3.2	1.123	1.1555	2.856
15.6	1.092	1.148	4.840
28.0	1.073	1.128	4.919
40.4	1.065	1.116	4.541
52.8	1.065	1.112	4.227
65.2	1.071	1.118	4.156
77.6	1.092	1.125	2.981
90.0	1.116	1.129	1.155

The numerical analysis results of penny-shape crack model show that the numerical solution technique gives acceptable results. The maximum percent error values are calculated for material IV. The figures of the tabulated stress intensity factor results are given in Figure 4.17 and Figure 4.18.

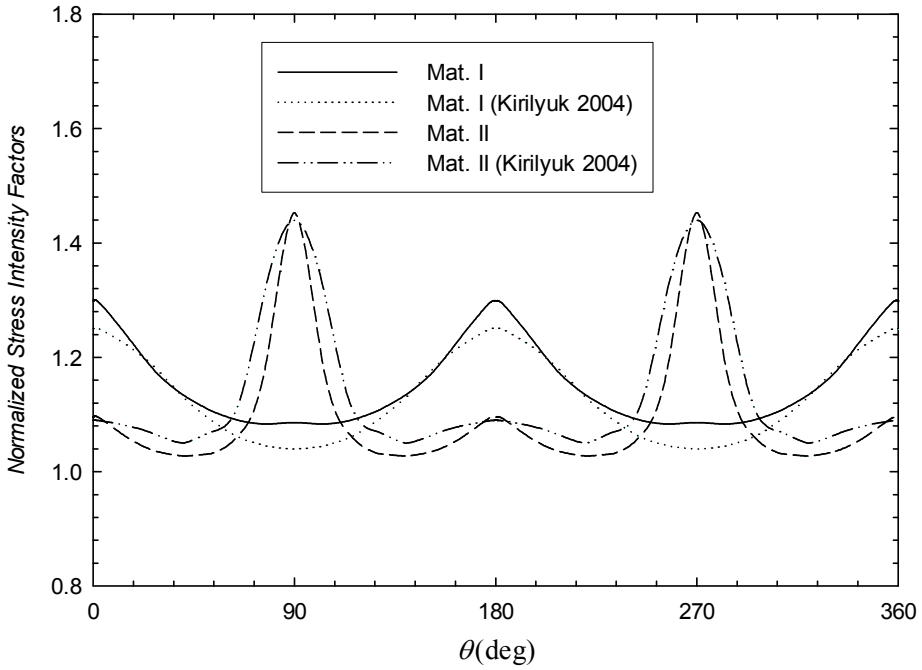

Figure 4 . 17 Uniform tension for internal penny-shape crack

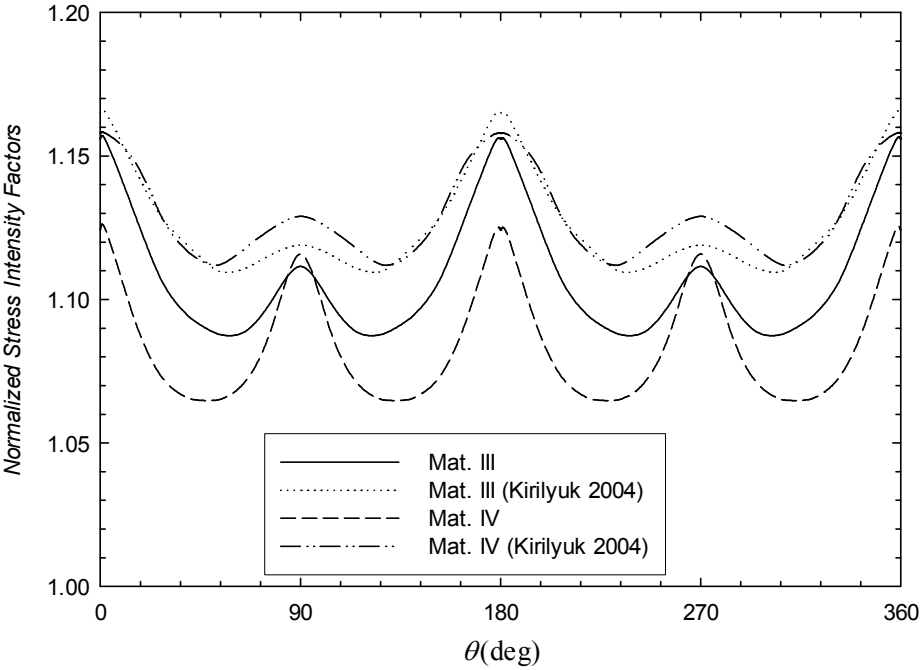

Figure 4 . 18 Uniform tension for internal penny-shape crack

4.5 Comparisons for Thermal Loading

In this section, three-dimensional homogeneous isotropic structure with semi-elliptical surface crack subjected to thermal loading is analyzed. The results are compared with the results given in literature [9].

In this type of loading condition, material is assumed as stress free at a temperature of 1273 K. Then, the material is exposed to an environment with a temperature of 300 K. For this type of loading condition, the surface of the structure at which the crack exists, exposed to a forced convection. At the surface, $x = h$, the convection coefficient is $h = 10000$ W/(m^{2}K). At the other surfaces, there are free convection with a convection coefficient $h = 5$ W/(m^{2}K). For this type of loading, material properties calculated at the mid temperature, $T_m = 786.5$ K.

The boundary conditions and the loading case are given in the Figure 4.19.

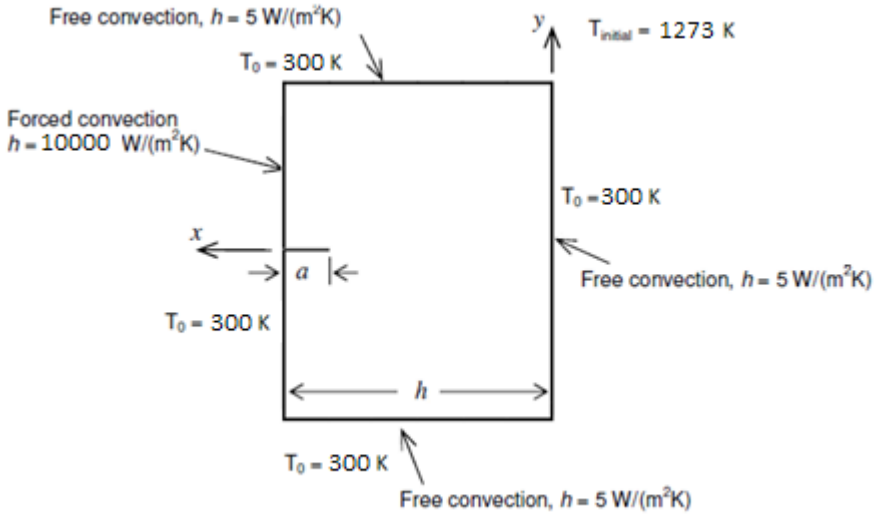

Figure 4 . 19 The boundary conditions for transient thermal loading [9]

The stress intensity factors are analyzed for homogeneous isotropic material with a semi-elliptical surface crack. Comparisons of the results are shown in Figure 4.20 and 4.21.

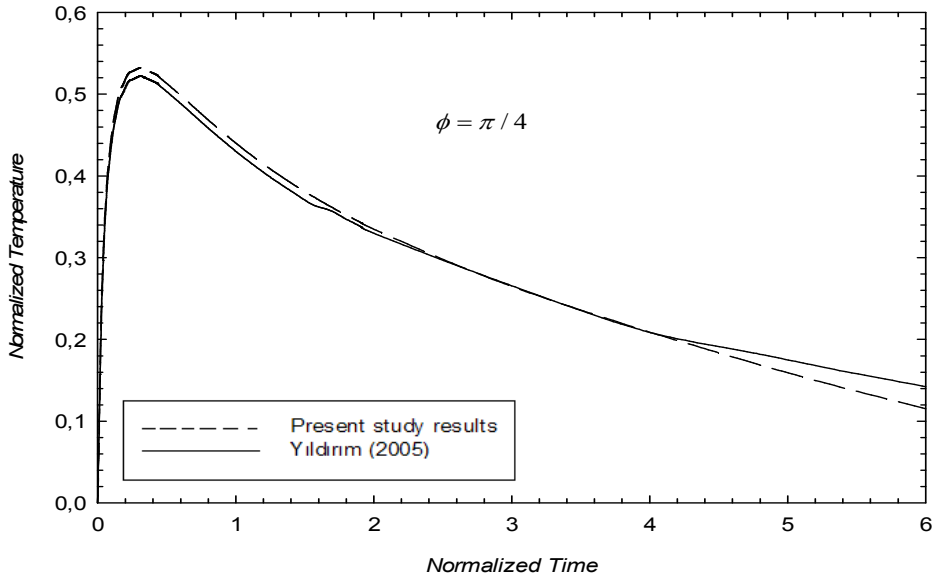

Figure 4 . 20 Temperature versus normalized time for thermal loading ($\phi = \pi/4$)

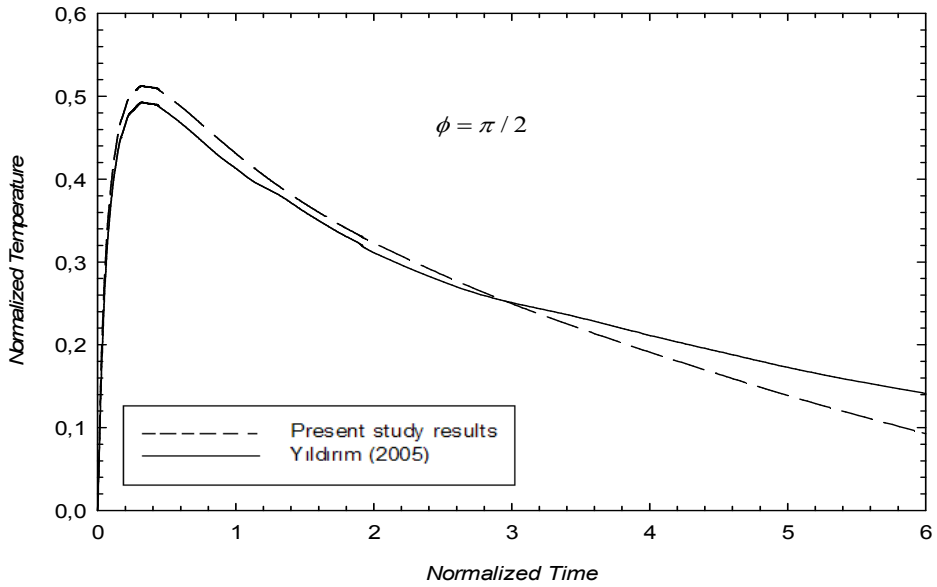

Figure 4 . 21 Temperature versus normalized time for thermal loading ($\phi = \pi/2$)

4.6 Present Study Results

4.6.1 Mechanical Loading on the Three-Dimensional Orthotropic Material

In this study, semi-elliptical cracks in three-dimensional orthotropic materials are investigated. The orthotropic homogeneous body is shown in Figure 4.22. The thickness of the orthotropic material is taken as h. The semi-elliptical crack length is taken as $2c$ and the half-length is taken as a, which is the length for the depth of the surface semi-elliptic crack. The orthotropic material dimensions used in this study are as follows $h = 12.5$ mm, $b = 20$ mm and $l = 20$ mm. These dimensions are chosen as same as the dimensions given by Lee and Erdogan [31].

Three-dimensional finite element model for mechanical loading cases are verified in the previous sections. After verification of the geometry of the model and the anisotropic expressions for the degeneracy case, the finite element solution is applied to the orthotropic materials. In this section present study results are presented. Material properties for orthotropic materials are taken as same as properties given in the reference study [32]. The material properties are tabulated in Table 4.18. The various anisotropic materials are subjected to mechanical loading such as uniform tension and fixed grip tension.

In finite element analysis anisotropic asymptotic field expressions and constants are used to obtain stress intensity factor.

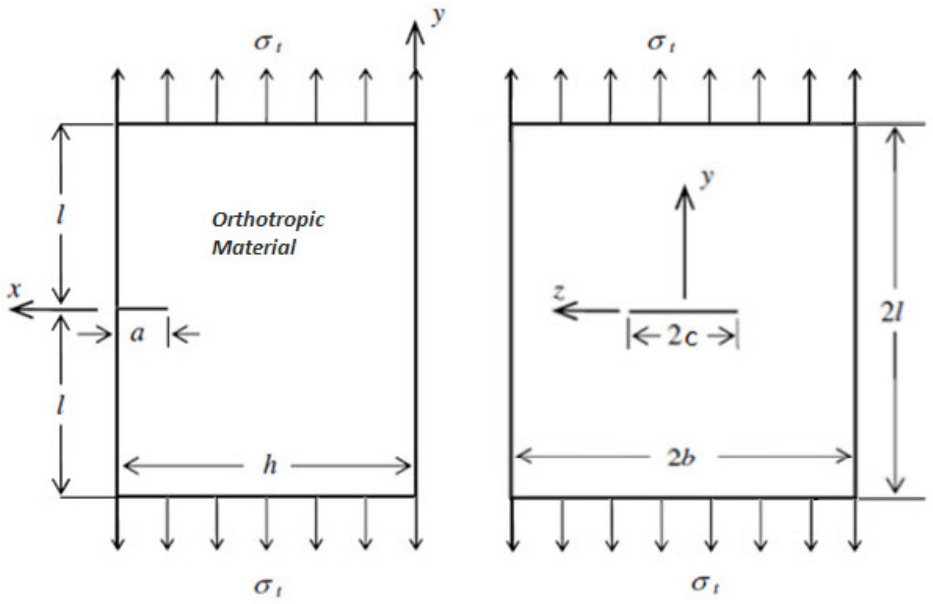

Figure 4 . 22 Orthotropic body subjected to uniform tension at the ends $y = \pm l$

Table 4 . 18 Orthotropic material properties used in numerical examples (Elastic moduli units given in Pa) [31]

	Mat. A	*Mat. B*	*Mat. C*	*Mat. D*
E_x	55.16x10^9	171.0 x10^9	128.9 x10^9	173.1 x10^9
E_y	171.0 x10^9	55.16x10^9	128.9 x10^9	122.0 x10^9
E_z	55.16 x10^9	171.0 x10^9	128.9 x10^9	173.1 x10^9
v_{xy}	0.036	0.111	0.380	0.370
v_{yz}	0.111	0.036	0.380	0.262
v_{xz}	0.036	0.111	0.380	0.370
G_{xy}	4.826 x10^9	4.826 x10^9	127.6 x10^9	124.8 x10^9
G_{yz}	4.826 x10^9	4.826 x10^9	127.6 x10^9	124.8 x10^9
G_{xz}	26.61 x10^9	76.53 x10^9	127.6 x10^9	63.02 x10^9

4.6.1.1 Uniform Tension on the Three-Dimensional Orthotropic Material

In this section, stress intensity factors are calculated for three-dimensional orthotropic and isotropic materials under uniform tension. The anisotropy effect is shown by using different type of materials. The materials are chosen as same as with

the numerical reference solution [32]. The properties are given in Table 4.18. In addition to these materials for isotropic case, the elastic modulus is chosen as $E = 206.84x10^9\ Pa\ (30x10^6 psi)$ and Poisson's ratio $v = 0.25$. Tensile loading is applied by amount stress value $\sigma_0 = 1$. The width of the strip is $2a$ and the crack depth is a.

After obtaining the stress intensity factors for the structure, normalized mode I stress intensity factors are calculated using the formula:

$$K_{ln} = \frac{K_I}{\sigma_t \sqrt{\frac{\pi\, a}{Q}}} \tag{4.1}$$

where σ_t is the applied uniform stress, a is the depth of the crack and Q is the shape factor for semi-elliptical crack. The shape factor is calculated with the formula expressed in the reference [24]. The semi elliptic surface cracked body is given in Figure 4.7.

$$Q = \begin{cases} 1 + 1.464\ (a/c)^{1.65} & for\ \ (a/c) \leq 1 \\ 1 + 1.464\ (c/a)^{1.65} & for\ \ (a/c) > 1 \end{cases} \tag{4.2}$$

Tabulated results are given in Table 4.19 - 4.24.

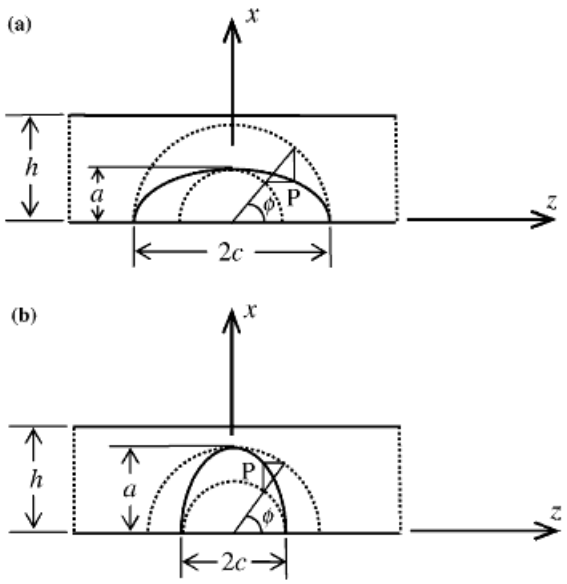

Figure 4 . 23 Plan view of the semi-elliptic cracked structure by Walters et al. (2004), (a) a/c < 1 and (b) a/c >1

Normalized mode I stress intensity factors for three-dimensional orthotropic materials subjected to uniform tension are given in Table 4.19 - 4.24.

Table 4 . 19 Normalized mode I stress intensity factors Kln for three-dimensional models subjected to uniform tension.

	a/h=0.2, a/c=2/3					*a/h=0.4, a/c=2/3*				
$2\phi/\pi$	*Mat. A*	*Mat. B*	*Mat. C*	*Mat. D.*	*Isotropic*	*Mat. A*	*Mat. B*	*Mat. C*	*Mat. D.*	*Isotropic*
0.05	1.075	0.939	0.997	0.985	0.999	1.228	1.080	1.105	1.119	1.129
0.10	0.944	0.862	1.044	1.014	0.994	1.074	0.989	1.189	1.169	1.139
0.15	0.886	0.774	1.031	1.004	0.973	1.004	0.887	1.171	1.153	1.110
0.20	0.845	0.700	1.021	1.002	0.959	0.955	0.802	1.156	1.146	1.090
0.25	0.810	0.638	1.018	1.008	0.951	0.913	0.733	1.149	1.148	1.077
0.30	0.778	0.586	1.021	1.022	0.949	0.876	0.675	1.148	1.158	1.071
0.35	0.750	0.544	1.029	1.041	0.952	0.841	0.626	1.153	1.174	1.069
0.40	0.723	0.509	1.039	1.065	0.957	0.809	0.585	1.161	1.197	1.071
0.45	0.700	0.480	1.051	1.093	0.965	0.781	0.552	1.171	1.223	1.076
0.50	0.678	0.456	1.063	1.124	0.975	0.757	0.525	1.182	1.254	1.084
0.55	0.659	0.435	1.075	1.157	0.986	0.734	0.502	1.192	1.287	1.093
0.60	0.642	0.419	1.086	1.192	0.997	0.715	0.483	1.202	1.321	1.103
0.65	0.627	0.404	1.095	1.226	1.009	0.698	0.467	1.209	1.356	1.113
0.70	0.615	0.393	1.103	1.260	1.020	0.684	0.454	1.213	1.389	1.123
0.75	0.605	0.384	1.109	1.292	1.032	0.673	0.444	1.217	1.420	1.134
0.80	0.598	0.376	1.113	1.321	1.043	0.664	0.436	1.220	1.449	1.144
0.85	0.592	0.371	1.117	1.347	1.054	0.658	0.430	1.223	1.475	1.155
0.90	0.590	0.367	1.119	1.368	1.064	0.656	0.426	1.224	1.497	1.165
0.95	0.591	0.365	1.121	1.384	1.072	0.657	0.424	1.225	1.514	1.174
1.00	0.596	0.365	1.122	1.394	1.078	0.662	0.423	1.225	1.524	1.180

Table 4 . 20 Normalized mode I stress intensity factors K_{In} for three-dimensional models subjected to uniform tension.

	a/h=0.2, a/c=1					*a/h=0.4, a/c=1*				
$2\phi/\pi$	*Mat. A*	*Mat. B*	*Mat. C*	*Mat. D.*	*Isotropic*	*Mat. A*	*Mat. B*	*Mat. C*	*Mat. D.*	*Isotropic*
0.05	1.292	1.183	1.156	1.141	1.169	1.402	1.301	1.208	1.217	1.245
0.10	1.141	1.062	1.232	1.193	1.180	1.235	1.165	1.325	1.294	1.275
0.15	1.062	0.937	1.216	1.182	1.150	1.147	1.026	1.304	1.279	1.240
0.20	1.001	0.834	1.196	1.172	1.124	1.078	0.910	1.280	1.265	1.208
0.25	0.947	0.747	1.179	1.168	1.102	1.017	0.815	1.260	1.256	1.182
0.30	0.896	0.675	1.167	1.169	1.084	0.960	0.736	1.243	1.253	1.159
0.35	0.848	0.614	1.156	1.174	1.070	0.907	0.670	1.229	1.255	1.141
0.40	0.803	0.563	1.148	1.183	1.058	0.858	0.614	1.217	1.261	1.126
0.45	0.763	0.520	1.141	1.195	1.049	0.814	0.568	1.208	1.271	1.114
0.50	0.726	0.485	1.134	1.210	1.042	0.775	0.530	1.199	1.283	1.104
0.55	0.694	0.455	1.127	1.226	1.037	0.740	0.498	1.189	1.297	1.097
0.60	0.666	0.430	1.120	1.244	1.033	0.710	0.471	1.179	1.313	1.091
0.65	0.642	0.410	1.112	1.263	1.031	0.684	0.449	1.169	1.330	1.086
0.70	0.622	0.393	1.104	1.281	1.031	0.663	0.431	1.159	1.346	1.084
0.75	0.605	0.379	1.096	1.299	1.031	0.645	0.416	1.150	1.363	1.083
0.80	0.592	0.368	1.089	1.317	1.033	0.631	0.405	1.142	1.379	1.084
0.85	0.582	0.359	1.083	1.332	1.036	0.620	0.396	1.134	1.394	1.086
0.90	0.576	0.353	1.078	1.345	1.039	0.614	0.389	1.129	1.406	1.089
0.95	0.574	0.349	1.074	1.354	1.043	0.612	0.384	1.125	1.415	1.092
1.00	0.577	0.347	1.072	1.360	1.046	0.615	0.383	1.122	1.421	1.095

Table 4 . 21 Normalized mode I stress intensity factors K_{In} for three-dimensional models subjected to uniform tension.

	a/h=0.2, a/c=3/2					*a/h=0.4, a/c=3/2*				
$2\phi/\pi$	*Mat. A*	*Mat. B*	*Mat. C*	*Mat. D.*	*Isotropic*	*Mat. A*	*Mat. B*	*Mat. C*	*Mat. D.*	*Isotropic*
0.05	1.031	0.987	0.907	0.899	0.924	1.075	1.036	0.910	0.919	0.945
0.10	0.922	0.881	0.970	0.945	0.939	0.960	0.923	1.004	0.985	0.977
0.15	0.858	0.771	0.954	0.934	0.914	0.893	0.808	0.986	0.972	0.950
0.20	0.807	0.680	0.933	0.923	0.889	0.838	0.712	0.963	0.959	0.922
0.25	0.759	0.605	0.913	0.914	0.866	0.787	0.632	0.942	0.948	0.897
0.30	0.712	0.541	0.895	0.907	0.845	0.737	0.565	0.922	0.940	0.874
0.35	0.667	0.486	0.878	0.902	0.826	0.690	0.508	0.904	0.934	0.853
0.40	0.625	0.441	0.862	0.900	0.809	0.646	0.459	0.886	0.929	0.834
0.45	0.586	0.402	0.846	0.898	0.792	0.605	0.419	0.869	0.926	0.816
0.50	0.550	0.369	0.830	0.898	0.777	0.568	0.385	0.852	0.924	0.799
0.55	0.518	0.341	0.814	0.898	0.762	0.535	0.355	0.834	0.922	0.783
0.60	0.489	0.317	0.797	0.898	0.748	0.505	0.331	0.816	0.921	0.767
0.65	0.464	0.297	0.779	0.897	0.735	0.478	0.310	0.797	0.919	0.753
0.70	0.442	0.279	0.761	0.897	0.722	0.455	0.292	0.778	0.917	0.740
0.75	0.423	0.265	0.744	0.896	0.712	0.436	0.278	0.760	0.915	0.728
0.80	0.407	0.253	0.727	0.894	0.702	0.420	0.266	0.743	0.913	0.718
0.85	0.394	0.244	0.713	0.893	0.695	0.407	0.256	0.728	0.911	0.710
0.90	0.385	0.236	0.701	0.891	0.689	0.398	0.249	0.716	0.909	0.704
0.95	0.380	0.231	0.693	0.890	0.686	0.393	0.244	0.707	0.907	0.700
1.00	0.380	0.228	0.687	0.889	0.684	0.393	0.241	0.702	0.906	0.698

Table 4 . 22 Normalized mode I stress intensity factors K_{In} for three-dimensional models subjected to uniform tension.

	a/h=0.6, a/c=2/3					*a/h=0.8, a/c=2/3*				
$2\phi/\pi$	*Mat. A*	*Mat. B*	*Mat. C*	*Mat. D.*	*Isotropic*	*Mat. A*	*Mat. B*	*Mat. C*	*Mat. D.*	*Isotropic*
0.05	1.625	1.482	1.419	1.457	1.468	2.614	2.543	2.140	2.200	2.239
0.10	1.407	1.337	1.540	1.524	1.480	2.215	2.222	2.314	2.276	2.226
0.15	1.298	1.185	1.504	1.490	1.428	1.990	1.912	2.227	2.185	2.105
0.20	1.220	1.062	1.473	1.466	1.387	1.826	1.678	2.148	2.114	2.005
0.25	1.155	0.964	1.451	1.455	1.357	1.687	1.498	2.082	2.060	1.923
0.30	1.098	0.885	1.439	1.454	1.336	1.569	1.357	2.028	2.024	1.857
0.35	1.046	0.818	1.433	1.462	1.322	1.466	1.244	1.983	1.999	1.803
0.40	1.000	0.763	1.431	1.477	1.313	1.375	1.147	1.948	1.987	1.759
0.45	0.959	0.717	1.432	1.498	1.309	1.296	1.065	1.915	1.983	1.723
0.50	0.923	0.679	1.435	1.523	1.308	1.227	0.995	1.886	1.985	1.693
0.55	0.891	0.647	1.436	1.551	1.309	1.168	0.935	1.860	1.992	1.669
0.60	0.864	0.621	1.437	1.581	1.312	1.118	0.885	1.829	1.999	1.648
0.65	0.840	0.599	1.435	1.610	1.316	1.075	0.844	1.797	2.008	1.630
0.70	0.820	0.581	1.432	1.639	1.321	1.040	0.809	1.766	2.016	1.616
0.75	0.805	0.567	1.428	1.667	1.328	1.012	0.780	1.731	2.023	1.605
0.80	0.793	0.556	1.423	1.692	1.335	0.991	0.758	1.697	2.028	1.597
0.85	0.783	0.547	1.419	1.714	1.343	0.975	0.741	1.669	2.034	1.591
0.90	0.779	0.541	1.414	1.731	1.350	0.967	0.729	1.643	2.037	1.588
0.95	0.780	0.538	1.411	1.745	1.357	0.966	0.724	1.627	2.042	1.588
1.00	0.785	0.537	1.407	1.753	1.362	0.972	0.722	1.615	2.043	1.588

Table 4 . 23 Normalized mode I stress intensity factors K_{In} for three-dimensional models subjected to uniform tension.

	a/h=0.6, a/c=1					*a/h=0.8, a/c=1*				
$2\phi/\pi$	*Mat. A*	*Mat. B*	*Mat. C*	*Mat. D.*	*Isotropic*	*Mat. A*	*Mat. B*	*Mat. C*	*Mat. D.*	*Isotropic*
0.05	1.649	1.580	1.362	1.404	1.436	2.092	2.104	1.648	1.717	1.764
0.10	1.445	1.404	1.515	1.500	1.475	1.803	1.831	1.832	1.827	1.799
0.15	1.329	1.224	1.484	1.473	1.426	1.633	1.575	1.781	1.776	1.719
0.20	1.240	1.079	1.449	1.447	1.379	1.509	1.381	1.723	1.729	1.647
0.25	1.162	0.963	1.419	1.428	1.339	1.398	1.221	1.669	1.690	1.583
0.30	1.091	0.868	1.392	1.416	1.306	1.300	1.093	1.622	1.658	1.527
0.35	1.026	0.788	1.369	1.409	1.277	1.211	0.988	1.580	1.634	1.478
0.40	0.967	0.722	1.349	1.407	1.253	1.133	0.901	1.543	1.616	1.436
0.45	0.914	0.666	1.331	1.408	1.233	1.064	0.828	1.509	1.602	1.399
0.50	0.867	0.621	1.314	1.413	1.215	1.004	0.768	1.476	1.593	1.368
0.55	0.826	0.583	1.296	1.420	1.200	0.952	0.717	1.447	1.588	1.341
0.60	0.791	0.551	1.279	1.428	1.188	0.906	0.674	1.415	1.584	1.317
0.65	0.761	0.525	1.260	1.438	1.178	0.869	0.639	1.382	1.581	1.297
0.70	0.736	0.504	1.244	1.449	1.171	0.837	0.609	1.352	1.579	1.280
0.75	0.715	0.487	1.230	1.460	1.166	0.811	0.585	1.326	1.579	1.267
0.80	0.699	0.473	1.217	1.470	1.163	0.791	0.567	1.301	1.577	1.257
0.85	0.687	0.462	1.204	1.480	1.163	0.776	0.551	1.276	1.575	1.249
0.90	0.679	0.454	1.195	1.488	1.164	0.766	0.540	1.256	1.572	1.244
0.95	0.677	0.449	1.189	1.494	1.165	0.763	0.534	1.242	1.571	1.242
1.00	0.680	0.447	1.184	1.498	1.167	0.766	0.530	1.233	1.570	1.241

Table 4 . 24 Normalized mode I stress intensity factors K_{In} for three-dimensional models subjected to uniform tension.

	a/h=0.6, a/c=3/2					*a/h=0.8, a/c=3/2*				
$2\phi/\pi$	*Mat. A*	*Mat. B*	*Mat. C*	*Mat. D.*	*Isotropic*	*Mat. A*	*Mat. B*	*Mat. C*	*Mat. D.*	*Isotropic*
0.05	1.175	1.152	0.964	0.989	1.018	1.324	1.336	1.047	1.089	1.124
0.10	1.044	1.019	1.076	1.065	1.056	1.171	1.177	1.176	1.175	1.166
0.15	0.965	0.886	1.053	1.047	1.021	1.072	1.011	1.146	1.149	1.121
0.20	0.901	0.777	1.025	1.028	0.987	0.994	0.880	1.112	1.122	1.078
0.25	0.843	0.687	0.999	1.012	0.957	0.925	0.778	1.080	1.100	1.039
0.30	0.787	0.612	0.975	0.999	0.928	0.858	0.689	1.050	1.080	1.002
0.35	0.734	0.549	0.953	0.989	0.903	0.796	0.616	1.021	1.063	0.969
0.40	0.685	0.497	0.932	0.980	0.879	0.740	0.556	0.994	1.048	0.938
0.45	0.641	0.453	0.911	0.973	0.857	0.688	0.505	0.968	1.035	0.910
0.50	0.600	0.416	0.891	0.967	0.836	0.643	0.464	0.941	1.022	0.883
0.55	0.564	0.385	0.869	0.962	0.817	0.603	0.429	0.913	1.011	0.858
0.60	0.532	0.359	0.848	0.956	0.798	0.567	0.399	0.887	1.000	0.835
0.65	0.504	0.337	0.825	0.951	0.781	0.536	0.375	0.859	0.989	0.814
0.70	0.480	0.319	0.804	0.946	0.766	0.510	0.355	0.833	0.979	0.795
0.75	0.459	0.303	0.783	0.940	0.752	0.488	0.337	0.808	0.969	0.777
0.80	0.442	0.291	0.764	0.935	0.740	0.469	0.323	0.785	0.958	0.762
0.85	0.429	0.281	0.748	0.930	0.730	0.455	0.313	0.765	0.948	0.751
0.90	0.419	0.274	0.734	0.926	0.723	0.446	0.305	0.748	0.939	0.742
0.95	0.414	0.269	0.724	0.923	0.719	0.441	0.300	0.735	0.932	0.736
1.00	0.414	0.266	0.718	0.920	0.716	0.441	0.297	0.727	0.927	0.732

Tabulated results for uniform tension case are shown in Figure 4.24 – Figure 4.35.

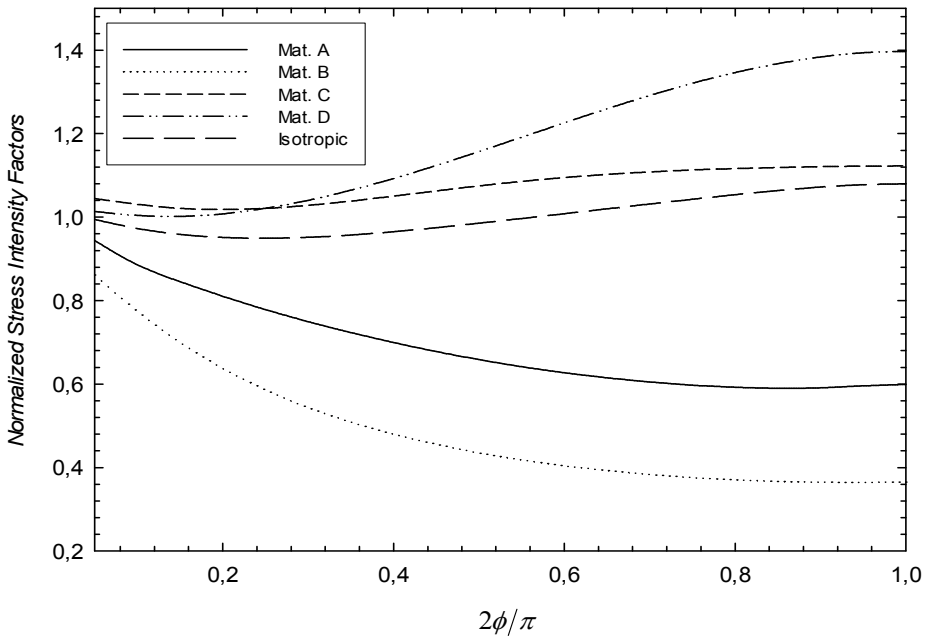

Figure 4 . 24 Uniform tension, K_{In} versus ϕ for a/h=0.2, a/c=2/3

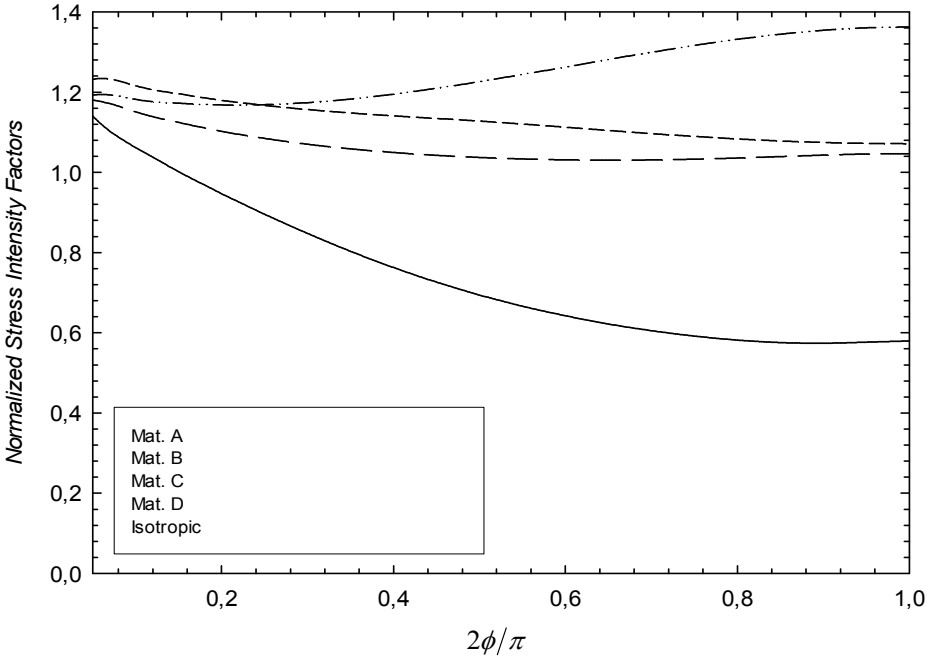

Figure 4 . 25 Uniform tension, K_{In} versus ϕ for a/h=0.2, a/c=1

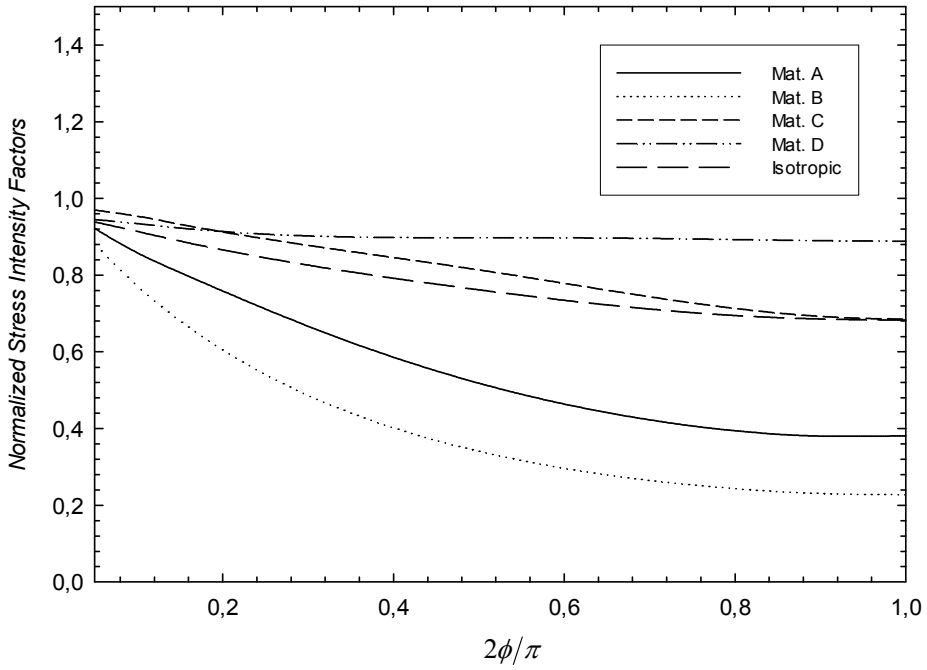

Figure 4 . 26 Uniform tension, K_{In} versus ϕ for a/h=0.2, a/c=3/2

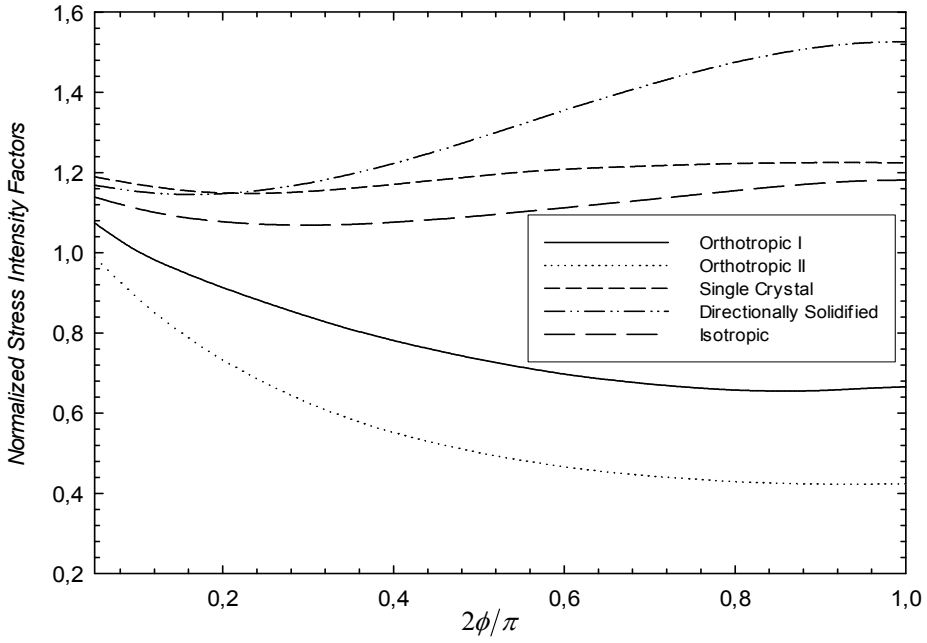

Figure 4 . 27 Uniform tension, K_{In} versus ϕ for a/h=0.4, a/c=2/3

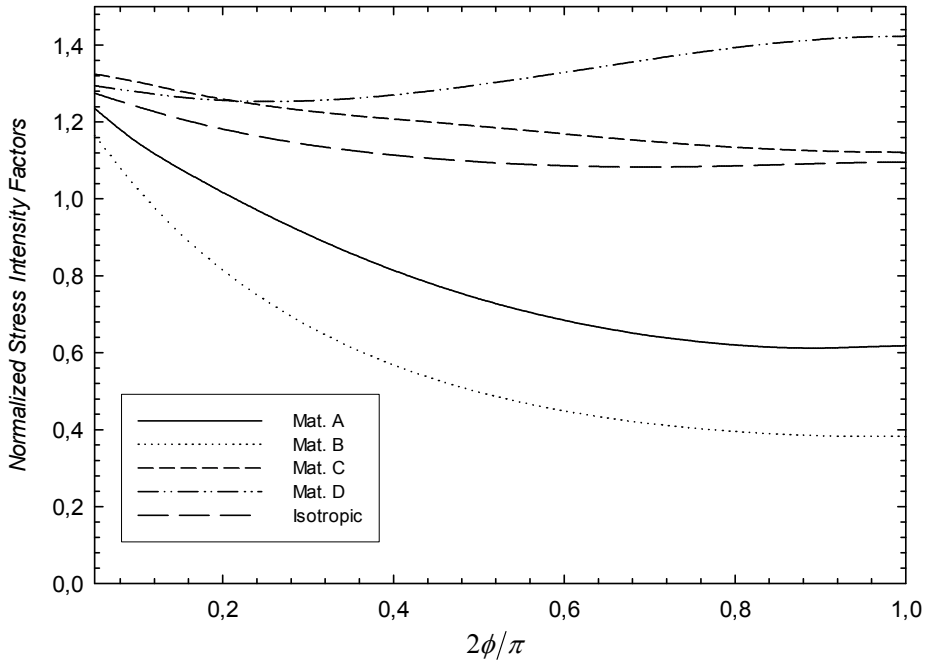

Figure 4 . 28 Uniform tension, K_{In} versus ϕ for a/h=0.4, a/c=1

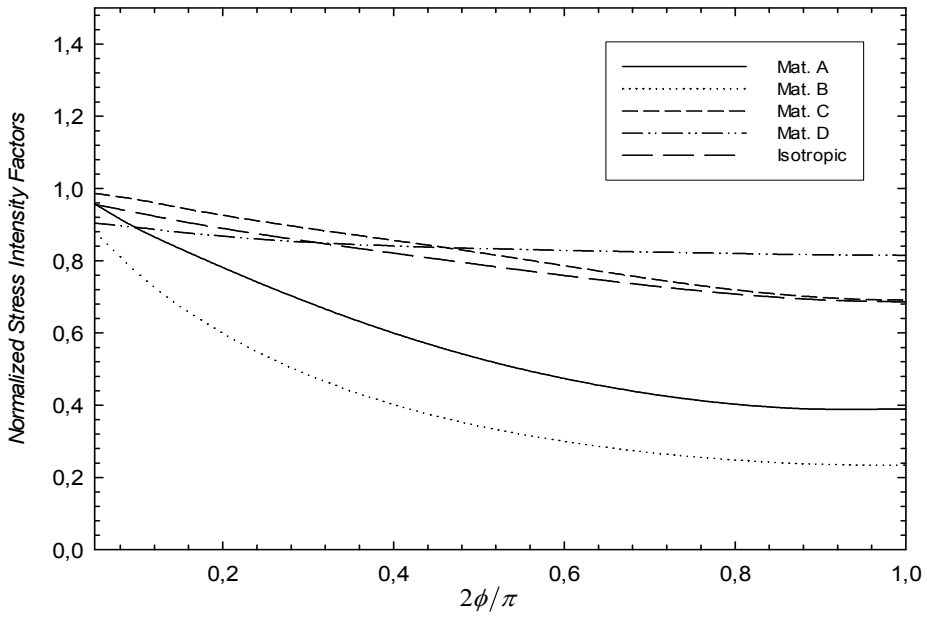

Figure 4 . 29 Uniform tension, K_{In} versus ϕ for a/h=0.4, a/c=3/2

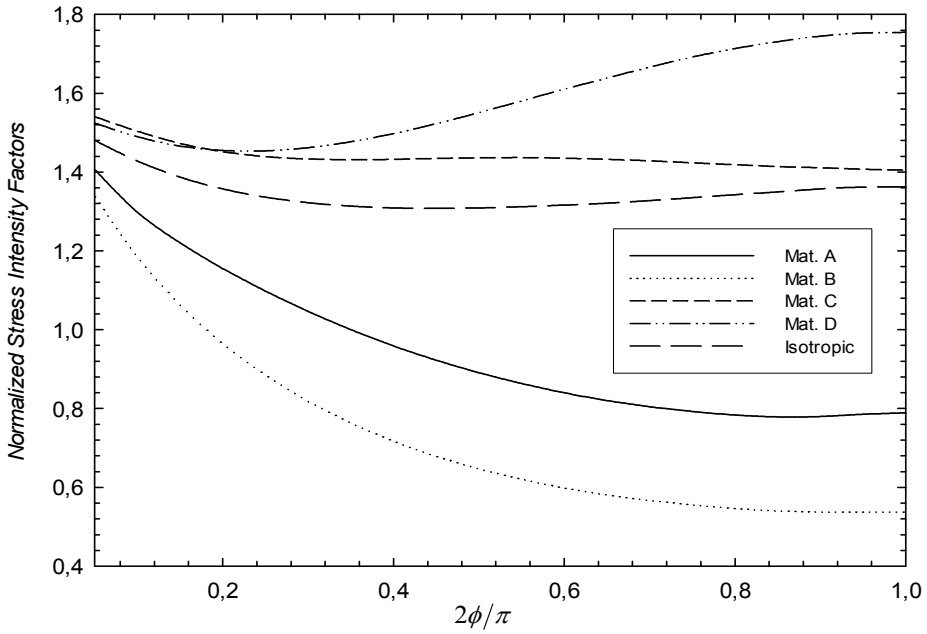

Figure 4 . 30 Uniform tension, K_{In} versus ϕ for a/h=0.6, a/c=2/3

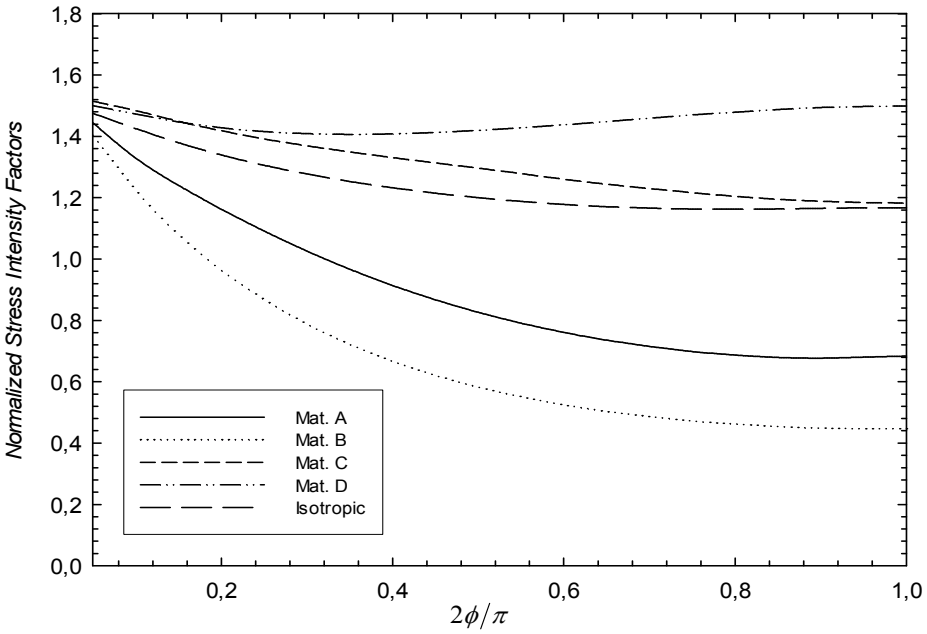

Figure 4 . 31 Uniform tension, K_{In} versus ϕ for a/h=0.6, a/c=1

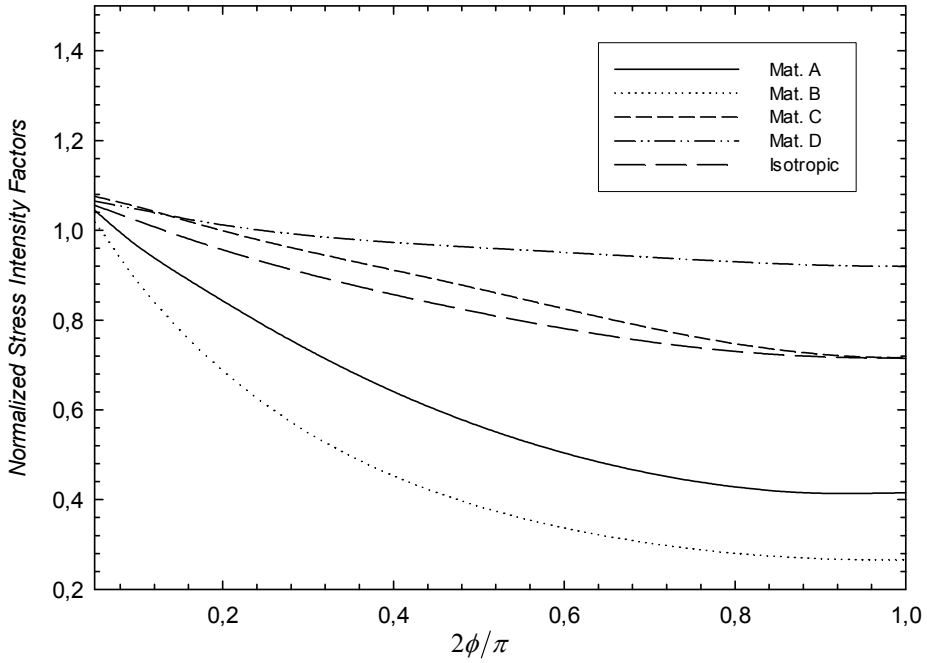

Figure 4 . 32 Uniform tension, K_{In} versus ϕ for a/h=0.6, a/c=3/2

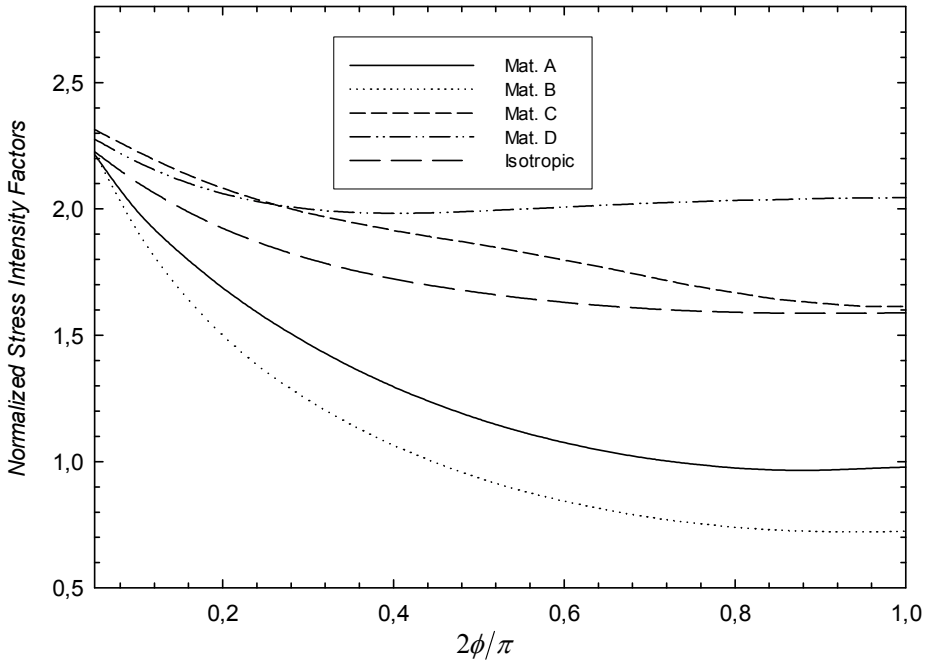

Figure 4 . 33 Uniform tension, K_{In} versus ϕ for a/h=0.8, a/c=2/3

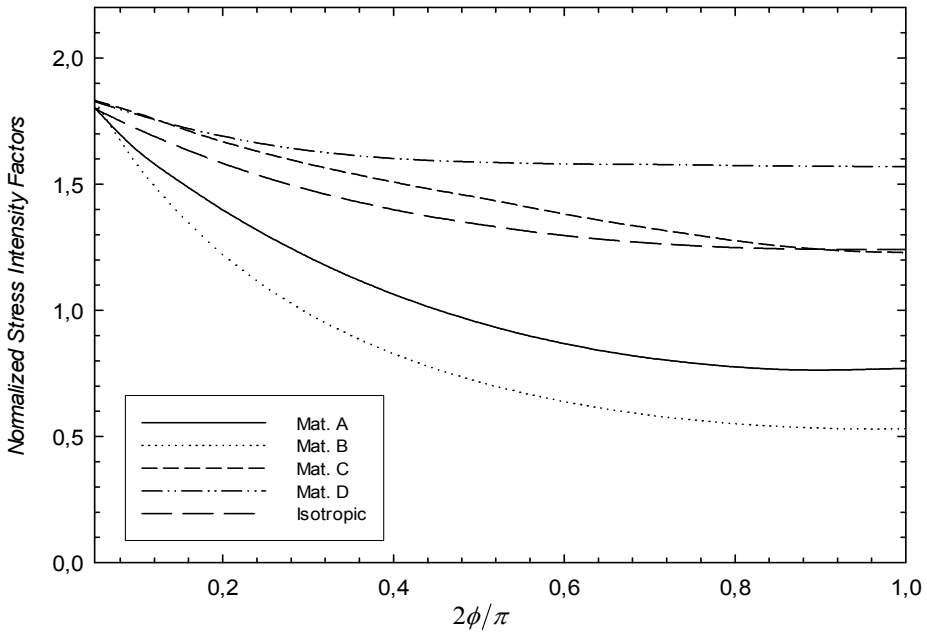

Figure 4 . 34 Uniform tension, K_{In} versus ϕ for a/h=0.8, a/c=1

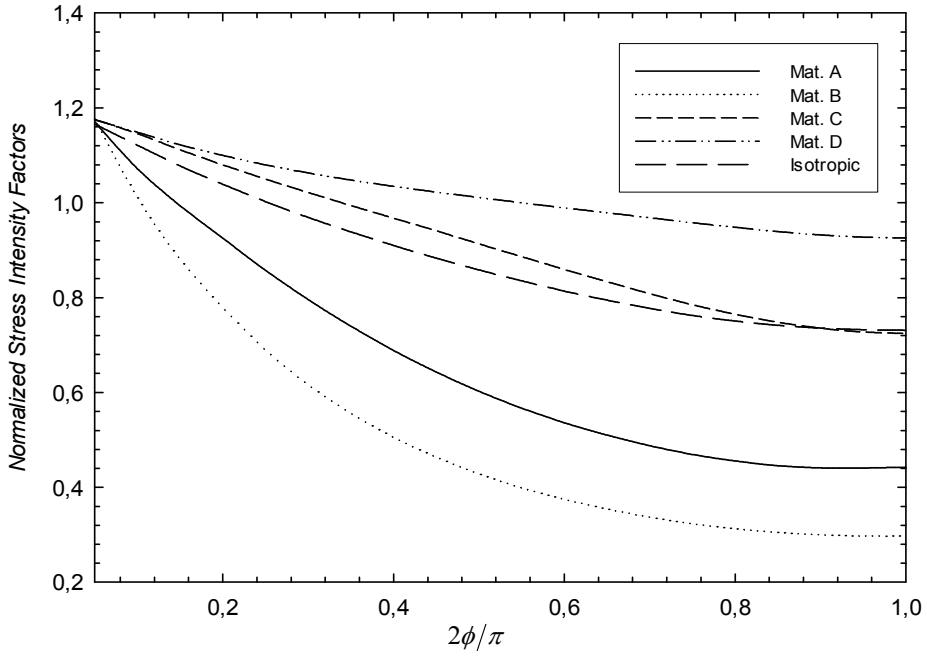

Figure 4 . 35 Uniform tension, K_{In} versus ϕ for a/h=0.8, a/c=3/2

4.6.1.2 Fixed Grip Tension on the Three-Dimensional Orthotropic Material

In this section, stress intensity factors are calculated for three-dimensional orthotropic and isotropic materials under fixed grip tension.

The materials are chosen same with the numerical reference solution [32]. The properties are given in Table 4.18. For isotropic case elastic modulus is chosen as $E = 206.84x10^9\ Pa\ (30x10^6 psi)$ and Poisson's ratio $v = 0.25$.

The edge crack is embedded in the orthotropic medium. Fixed grip tension loading type is applied by amount normal displacement v_0. The displacement is applied at the ends $y = \pm l$ as shown in Figure 4.36. The uniform normal displacement is taken as 0.0001 mm. The width of the strip is $2a$ and the crack depth is a.

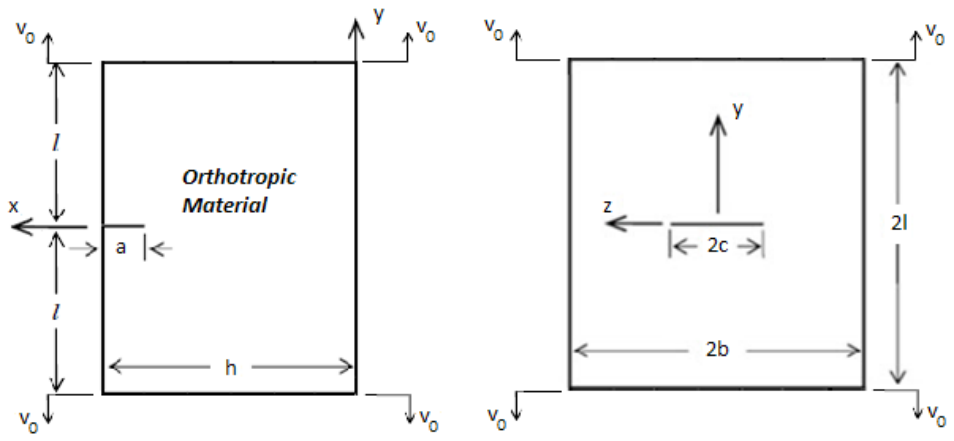

Figure 4 . 36 Orthotropic body subjected to fixed grip tension at the ends $y = \pm l$

For fixed grip tension, normalized mode I stress intensity factor can be defined in the below expression. The elastic modulus is used parallel to the direction of the applied load for crack opening type of loading.

$$K_{ln} = \frac{K_I}{E_y\,(v_0/l)\sqrt{\frac{\pi\,a}{Q}}} \tag{4.3}$$

Normalized mode I stress intensity factors for three-dimensional orthotropic materials subjected to fixed grip tension are given in Table 4.25 – Table 4.30.

Table 4 . 25 Normalized mode I stress intensity factors K_{ln} for three-dimensional models subjected to fixed grip tension.

	a/h=0.2, a/c=2/3					*a/h=0.4, a/c=2/3*				
$2\phi/\pi$	*Mat. A*	*Mat. B*	*Mat. C*	*Mat. D.*	*Isotropic*	*Mat. A*	*Mat. B*	*Mat. C*	*Mat. D.*	*Isotropic*
0.05	1.056	0.919	0.986	0.970	0.982	1.089	0.941	1.022	0.999	1.007
0.10	0.927	0.844	1.033	0.997	0.978	0.954	0.863	1.102	1.046	1.018
0.15	0.871	0.758	1.020	0.988	0.957	0.894	0.775	1.086	1.033	0.994
0.20	0.831	0.685	1.010	0.986	0.943	0.851	0.701	1.074	1.029	0.977
0.25	0.797	0.624	1.008	0.992	0.936	0.815	0.640	1.069	1.032	0.968
0.30	0.765	0.574	1.011	1.006	0.935	0.783	0.589	1.070	1.043	0.964
0.35	0.737	0.532	1.018	1.025	0.937	0.753	0.546	1.076	1.060	0.964
0.40	0.711	0.498	1.028	1.049	0.943	0.726	0.511	1.085	1.082	0.967
0.45	0.688	0.470	1.040	1.077	0.951	0.702	0.482	1.096	1.108	0.974
0.50	0.667	0.446	1.053	1.108	0.960	0.680	0.458	1.107	1.137	0.982
0.55	0.648	0.426	1.065	1.140	0.971	0.661	0.438	1.118	1.169	0.991
0.60	0.631	0.409	1.075	1.174	0.982	0.643	0.421	1.128	1.201	1.002
0.65	0.617	0.396	1.085	1.209	0.994	0.628	0.407	1.136	1.234	1.012
0.70	0.605	0.384	1.092	1.242	1.005	0.616	0.395	1.141	1.265	1.022
0.75	0.595	0.375	1.098	1.273	1.017	0.606	0.386	1.145	1.295	1.033
0.80	0.588	0.368	1.103	1.302	1.028	0.599	0.379	1.149	1.323	1.044
0.85	0.583	0.363	1.106	1.328	1.039	0.593	0.373	1.152	1.348	1.054
0.90	0.581	0.359	1.109	1.349	1.049	0.591	0.370	1.154	1.368	1.064
0.95	0.582	0.357	1.110	1.364	1.057	0.592	0.368	1.155	1.384	1.072
1.00	0.586	0.356	1.112	1.374	1.062	0.597	0.367	1.155	1.393	1.077

Table 4 . 26 Normalized mode I stress intensity factors K_{In} for three-dimensional models subjected to fixed grip tension.

	a/h=0.2, a/c=1					a/h=0.4, a/c=1				
$2\phi/\pi$	*Mat. A*	*Mat. B*	*Mat. C*	*Mat. D.*	Isotropic	*Mat. A*	*Mat. B*	*Mat. C*	*Mat. D.*	Isotropic
0.05	1.279	1.168	1.149	1.131	1.159	1.306	1.193	1.160	1.144	1.169
0.10	1.129	1.049	1.224	1.182	1.169	1.151	1.070	1.273	1.218	1.198
0.15	1.051	0.926	1.209	1.171	1.140	1.070	0.943	1.255	1.204	1.167
0.20	0.991	0.823	1.189	1.162	1.114	1.007	0.838	1.232	1.192	1.138
0.25	0.938	0.738	1.173	1.158	1.093	0.951	0.751	1.214	1.186	1.114
0.30	0.887	0.667	1.160	1.159	1.075	0.899	0.679	1.198	1.184	1.095
0.35	0.839	0.607	1.150	1.164	1.061	0.851	0.618	1.186	1.187	1.079
0.40	0.795	0.556	1.142	1.173	1.049	0.806	0.567	1.176	1.194	1.066
0.45	0.755	0.514	1.135	1.185	1.040	0.766	0.525	1.168	1.205	1.055
0.50	0.720	0.479	1.128	1.200	1.034	0.729	0.490	1.160	1.218	1.047
0.55	0.688	0.449	1.122	1.216	1.029	0.697	0.460	1.151	1.232	1.041
0.60	0.660	0.425	1.114	1.234	1.025	0.670	0.436	1.143	1.248	1.036
0.65	0.637	0.405	1.107	1.253	1.023	0.646	0.416	1.134	1.265	1.033
0.70	0.616	0.388	1.099	1.271	1.022	0.626	0.399	1.124	1.282	1.032
0.75	0.600	0.374	1.091	1.289	1.023	0.609	0.386	1.116	1.299	1.032
0.80	0.586	0.363	1.084	1.306	1.025	0.596	0.375	1.109	1.316	1.033
0.85	0.577	0.355	1.078	1.321	1.028	0.587	0.367	1.102	1.330	1.036
0.90	0.571	0.349	1.073	1.334	1.031	0.581	0.361	1.097	1.342	1.039
0.95	0.569	0.344	1.069	1.344	1.035	0.579	0.357	1.093	1.352	1.042
1.00	0.572	0.343	1.067	1.350	1.038	0.582	0.356	1.091	1.357	1.045

Table 4 . 27 Normalized mode I stress intensity factors K_{In} for three-dimensional models subjected to fixed grip tension.

	a/h=0.2, a/c=3/2					a/h=0.4, a/c=3/2				
$2\phi/\pi$	*Mat. A*	*Mat. B*	*Mat. C*	*Mat. D.*	Isotropic	*Mat. A*	*Mat. B*	*Mat. C*	*Mat. D.*	Isotropic
0.05	1.025	0.980	0.904	0.895	0.919	1.034	0.987	0.892	0.891	0.915
0.10	0.916	0.874	0.967	0.941	0.934	0.924	0.880	0.985	0.955	0.946
0.15	0.853	0.766	0.951	0.930	0.910	0.859	0.771	0.968	0.944	0.920
0.20	0.802	0.676	0.930	0.919	0.885	0.807	0.680	0.946	0.931	0.894
0.25	0.754	0.601	0.910	0.910	0.862	0.759	0.605	0.925	0.921	0.871
0.30	0.708	0.537	0.892	0.903	0.841	0.712	0.540	0.906	0.914	0.849
0.35	0.663	0.483	0.875	0.899	0.822	0.667	0.486	0.889	0.908	0.829
0.40	0.621	0.438	0.859	0.896	0.805	0.625	0.440	0.872	0.905	0.811
0.45	0.583	0.399	0.844	0.895	0.789	0.586	0.402	0.855	0.902	0.794
0.50	0.548	0.367	0.828	0.894	0.773	0.550	0.369	0.839	0.901	0.778
0.55	0.516	0.339	0.812	0.894	0.759	0.518	0.341	0.822	0.900	0.763
0.60	0.487	0.315	0.795	0.894	0.745	0.489	0.318	0.804	0.899	0.748
0.65	0.462	0.295	0.777	0.894	0.732	0.464	0.298	0.785	0.898	0.735
0.70	0.440	0.278	0.759	0.893	0.720	0.442	0.281	0.767	0.896	0.722
0.75	0.421	0.263	0.742	0.892	0.709	0.423	0.267	0.750	0.895	0.711
0.80	0.405	0.252	0.726	0.891	0.700	0.408	0.256	0.733	0.893	0.702
0.85	0.392	0.242	0.712	0.889	0.692	0.396	0.247	0.719	0.891	0.694
0.90	0.383	0.235	0.700	0.888	0.687	0.387	0.240	0.707	0.889	0.688
0.95	0.379	0.230	0.691	0.886	0.683	0.382	0.235	0.698	0.888	0.685
1.00	0.378	0.227	0.686	0.886	0.681	0.382	0.233	0.693	0.887	0.683

Table 4 . 28 Normalized mode I stress intensity factors K_{In} for three-dimensional models subjected to fixed grip tension.

	a/h=0.6, a/c=2/3					a/h=0.8, a/c=2/3				
$2\phi/\pi$	*Mat. A*	*Mat. B*	*Mat. C*	*Mat. D.*	Isotropic	*Mat. A*	*Mat. B*	*Mat. C*	*Mat. D.*	Isotropic
0.05	1.137	0.984	1.111	1.043	1.047	1.209	1.042	1.216	1.077	1.089
0.10	0.991	0.895	1.213	1.097	1.062	1.040	0.932	1.332	1.129	1.099
0.15	0.922	0.798	1.190	1.079	1.032	0.954	0.820	1.298	1.101	1.055
0.20	0.874	0.718	1.172	1.069	1.009	0.895	0.732	1.268	1.082	1.023
0.25	0.833	0.653	1.161	1.068	0.994	0.845	0.661	1.246	1.072	0.999
0.30	0.798	0.601	1.158	1.075	0.986	0.802	0.603	1.231	1.072	0.983
0.35	0.765	0.556	1.159	1.088	0.983	0.764	0.556	1.222	1.078	0.972
0.40	0.736	0.519	1.164	1.106	0.983	0.729	0.515	1.218	1.089	0.966
0.45	0.709	0.488	1.171	1.129	0.985	0.698	0.481	1.216	1.106	0.963
0.50	0.685	0.463	1.179	1.155	0.991	0.670	0.452	1.216	1.126	0.962
0.55	0.664	0.442	1.187	1.182	0.997	0.645	0.428	1.216	1.147	0.963
0.60	0.646	0.424	1.193	1.211	1.004	0.623	0.407	1.214	1.168	0.965
0.65	0.630	0.409	1.196	1.239	1.012	0.604	0.389	1.209	1.190	0.968
0.70	0.616	0.397	1.198	1.266	1.020	0.587	0.374	1.203	1.210	0.971
0.75	0.605	0.387	1.199	1.292	1.028	0.574	0.361	1.194	1.229	0.974
0.80	0.597	0.379	1.199	1.316	1.037	0.564	0.351	1.184	1.245	0.979
0.85	0.590	0.372	1.198	1.336	1.045	0.556	0.343	1.176	1.260	0.983
0.90	0.587	0.367	1.196	1.353	1.053	0.552	0.337	1.167	1.272	0.987
0.95	0.587	0.365	1.195	1.366	1.060	0.552	0.333	1.164	1.281	0.992
1.00	0.592	0.364	1.193	1.373	1.064	0.555	0.332	1.159	1.287	0.995

Table 4 . 29 Normalized mode I stress intensity factors K_{In} for three-dimensional models subjected to fixed grip tension.

	a/h=0.6, a/c=1					a/h=0.8, a/c=1				
$2\phi/\pi$	*Mat. A*	*Mat. B*	*Mat. C*	*Mat. D.*	Isotropic	*Mat. A*	*Mat. B*	*Mat. C*	*Mat. D.*	Isotropic
0.05	1.338	1.222	1.207	1.172	1.194	1.362	1.238	1.275	1.189	1.212
0.10	1.176	1.092	1.347	1.257	1.232	1.185	1.094	1.429	1.277	1.248
0.15	1.087	0.958	1.324	1.239	1.195	1.086	0.954	1.400	1.253	1.204
0.20	1.020	0.849	1.297	1.223	1.162	1.017	0.847	1.365	1.231	1.165
0.25	0.961	0.761	1.274	1.212	1.133	0.954	0.757	1.332	1.216	1.132
0.30	0.907	0.688	1.254	1.206	1.110	0.899	0.683	1.306	1.206	1.105
0.35	0.857	0.626	1.238	1.206	1.091	0.847	0.622	1.283	1.201	1.081
0.40	0.811	0.576	1.224	1.209	1.075	0.801	0.571	1.263	1.200	1.063
0.45	0.770	0.533	1.211	1.216	1.062	0.760	0.529	1.246	1.203	1.047
0.50	0.734	0.498	1.199	1.225	1.051	0.723	0.494	1.229	1.208	1.034
0.55	0.702	0.469	1.187	1.236	1.043	0.691	0.465	1.215	1.216	1.024
0.60	0.674	0.445	1.174	1.248	1.036	0.663	0.440	1.197	1.225	1.015
0.65	0.650	0.425	1.161	1.261	1.031	0.640	0.420	1.178	1.234	1.008
0.70	0.630	0.408	1.149	1.274	1.028	0.619	0.403	1.161	1.243	1.002
0.75	0.614	0.396	1.138	1.288	1.026	0.603	0.388	1.146	1.252	0.999
0.80	0.601	0.385	1.128	1.300	1.026	0.591	0.378	1.131	1.260	0.998
0.85	0.591	0.377	1.119	1.311	1.027	0.581	0.369	1.116	1.266	0.997
0.90	0.586	0.371	1.111	1.321	1.030	0.575	0.362	1.103	1.271	0.997
0.95	0.584	0.367	1.106	1.328	1.033	0.574	0.358	1.093	1.274	0.999
1.00	0.587	0.365	1.103	1.332	1.035	0.576	0.356	1.088	1.276	1.000

Table 4 . 30 Normalized mode I stress intensity factors K_{In} for three-dimensional models subjected to fixed grip tension.

	a/h=0.6, a/c=3/2					a/h=0.8, a/c=3/2				
$2\phi/\pi$	*Mat. A*	*Mat. B*	*Mat. C*	*Mat. D.*	Isotropic	*Mat. A*	*Mat. B*	*Mat. C*	*Mat. D.*	Isotropic
0.05	1.048	1.000	0.910	0.903	0.926	1.051	0.999	0.929	0.906	0.927
0.10	0.934	0.888	1.017	0.975	0.963	0.934	0.887	1.049	0.983	0.968
0.15	0.865	0.774	0.997	0.961	0.934	0.861	0.769	1.026	0.967	0.936
0.20	0.811	0.682	0.973	0.946	0.905	0.804	0.676	1.000	0.950	0.905
0.25	0.761	0.605	0.950	0.933	0.879	0.755	0.603	0.976	0.936	0.879
0.30	0.713	0.541	0.929	0.924	0.856	0.706	0.538	0.953	0.925	0.853
0.35	0.667	0.487	0.909	0.916	0.834	0.661	0.485	0.932	0.916	0.831
0.40	0.625	0.442	0.891	0.911	0.815	0.619	0.440	0.911	0.909	0.810
0.45	0.586	0.404	0.873	0.907	0.796	0.580	0.403	0.890	0.903	0.790
0.50	0.551	0.372	0.855	0.903	0.779	0.546	0.372	0.870	0.898	0.772
0.55	0.519	0.346	0.836	0.900	0.763	0.515	0.346	0.848	0.893	0.755
0.60	0.491	0.323	0.816	0.897	0.748	0.487	0.324	0.826	0.888	0.739
0.65	0.466	0.304	0.796	0.894	0.733	0.463	0.306	0.804	0.883	0.724
0.70	0.445	0.288	0.776	0.891	0.720	0.443	0.291	0.783	0.878	0.710
0.75	0.426	0.275	0.757	0.888	0.708	0.425	0.278	0.762	0.873	0.698
0.80	0.411	0.264	0.740	0.884	0.698	0.410	0.268	0.742	0.867	0.687
0.85	0.399	0.255	0.724	0.881	0.690	0.399	0.260	0.725	0.862	0.678
0.90	0.391	0.249	0.712	0.878	0.684	0.391	0.254	0.711	0.856	0.672
0.95	0.386	0.244	0.703	0.875	0.680	0.388	0.250	0.700	0.852	0.668
1.00	0.386	0.242	0.697	0.874	0.678	0.388	0.248	0.693	0.849	0.665

Tabulated results for fixed grip tension case are shown in Figure 4.37 – Figure 4.48.

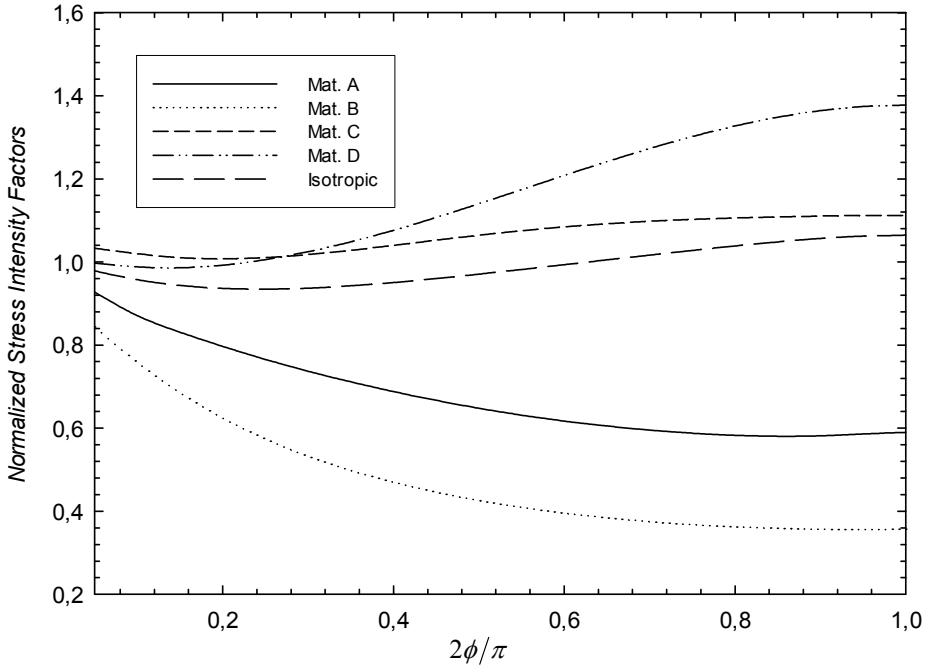

Figure 4 . 37 Fixed grip tension, K_{In} versus ϕ for a/h=0.2, a/c=2/3

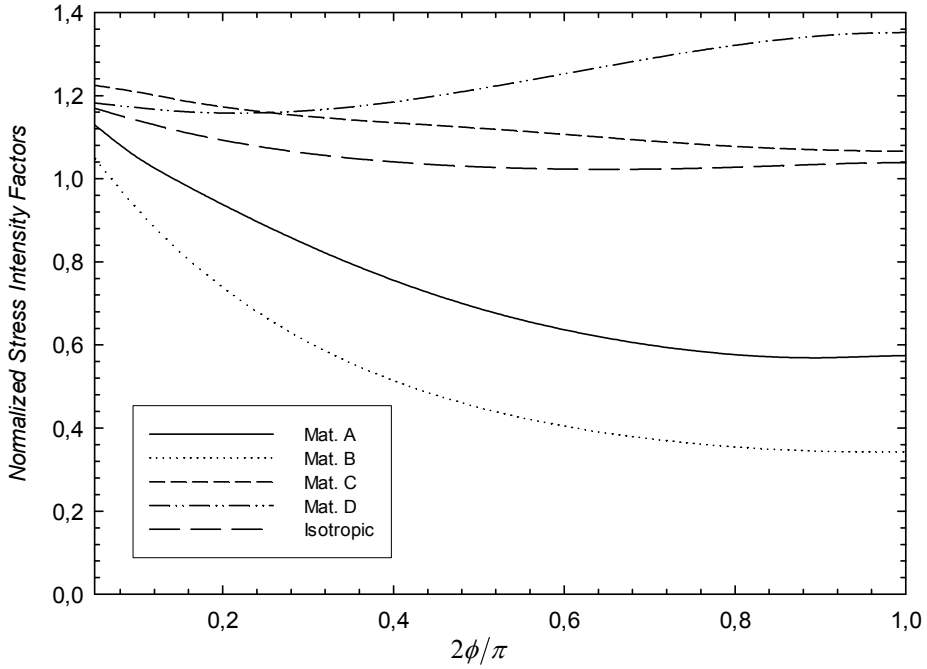

Figure 4 . 38 Fixed grip tension, K_{In} versus ϕ for a/h=0.2, a/c=1

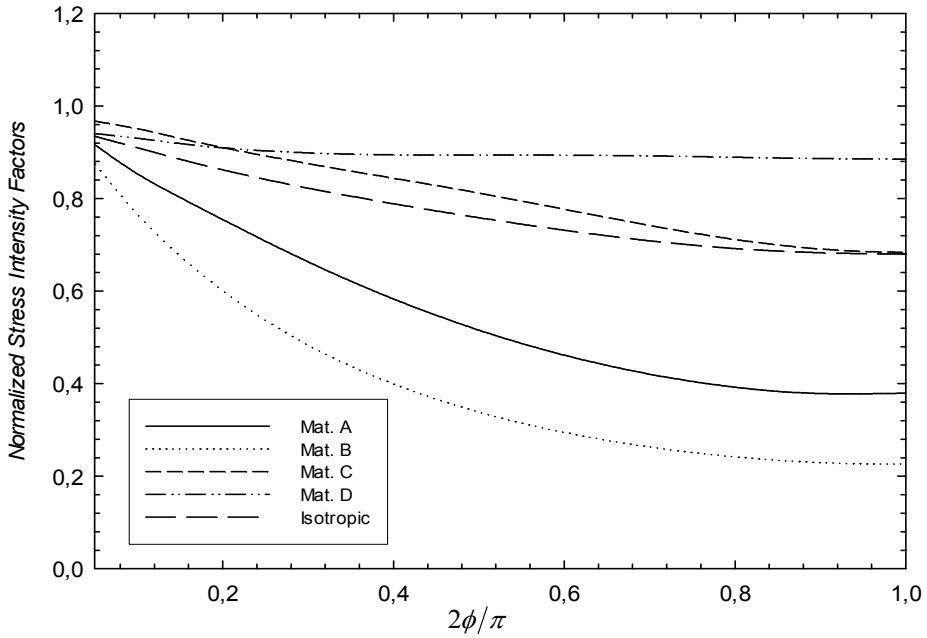

Figure 4 . 39 Fixed grip tension, K_{In} versus ϕ for a/h=0.2, a/c=3/2

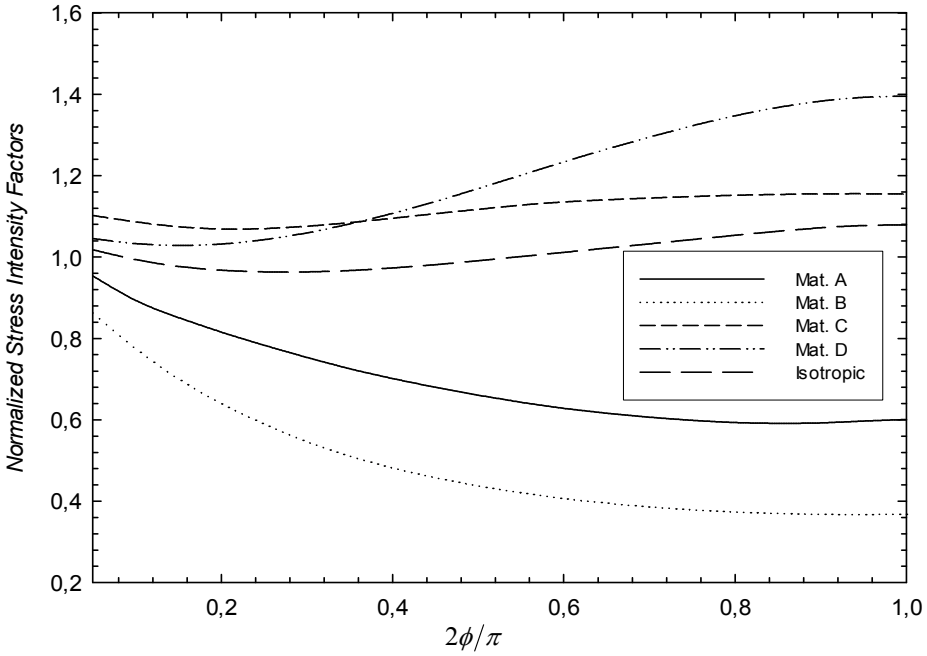

Figure 4 . 40 Fixed grip tension, K_{In} versus ϕ for a/h=0.4, a/c=2/3

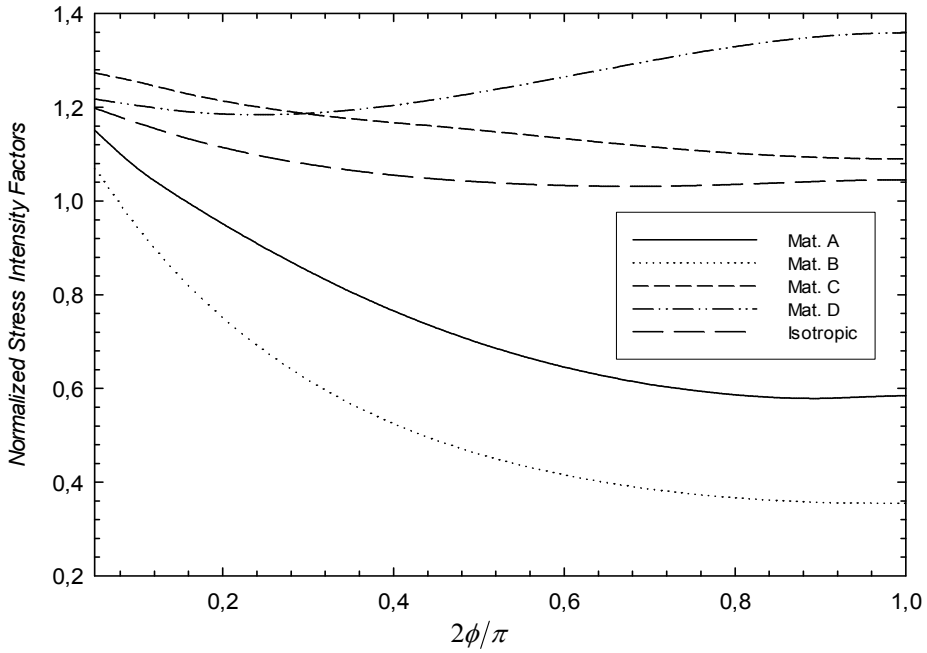

Figure 4 . 41 Fixed grip tension, K_{In} versus ϕ for a/h=0.4, a/c=1

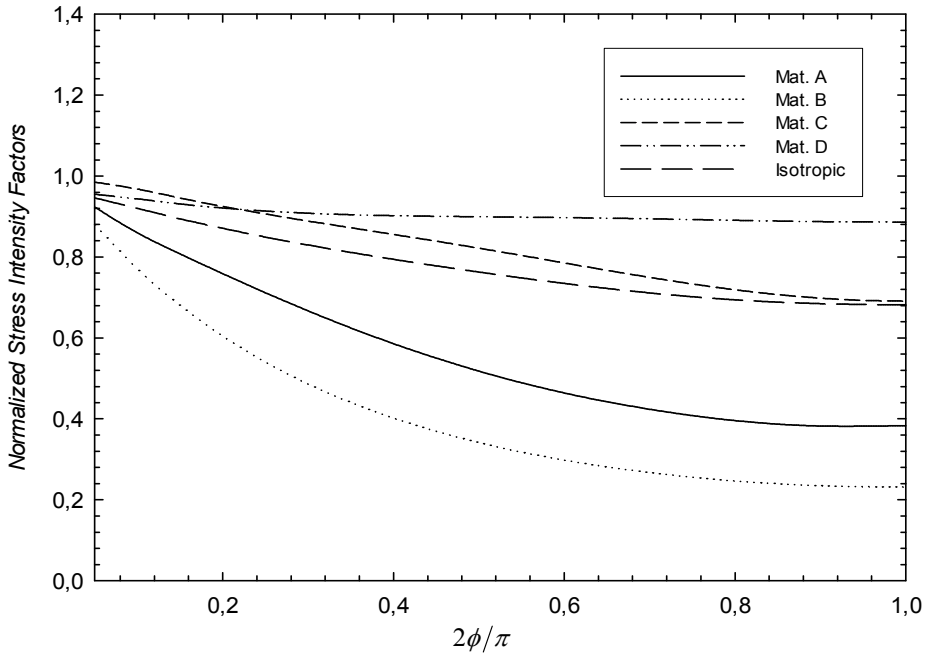

Figure 4 . 42 Fixed grip tension, K_{In} versus ϕ for a/h=0.4, a/c=3/2

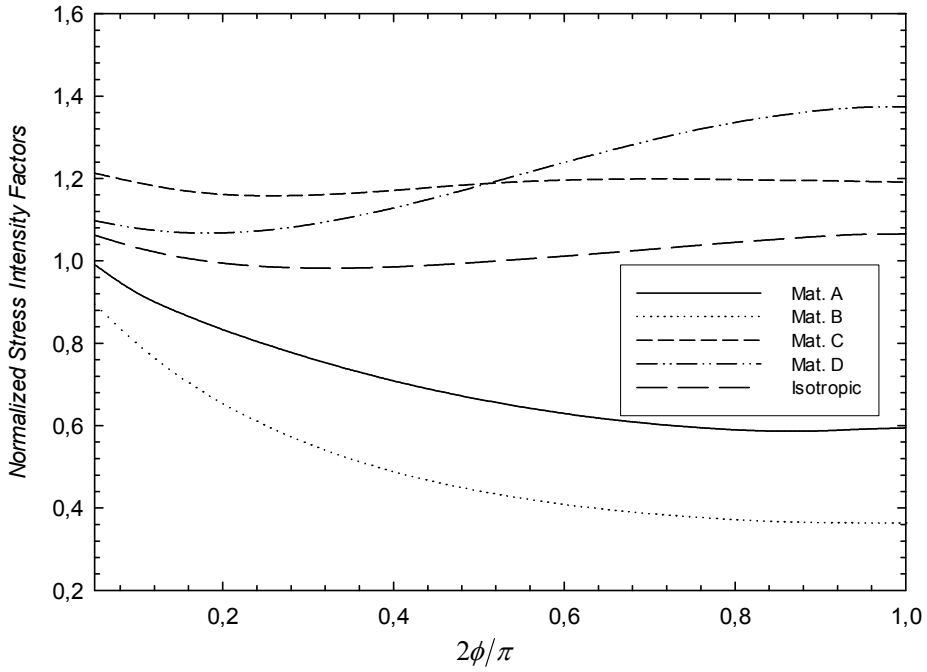

Figure 4 . 43 Fixed grip tension, K_{In} versus ϕ for a/h=0.6, a/c=2/3

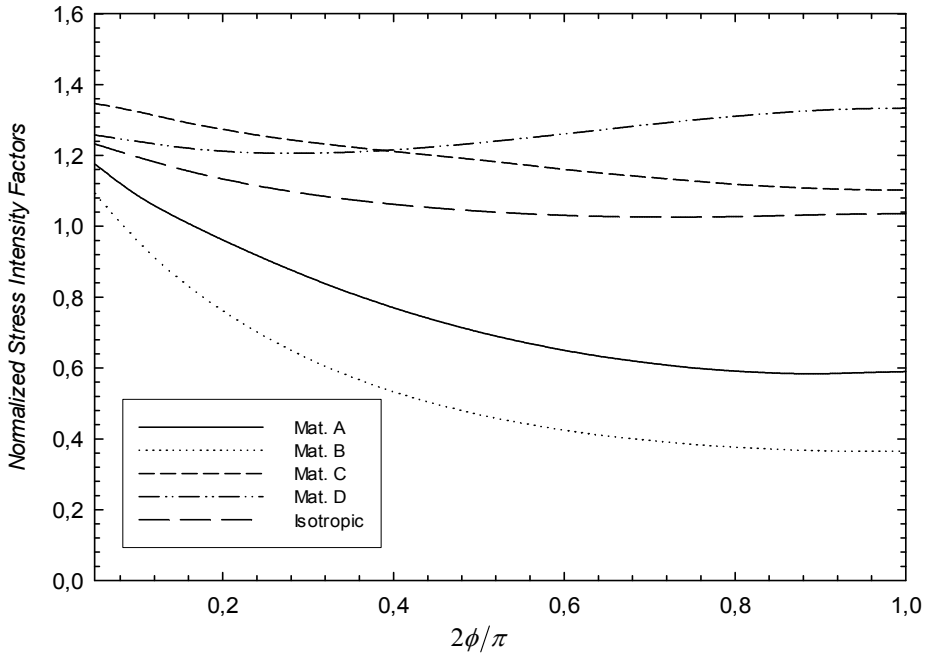

Figure 4 . 44 Fixed grip tension, K_{In} versus ϕ for a/h=0.6, a/c=1

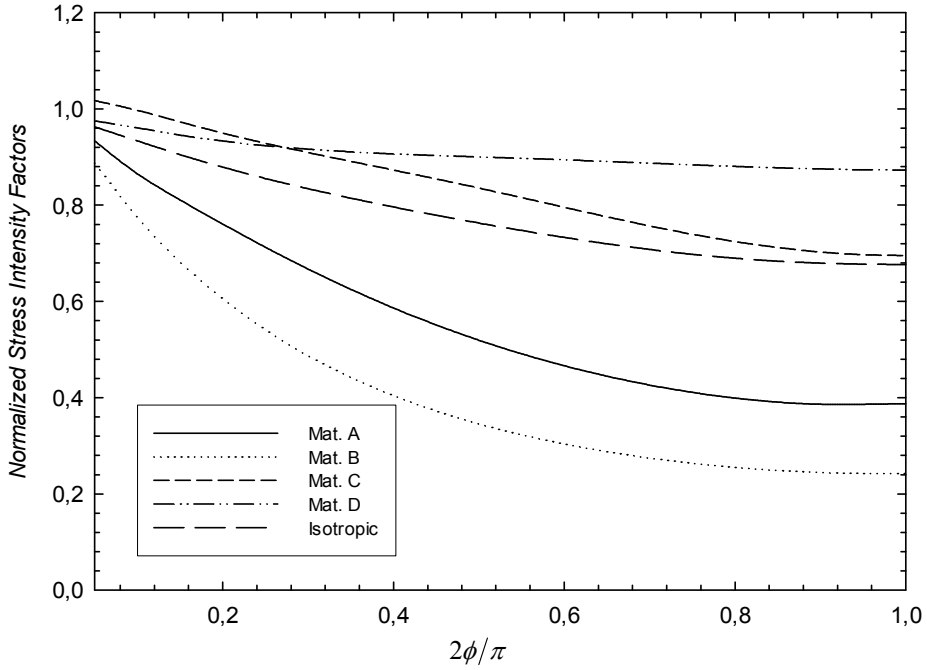

Figure 4 . 45 Fixed grip tension, K_{In} versus ϕ for a/h=0.6, a/c=3/2

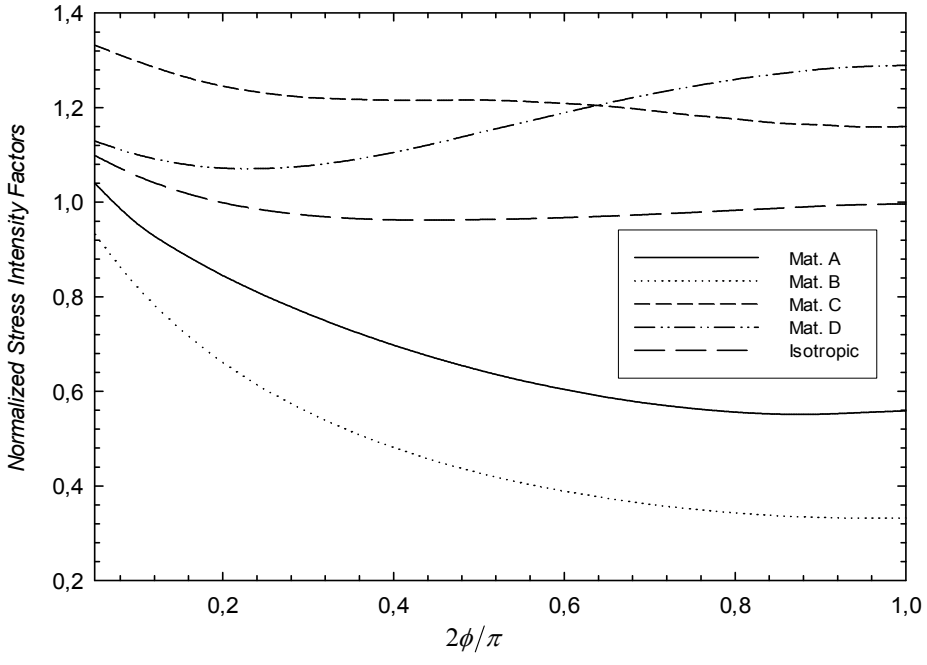

Figure 4 . 46 Fixed grip tension, K_{In} versus ϕ for a/h=0.8, a/c=2/3

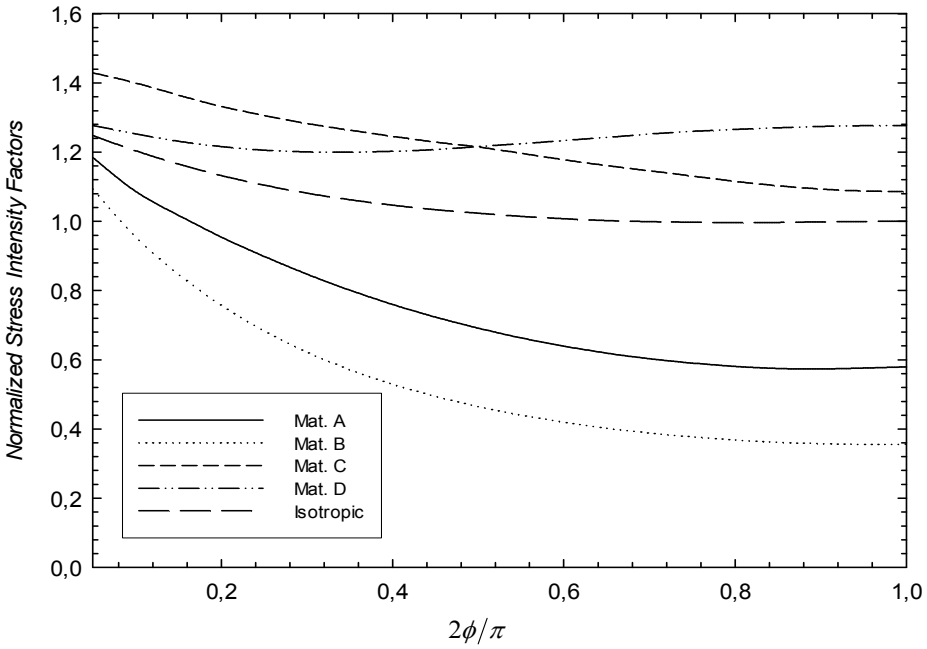

Figure 4 . 47 Fixed grip tension, K_{In} versus ϕ for a/h=0.8, a/c=1

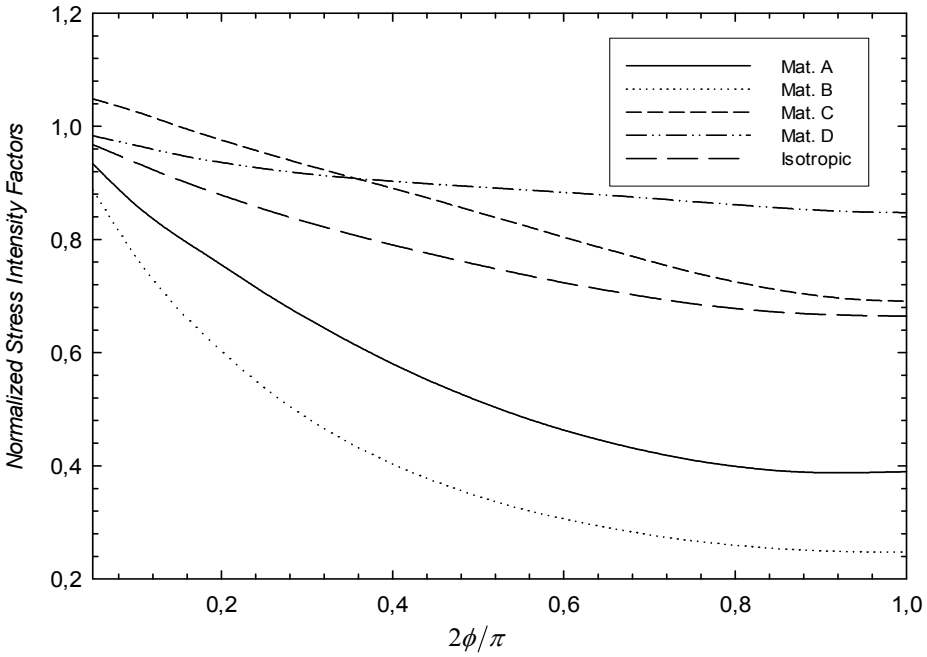

Figure 4 . 48 Fixed grip tension, K_{In} versus ϕ for a/h=0.8, a/c=3/2

4.6.2 Thermal Loading on the Three-Dimensional Orthotropic Material

In this type of loading condition, orthotropic medium is Polystal. It is glass fiber woven fabric reinforced PA-6. For this type of material seven thermal properties are given, namely, the specific heat capacity c_p, the thermal conductivity in the three principal material directions, k_1, k_2 and k_3, and similarly three thermal expansion coefficients, a_1, a_2 and a_3. To characterize an orthotropic material it is required to define nine mechanical properties, namely Elastic moduli, E_{11}, E_{22} and E_{33}, the Poisson's ratio v_{12}, v_{23} and v_{13}, and the shear moduli G_{12}, G_{23} and G_{13} [33]. The material properties are given in Table 4.31.

Table 4 . 31 Properties of Polystal vs. Temperature

Model		*Temperature (C)*			
		20	*80*	*120*	*220*
$E_{11}\ (MPa)$	*Fiber Undulation*	*24*	*20*	*29*	*19*
$E_{22}(MPa)$	Mosaic Series	19	13	12	12
$E_{33}(MPa)$	Inv rom	6.1	3.2	2.6	2.4
$G_{12}(GPa)$	Fiber Undulation	3.1	1.6	1.3	1.2
$G_{23}(GPa)$	Assumed	2.5	1.5	1.4	1.2
$G_{13}(GPa)$	Assumed	2.5	1.5	1.4	1.2
v_{12}	Mosaic Series	0.16	0.11	0.10	0.11
v_{23}	Assumed	0.25	0.25	0.25	2.5
v_{13}	Assumed	0.25	0.25	0.25	2.5
$a_1 x10^6/C$	Experiment	14	14	13	13
$a_2\ x10^6/C$	Experiment	13	13	13	12
$a_3\ x10^6/C$	Rule of Mixtures	53	53	53	53
$k_1(W/mK)$	Knappe/Martinez	0.53	0.57	0.60	0.60
$k_2(W/mK)$	Knappe/Martinez	0.50	0.53	0.56	0.56
$k_3(W/mK)$	Knappe/Martinez	0.51	0.54	0.57	0.57
$c_p(kJ/kg\ K)$	Rule of Mixtures	1.2	1.2	1.2	2.9

In this type of loading condition, material is assumed as stress free at a temperature of 493 K. Then, the material is exposed to an environment with a temperature of 293 K. For this type of loading condition, the surface of the structure at which the crack exists, exposed to a forced convection. At the surface, $x = h$, the convection

coefficient is $h = 100$ W/(m^{2}K). At the other surfaces, there are free convection with a convection coefficient $h = 5$ W/(m^{2}K). For this type of loading, material properties calculated at the mid temperature, $T_m = 393$ K.

In transient problem, firstly, the temperature distribution is computed. These computed temperatures are used as an input for structural problem. The deformations and the displacements are computed to obtain stress intensity factors at the crack front.

The boundary conditions and the loading case are given in the Figure 4.49.

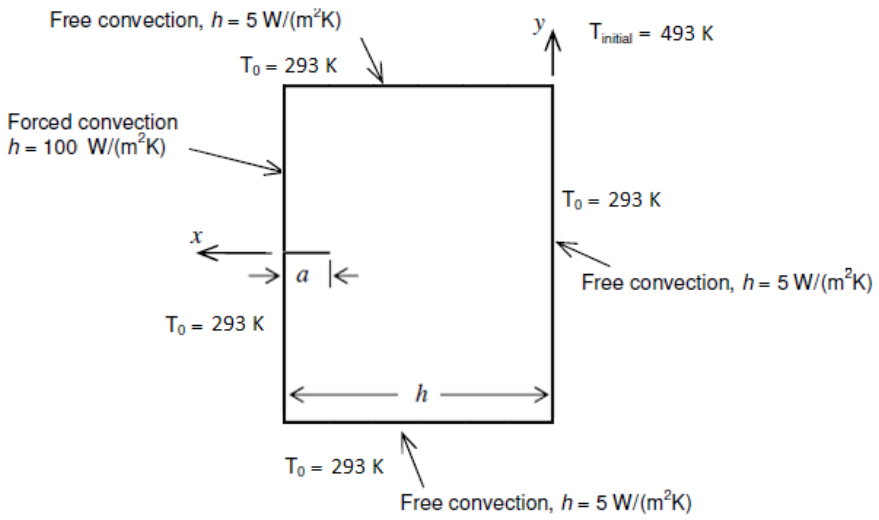

Figure 4 . 49 The boundary conditions for transient thermal loading

The geometry of the crack is semi-elliptic with an aspect ratio of $a/c = 1/2$. The crack depth to thickness ratio is chosen as $a/h = 0.4$. Material properties are given in Table 4.31.

After obtaining the stress intensity factors for the structure, normalized mode I stress intensity factors are calculated for transient thermal loading type by using the formula:

$$K_{ln} = \frac{K_I}{S\sqrt{\frac{\pi\, a}{Q}}} \tag{4.4}$$

where S is the normalization stress and described by

$$S = \alpha_y\, E_y\, T_m \tag{4.5}$$

where α and E are the thermal expansion coefficient and elastic modulus in the crack opening direction (y- direction), respectively. T_m is the mid temperature at which the mechanical and thermal propertie0s, that are given in Table 4.31,are used. For the transient part of the problem, to define normalized mode-I stress intensity factors, normalized time is defined by

$$\tau = \frac{D\, t}{h^2} \tag{4.6}$$

where t is the time and the thickness of the structure is h. In addition to these, D is the thermal diffusivity coefficient of the material defined by

$$D = \frac{k_{xy}}{\rho\, c_{xy}} \tag{4.7}$$

where k, ρ and c are the thermal diffusivity coefficients of the orthotropic material.

In the finite element code, anisotropic asymptotic field expressions and constants are used to obtain stress intensity factors. The variation of the normalized temperature and the normalized mode I stress intensity factor for at a given point around the crack front ($\phi = \pi/4$ and $\phi = \pi/2$) with respect to normalized time are shown in Figure 4.50 – Figure 4.53.

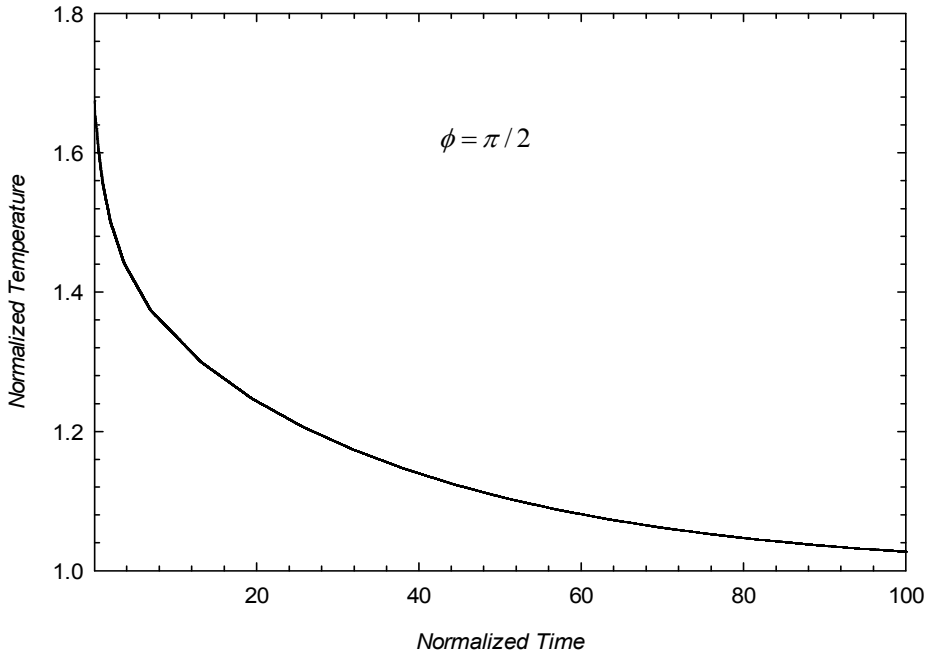

Figure 4 . 50 Temperature versus normalized time for thermal loading ($\phi = \pi/2$)

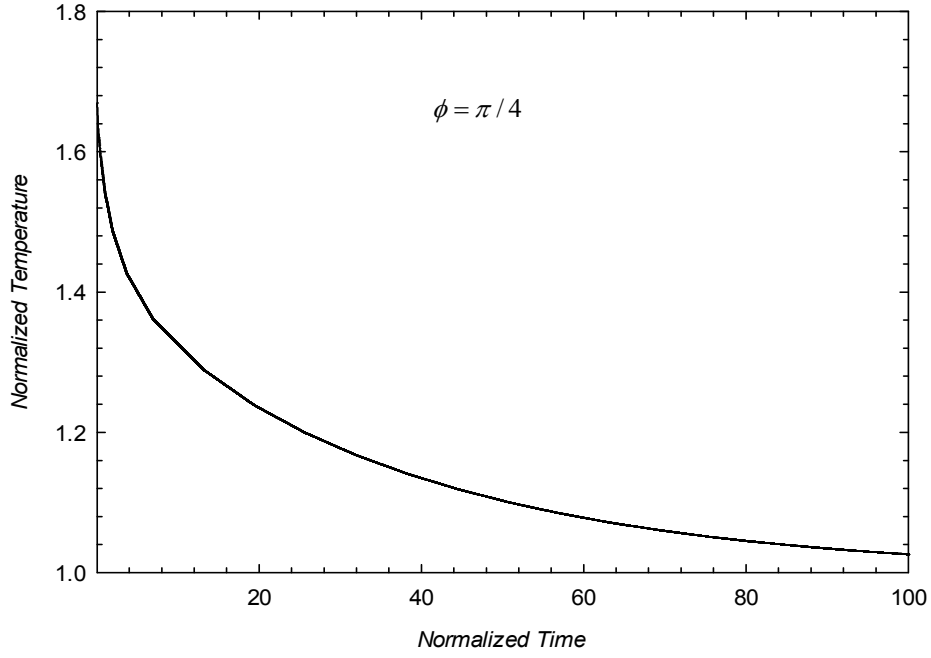

Figure 4 . 51 Temperature versus normalized time for thermal loading ($\phi = \pi/4$)

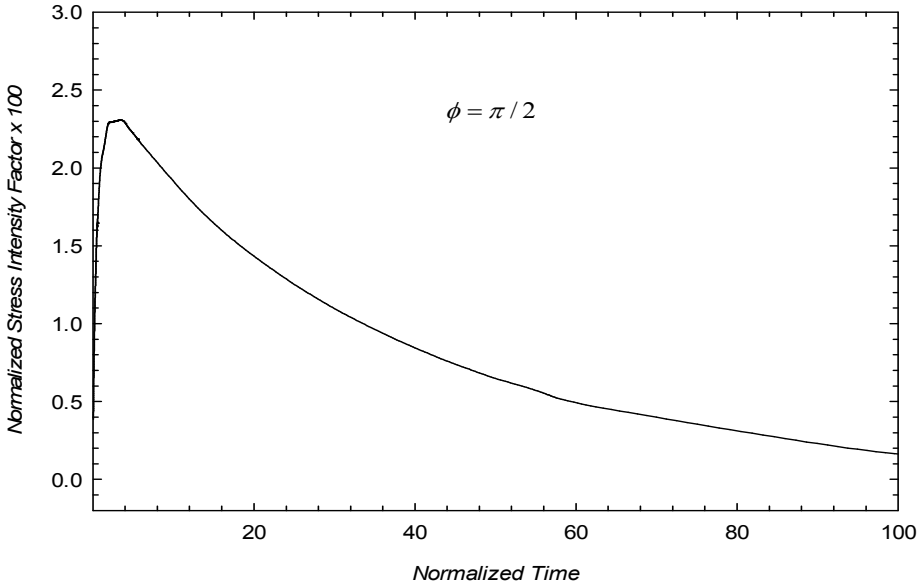

Figure 4 . 52 Normalized stress intensity factor vs. normalized time ($\phi = \pi/2$)

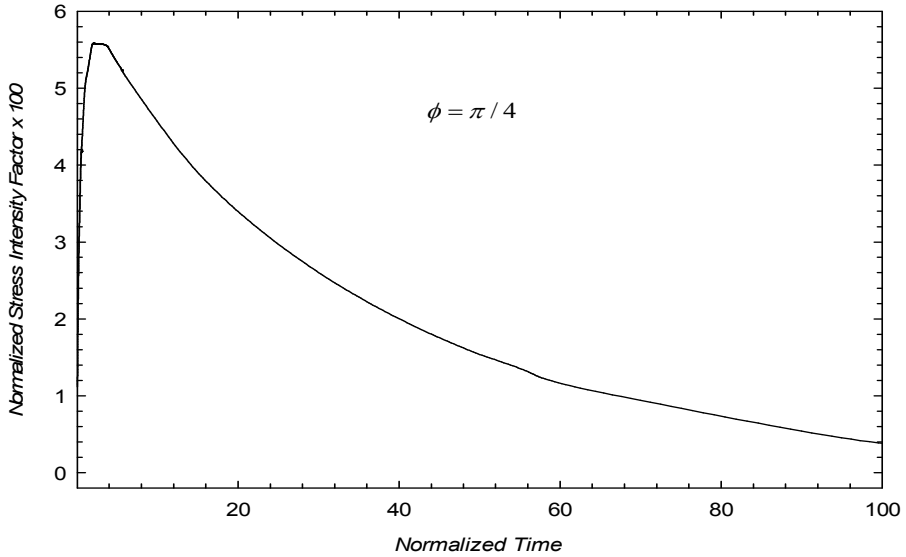

Figure 4 . 53 Normalized stress intensity factor vs. normalized time ($\phi = \pi/4$)

The tabulated results are given in Table 4.32.

Table 4 . 32 Normalized mode I stress intensity factors K_{In} for polystal material subjected to transient thermal load at $\tau = 0.0625$ and $\tau = 0.125$

$2\phi/\pi$	a/h=0.4, a/c=0.5 at $\tau = 0.0625$	a/h=0.4, a/c=0.5 at $\tau = 0.125$
	Polystal ($K_{In}x10^2$)	
0.00	0.1988	0.3131
0.10	0.1727	0.2791
0.20	0.1535	0.2554
0.30	0.1359	0.2320
0.40	0.1199	0.2094
0.50	0.1084	0.1932
0.60	0.1012	0.1829
0.70	0.0925	0.1694
0.80	0.0870	0.1604
0.90	0.0857	0.1580
1.00	0.0850	0.1578

The stress intensity factors around the semi-elliptical surface crack for $\tau = 0.0625$, and $\tau = 0.125$ are presented in Figure 4.54.

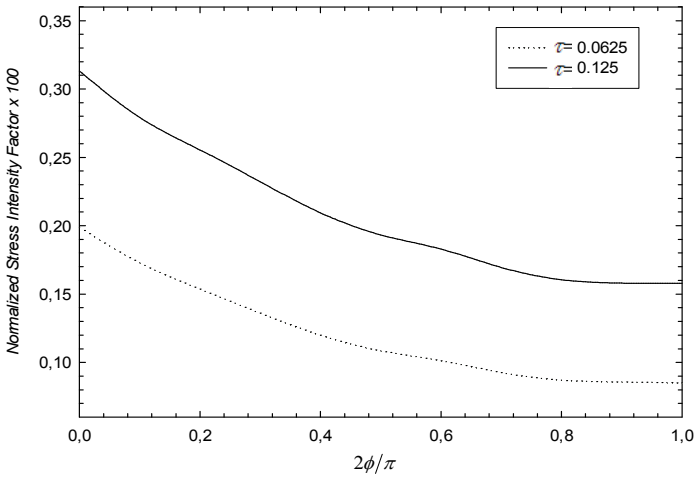

Figure 4 . 54 Normalized mode I stress intensity factor vs. normalized time distribution around the crack front for thermal loading, a/h=0.4, a/c=0.5

CHAPTER 5

CONCLUSION

In the present study, three-dimensional semi elliptic crack problems are studied for orthotropic materials and stress intensity factors around crack front are numerically calculated. The numerical code is written in the software, ANSYS parametric design language (APDL).

The crack is observed under several loading conditions for different type of materials. Displacement correlation technique gives accurate results for orthotropic and isotropic materials. It is an effective and accurate technique to obtain stress intensity factors around the crack front.

In the calculation of the stress intensity factors both displacement correlation techniques and anisotropic asymptotic stress and strain field expressions are used. The geometries of the models are created as same as in the reference models and the asymptotic stress and strain field expressions are verified with the results provided in the literature. Then, the percent differences are observed. Since results have small percent differences for all crack dimensions, loading types and material properties, it is accomplished that the numerical solution technique to solve the stress intensity factors of the orthotropic materials is satisfactorily accurate.

Considering the results of the finite element analysis results, it is seen that stress intensity factors at the surfaces where the crack intersects the free surface cannot be determined accurately. Due to the fact that stress singularity is different at these free surfaces. Therefore, the stress intensity factors cannot be found accurately, due to the negligence of the boundary zone effect near these surfaces. However, the results at the crack front regions are also approximate and applicable for the semi-elliptic surface cracks at the free surfaces.

For orthotropic material analysis, properties are given in tables as same as the reference values. Furthermore, the asymptotic stress and strain field expressions, used for anisotropic materials and the derivation, are given in Chapter 3. Considering the degeneracy cases, the correct formulation and expressions are used in the numerical analysis. In fact, in this study, fully anisotropic material is not analyzed; instead, it is focused on the degeneracy situations. For these cases, such as anti plane shear and plane strain decoupling case and the x-y plane isotropy case, different type of materials are investigated under various loading conditions, such as uniform tension, fixed grip tension, transient thermal loading etc.

Considering the mechanical loading cases, the stress intensity factors are higher at the free surface regions. For uniform tension loading type, the value of the stress intensity factor generally decreases when the thickness and polar angle increase. This leads to the conclusion that for three-dimensional surface edge cracks, the propagation of the crack front is slower in the direction of the thickness. However, in some loading types, the maximum and the

minimum points are altering while crack length and material thicknesses are changing.

In transient thermal loading, due to the boundary conditions the temperature of the free surface drops instantaneously. For polystal material, in transient thermal analysis stress intensity factor has the minimum value where the polar angle is $\pi/2$. This leads to the conclusion that the crack propagation is larger where the crack intersects the free surface and smaller in the thickness direction.

As a future work, extension of this present study, three-dimensional fracture analysis of the semi elliptical crack can be studied in a fully anisotropic structure subjected to thermal and mechanical loading. Another extension can be the mixed mode loading of the anisotropic structure. For this task, mixed mode stress intensity factors can be obtained, and after developing reliable models, inclined surface cracks can be embedded to the material, which is orthotropic or anisotropic. Moreover, the model and the code can be modified considering the crack closure methods to obtain accurate results for negative stress intensity factors.

REFERENCES

[1] *Near Tip Behavior of a Crack in a Plane Anisotopic Elastic Body.* Hoenig, Alan., Engineering Fracture Mechanics, Vol. 16, pp. 393-403, 1982

[2] *Elastic Crack Growth In Finite Elements with Minimal Remeshing.* Belytschko, T. and Black, T. s.l. : International Journal for Numerical Methods in Engineering, International Journal for Numerical Methods in Engineering, Vol. 45, pp. 601-620, 1999

[3] *Crack-Mounth Displacements for Semielliptical Surface Cracks Subjected to Remote Tension and Bending Loads.* Raju, I. S., Newman, J. C. and Atluri, S. N., Engineering Fracture Mechanics, Vol. 2, pp. 297-316, 1992

[4] *Three Dimensional Contact Fracture Problems Using Enriched Finite Elements.* Özkan, Ümit., Phd. Thesis Lehigh University, 2006

[5] *Analysis of Cracks In Anisotropic Materials Using ANSYS and 3DFAS.* Özkan, Ümit, et al. s.l. : Proceeding of IMECE2006, ASME, 2006.

[6] *A Critical Review of Crack Tip Stress Intensity Factors for Semi-Elliptic Cracks.* Scott, P. M. and Thorpe, T. W. 4, Fatigue and Fracture of Engineering Materials and Structures, Vol. 4, pp. 291-309, 2007

[7] *A Finite Element Alternating Method for Evaluation of Stress Intensity Factors for Part Circular Cracks Subjected to Arbitrary Loadings.* Liao, C. Y. and Atluri, S. N., Engineering Fracture Mechanics, Vol. 91, pp. 1253-1270, 1991

[8] *Stress Intensity Factors for Semi-Circular Cracks Part-2 Semi-Infinite Solid.* Smith, F. W., Emery, A. F. and Kobayashi, A. S., International Journal of Applied Mechanics, Vol. 34, pp. 947-952, 1967

[9] *Three Dimensional Fracture Analysis of FGM Coatings under Thermo-Mechanical Loading.* Yıldırım, B., Dag, S. and Erdogan, F., International Journal of Fracture Mechanics, Vol. 132, pp. 369-395, 2005

[10] *Stress Intensity Factors for a Wide Range of Semi-Elliptical Surface Cracks in Finite Thickness Plates.* Raju, I. S. and Newman, J. C., Engineering Fracture Mechanics, Vol. 11, pp. 817-829, 1979

[11] *On Cracks in Rectilinearly Anisotropic Bodies.* Sih, G. C., Chen and Paris, P. C., International Journal of Fracture Mechanics, Vol. 1, pp. 189-203, 1965

[12] *Cracks in Anisotropic Bodies in a State of Generalized Plane Deformation.* Embley, G., M.S. Thesis, Lehigh University, 1981

[13] *Cracks in Composite Materials.* Sih, G. C. and Chen. London : Martinus Nijhoff Publishers, EP Mechanics of Fracture 6, 1981

[14] *Stress Intensity Factors for Cracks in Anisotropic Materials Using Enriched Finite Elements.* Özkan, Ümit. PA. : s.n., M.S. Thesis, Lehigh University, 2003

[15] *Analysis of Three Dimensional Interface Cracks Using Enriched Finite Elements.* Ayhan, A. O., Kaya, A. C. and Nied, H. F., Engineering Fracture Mechanics, 2006

[16] *The Stress State of an Elastic Orthotropic Medium with a Penny-Shaped Crack*. Kirilyuk, V. S. 12, International Applied Mechanics, Vol. 40, pp. 1371-1377, 2004

[17] Kaw and Autar, K. *Mechanics of Composite Materials.* Fla. : Boca Raton. pp. 79-109. Vol. 29, 2003

[18] Jones, Robert M. *Mechanics of Composite Materials.* 2nd. s.l. : CRC Press., 1998.

[19] Springer, G. S. *Mechanics of Composite Structures.* Cambridge : U.P., 2003.

[20]. Bower, Alan F. *Applied Mechanics of Solids.* USA : CRC Press, 2009.

[21] *Wikipedia.* [Online] http://en.wikipedia.org/wiki/stress_intensity_factor.

[22] *Fracture and Size Effect in Concrete and Other Quasibrittle Materials.* Bazant, Z. P. and Planas, J. FL : CRC Press , Boca Raton, 1998.

[23] Library/Solid87, ANSYS Users Manual (Element Reference/I.Element. [prod.] ANSYS 12.1. 2010.

[24] *Stress Intensity Factors for Surface Cracks in Functionally Grade Materials Under Mode-I Thermomechanical Loading.* Walters, M. C., Glaucio, H. Paulino and Doods, H. Robert., International Journal of Solids and Structures, Vol. 41, pp. 1081-1118, 2004

[25] *Mathematical Analysis in the Mechanics of Fracture.* Rice, J. R. [ed.] H. Liebowitz. NY : Academic Press, Vol. 2, 1968

[26] *Three Dimensional Fracture Analysis of FGM Coatings.* İnan, Özgür. 2004.

[27] *Three Dimensional Mixed Mode Fracture Analysis of Functionally Graded Materials.* Köşker, Sadık. 2007.

[28] *An Empirical Stress-Intensity Factor Equation for the Surface Crack.* Newman, J. C. and Raju, I. S., Engineering Fracture Mechanics, Vol. 15, pp. 185-192, 1981

[29] *Stress Intensity Factor for Three Dimensional Surface Cracks Using Enriched Finite Elements.* Ayhan, A. O. and Nied, H. F., International Journal for Numerical Methods in Engineering, Vol. 54, pp. 889-921, 2002

[30] *Stress Intensity Factors and COD in an Orthotropic Strip.* Kaya, A. C. and Erdogan, F. 2, International Journal of Fracture Mechanics, Vol. 16, pp. 171-190, 1980

[31] *Interface Cracking of FGM Coatings Under Steady State Hear Flow.* Lee, Y. D. and Erdogan, F. 3, Engineering Fracture Mechanics, Vol. 59, pp. 361-380, 1998

[32] *Fracture Analysis of Anisotropic Materials Using Enriched Crack Tip Elements.* Özkan, Ümit, Nied, H. F. and Kaya, A. C., Engineering Fracture Mechanics, Vol. 77, pp. 1191-1202, 2010

[33] *Use of Micromechanical Modelling in the Material Characterisation of Overinjected Thermoplastic Composites.* Harte, A. M. and Mc. Namara, J. F. Galway, Ireland : s.n., Journal of Materials Processing Technology, Vol. 173, pp. 376-383, 2005

[34] *Theory of an Anisotropic Elastic Body.* Lekhnitskii, S. G. San Francisco : Holden Day, 1953.

APPENDIX A

A. SAMPLE ANISOTROPIC ASYMPTOTIC FIELD EXPRESSION CALCULATION FOR THE ORTHOTROPIC-I MATERIAL

Material properties are given as follows:

$$E_1 = 55.16x10^9 \qquad v_{12} = 0.036 \qquad G_{12} = 4.83x10^9$$
$$E_2 = 171.0x10^9 \qquad v_{23} = 0.111 \qquad G_{23} = 4.83x10^9$$
$$E_3 = 55.16x10^9 \qquad v_{13} = 0.036 \qquad G_{31} = 26.61x10^9 \qquad (A1)$$

Due to symmetry, following simplifications can be applied.

$$v_{21} = v_{12}\ , v_{32} = v_{23}, v_{31} = v_{13}, G_{21} = G_{12}, G_{32} = G_{23}, G_{31} = G_{13} \quad (A2)$$

The elements of compliance matrices can be written in terms of material properties.

$$S_{11} = \frac{1}{E_1} \qquad (A3)$$

$$S_{12} = \frac{-v_{21}}{E_2} \qquad (A4)$$

$$S_{13} = \frac{-v_{31}}{E_3} \qquad (A5)$$

$$S_{22} = \frac{1}{E_2} \qquad (A6)$$

$$S_{23} = \frac{-v_{32}}{E_3} \qquad (A7)$$

$$S_{33} = \frac{1}{E_3} \qquad (A8)$$

$$S_{44} = \frac{1}{G_{23}} \qquad (A9)$$

$$S_{44} = \frac{1}{G_{13}} \qquad (A10)$$

$$S_{44} = \frac{1}{G_{12}} \qquad (A11)$$

$$S_{14} = S_{15} = S_{16} = S_{24} = S_{25} = S_{26} = S_{34} = S_{35} = S_{36} = S_{45} = S_{46} = S_{56} = 0 \qquad (A12)$$

$$S_{43} = S_{34},\ S_{53} = S_{35},\ S_{63} = S_{36} \qquad (A13)$$

S =

$$\begin{bmatrix} 1.81\text{x}10^{-11} & -2.11\text{x}10^{-13} & -6.53\text{x}10^{-13} & 0 & 0 & 0 \\ -2.11\text{x}10^{-13} & 5.85\text{x}10^{-12} & 2.01\text{x}10^{-12} & 0 & 0 & 0 \\ -6.53\text{x}10^{-13} & 2.01\text{x}10^{-12} & 1.83\text{x}10^{-11} & 0 & 0 & 0 \\ 0 & 0 & 0 & 2.07\text{x}10^{-10} & 0 & 0 \\ 0 & 0 & 0 & 0 & 3.78\text{x}10^{-11} & 0 \\ 0 & 0 & 0 & 0 & 0 & 2.07\text{x}10^{-10} \end{bmatrix} \qquad (A14)$$

If the plane stress conditions exists material matrix elements calculated by the following expressions.

$$M_{ij} = M_{ij} - \frac{M_{i3}M_{j3}}{M_{33}} \qquad (A15)$$

$$I_2(x) = M_{22}x^2 - 2M_{45}x + M_{44} \qquad (A16)$$

$$I_3(x) = M_{15}x^3 - (M_{14} + M_{56})x^2 + (M_{25} + M_{46})x - M_{24} \qquad (A17)$$

$$I_4(x) = M_{11}x^4 - 2M_{16}x^3 + (2M_{12} + M_{66})x^2 - 2M_{26}x + M_{22} \qquad (A18)$$

Characteristic roots of these polynomials are calculated as:

$$roots\ of\ I_2(x) = \begin{pmatrix} -1.16525i \\ 1.16525i \\ -3.37291i \\ 3.37291i \end{pmatrix} \qquad (A19)$$

$$roots\ of\ I_4(x) = \begin{pmatrix} -6.06710i \\ 6.06710i \end{pmatrix} \quad (A20)$$

Characteristics roots are chosen such that, imaginary parts are positive.

$$N = \begin{pmatrix} 1 & 1 & 0 \\ -\mu_1 & -\mu_2 & 0 \\ 0 & 0 & -1 \end{pmatrix} = \begin{pmatrix} 1 & 1 & 0 \\ -1.165i & -3.373i & 0 \\ 0 & 0 & -1 \end{pmatrix} \quad (A21)$$

The inverse matrix is calculated as given

$$N^{-1} = \begin{pmatrix} 1.052 & -0.312i & 0 \\ -0.052 & 0.312i & 0 \\ 0 & 0 & -1 \end{pmatrix} \quad (A22)$$

The values of “p” are defined as follows:

$$p_{11} = M_{11}{\mu_1}^2 + M_{12} - M_{16}\mu_1 \quad (A23)$$

$$p_{12} = M_{11}{\mu_2}^2 + M_{12} - M_{16}\mu_2 \quad (A24)$$

$$p_{21} = M_{12}{\mu_1}^2 + \frac{M_{22}}{\mu_1} - M_{26} \quad (A25)$$

$$p_{22} = M_{12}{\mu_2}^2 + \frac{M_{22}}{\mu_2} - M_{26} \quad (A26)$$

$$p_{33} = \left(M_{45} + \frac{M_{44}}{\mu_3}\right) \tag{A27}$$

$$p_{23} = 0,\ p_{31} = 0,\ p_{32} = 0,\ p_{13} = 0 \tag{A28}$$

The calculation result for p matrix is given

$$p = \begin{pmatrix} p_{11} & p_{12} & p_{13} \\ p_{21} & p_{22} & p_{23} \\ p_{31} & p_{32} & p_{33} \end{pmatrix}$$
$$= \begin{pmatrix} -7.774x10^{-13} & -2.063x10^{-10} & 0 \\ -3.408ix10^{-11} & -2.622x10^{-12} & 0 \\ 0 & 0 & 3.412x10^{-11} \end{pmatrix} \tag{A29}$$

For mode-I loading the asymptotic displacement expression is given.

$$u_2(r,\theta) = \sqrt{\frac{2r}{\pi}K}\left(Re\left(p_{21}N_{11}\sqrt{\cos(\theta) + \mu_1\sin(\theta)}\right)\right.$$
$$+ Re\left(p_{22}N_{21}\sqrt{\cos(\theta) + \mu_2\sin(\theta)}\right)$$
$$\left. + Re\left(p_{23}N_{31}\sqrt{\cos(\theta) + \mu_3\sin(\theta)}\right)\right)$$
$$= 2.849x10^{-11} \tag{A30}$$

As $\theta \to \pi$ and $r \to 0$

$$u_2(r,\pi) \to 2.0144x10^{-11}\sqrt{2r}K \tag{A31}$$

Then the coefficient $C(\pi)$ is calculated as

$$C = 3.51x10^{10} \tag{A32}$$